

BRNO UNIVERSITY OF TECHNOLOGY
VYSOKÉ UČENÍ TECHNICKÉ V BRNĚ

FACULTY OF CIVIL ENGINEERING
INSTITUTE OF STRUCTURAL MECHANICS

FAKULTA STAVEBNÍ
ÚSTAV STAVEBNÍ MECHANIKY

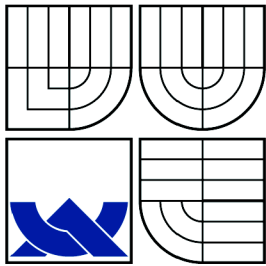
**MULTI-FILAMENT YARNS TESTING FOR
TEXTILE-REINFORCED CONCRETE**

MASTER'S THESIS
DIPLOMOVÁ PRÁCE

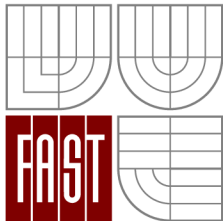
AUTHOR
AUTOR PRÁCE

Bc. JANA KADĚROVÁ

BRNO 2012



BRNO UNIVERSITY OF TECHNOLOGY
VYSOKÉ UČENÍ TECHNICKÉ V BRNĚ



FACULTY OF CIVIL ENGINEERING
INSTITUTE OF STRUCTURAL MECHANICS

FAKULTA STAVEBNÍ
ÚSTAV STAVEBNÍ MECHANIKY

MULTI-FILAMENT YARNS TESTING FOR TEXTILE-REINFORCED CONCRETE

TESTOVÁNÍ ODEZVY MNOHOVLÁKNITÝCH SVAZKŮ PRO TEXTILEM
VYZTUŽENÝ BETON

MASTER'S THESIS
DIPLOMOVÁ PRÁCE

AUTHOR
AUTOR PRÁCE

Bc. JANA KADĚROVÁ

SUPERVISOR
VEDOUČÍ PRÁCE

doc. Ing. MIROSLAV VOŘECHOVSKÝ, Ph.D.

BRNO 2012



VYSOKÉ UČENÍ TECHNICKÉ V BRNĚ FAKULTA STAVEBNÍ

Studijní program	N3607 Stavební inženýrství
Typ studijního programu	Navazující magisterský studijní program s prezenční formou studia
Studijní obor	3607T009 Konstrukce a dopravní stavby
Pracoviště	Ústav stavební mechaniky

ZADÁNÍ DIPLOMOVÉ PRÁCE

Diplomant	Bc. Kaděrová Jana
Název	Multi-filament yarns testing for textile-reinforced concrete
Vedoucí diplomové práce	doc. Ing. Miroslav Vořechovský, Ph.D.
Datum zadání diplomové práce	31. 3. 2011
Datum odevzdání diplomové práce	13. 1. 2012

V Brně dne 31. 3. 2011

.....
prof. Ing. Drahomír Novák, DrSc.
Vedoucí ústavu

.....
prof. Ing. Rostislav Drochytka, CSc.
Děkan Fakulty stavební VUT

Podklady a literatura

- [1] R. Chudoba, M. Vořechovský, and M. Konrad. Stochastic modeling of multi-filament yarns I: Random properties within the cross-section and size effect. *International Journal of Solids and Structures* (Elsevier), 43(3-4):413-434, 2006.
- [2] M. Vořechovský and R. Chudoba. Stochastic modeling of multi-filament yarns: II. Random properties over the length and size effect. *International Journal of Solids and Structures* (Elsevier), 43(3-4):435-458, 2006.
- [3] R. Chudoba, M. Vořechovský, V. Eckers, and T. Gries. Effect of twist, fineness, loading rate and length on tensile behavior of multifilament yarns (a multivariate study). *Textile Research Journal* (Sage), 77(11):880-891, 2007.
- [4] M. Vořechovský. Korekce zatěžovacích drah na netuhých lisech. In: Pejchalová a kol. (eds), *Směrování kateder/ústavu STM stavebních fakult ČR a SR 2005/2006*, p. 93-97, Mikulov, Czech Republic, 2006. Brno University of Technology, Fac. of Civil Engrg., Inst. of Struct. Mech.
- [5] D Tripathi and F. R Jones, Single fibre fragmentation test for assessing adhesion in fibre reinforced composites, *Journal of Materials Science*, 33(1):1-16, DOI: 10.1023/A:1004351606897
- [6] Feih, S., Wonsyld, K., Minzari, D. Westermann, P., Lilholt, H. Testing Procedure for the Single Fiber Fragmentation Test, Technical Report Riso-R-1483(EN) (ISSN: 0106-2840), pages: 30, 2004, RISØ.
- [7] Sborníky konferencí EURO-C, FraMCoS a konferencí zaměřených na textilní beton, vláknobeton a podobné kompozity

Zásady pro vypracování

The aim of the master's thesis is a study of the behavior of multi-filament used for textile-reinforced concrete. The strength and deformation characteristics of industrially manufactured glass yarns will be experimentally measured within the scope of the thesis by tensile testing.

Before performing the experiment with glass yarns, the student will suggest and perform necessary experiments to identify the deformation characteristics of the laboratory test machine and of the other components employed in the clamping of the sample and in the measurement of the force and deformation during the tensile loading. Based on this experience, the procedure of elimination of spurious deformations will be suggested.

The technology of the specimen preparation and the procedure of experimental testing have to be mastered to avoid any fundamental errors. The realization of a high number of experiment series is encouraged to obtain statistically significant data. Results from the experiment will be processed with the focus on the parameter identification for a numerical model of multi-filament bundle.

Předepsané přílohy

Licenční smlouva o zveřejňování vysokoškolských kvalifikačních prací

.....
doc. Ing. Miroslav Vořechovský, Ph.D.
Vedoucí diplomové práce

ABSTRACT

The scope of the presented master thesis was the experimental study of multi-filament yarns made of AR-glass and used for textile-reinforced concrete. The behavior under the tensile loading was investigated by laboratory tests. A high number of yarn specimens (over 300) of six different lengths (from 1 cm to 74 cm) was tested to obtain statistically significant data which were subsequently corrected and statistically processed. The numerical model of the multi-filament bundle was studied and applied for prediction of the yarn performance and for later results interpretation. The model of n parallel filaments describes the behavior of a bundle with varying parameters representing different sources of disorder of the response and provides the qualitative information about the influence of their randomization on the overall bundle response. The aim of the carried experiment was to validate the model presumptions and to identify the model parameters to fit the real load-displacement curves. Unfortunately, due to unsuccessful correction of measured displacements devalued by additional non-linear contribution of the unstiff experiment device the load-displacement diagrams were not applicable to model parameters identification. The statistical evaluation was carried only for the maximal load values and the effect of the specimen size (length) on its strength was demonstrated. The size effect curve did not exclude the existence of spatial correlation of material mechanical properties modifying the classical statistical Weibull theory.

KEYWORDS

filament, yarn, bundle model, size effect, Weibull theory, experiment, specimen, textile-reinforced concrete, AR-glass, probability

ABSTRAKT

Cílem předložené práce bylo experimentální studium mnohovláknitých svazů z alkalicky odolného skla, které se používají k výrobě textilně vyztuženého betonu. V rámci laboratorního testu byla zjišťována odezva na tahové zatížení. K získání statisticky významného souboru dat byl proveden vysoký počet zkoušek (přes 300) na vzorcích šesti různých délek (od 1 do 74 cm). K predikci a k pozdější interpretaci výsledků zkoušek byl prezentován numerický model svazku mnoha sériově zapojených vláken se znáhodněnými parametry, které zastupují různé vlivy způsobující odlišnost odezvy od ideálního svazku. Cílem experimentu bylo ověřit předpoklady modelu a případně identifikovat jeho parametry tak, aby odpovídal skutečně naměřeným zatěžovacím křivkám. Díky neúspěšnému pokusu o opravu naměřených křivek, jejichž deformace byly ovlivněny příspěvkem netuhých částí zatěžovacího stroje, nebyla identifikace parametrů modelu možná. K statistickému zpracování experimentu byla použita pouze data naměřených sil (tahových pevností), na kterých byl demonstrován vliv délky vzorku na jeho pevnost.

KLÍČOVÁ SLOVA

vlákno, svazek vláken, model svazku, vliv velikosti, Weibullova teorie, pokus, vzorek, textilně vyztužený beton, alkalicky odolné sklo, pravděpodobnost

KADĚROVÁ, Jana *Multi-filament yarns testing for textile-reinforced concrete*: master's thesis. Brno: Brno University of Technology, Faculty of Civil Engineering, INSTITUTE OF STRUCTURAL MECHANICS, 2012. 86+XVII p. Supervised by doc. Ing. Miroslav Vořechovský, Ph.D.

DECLARATION

I declare that I have elaborated my master's thesis on the theme of "Multi-filament yarns testing for textile-reinforced concrete" independently, under the supervision of the master's thesis supervisor and with the use of technical literature and other sources of information which are all quoted in the thesis and detailed in the list of literature at the end of the thesis.

As the author of the master's thesis I furthermore declare that, concerning the creation of this master's thesis, I have not infringed any copyright. In particular, I have not unlawfully encroached on anyone's personal copyright and I am fully aware of the consequences in the case of breaking Regulation § 11 and the following of the Copyright Act No 121/2000 Vol., including the possible consequences of criminal law resulted from Regulation § 152 of Criminal Act No 140/1961 Vol.

Brno

.....

(author's signature)

PODĚKOVÁNÍ

Na prvním místě bych chtěla poděkovat panu doc. Ing. Miroslavu Vořechovskému, Ph.D. za jeho motivaci, ochotu a pomoc při práci v laboratoři i při následném zpracovávání výsledků. Děkuji také panu Ing. Václavu Sadílkovi za jeho pomoc s realizací a zpracováváním zkoušek, panu Miroslavu Friedlovi za výrobu drah pro přípravu vzorků a technickou pomoc a panu Ing. Petru Frantíkovi, Ph.D. za pomoc s úpravou naměřených dat. Můj velký dík patří mé rodině a všem mým blízkým za jejich podporu a zájem (1182).

Práce vznikla v rámci projektů:

GAČR P105/10/J028

GAČR 103/09/H085

Typeset by L^AT_EX 2_ε

CONTENTS

Introduction	19
1 Behavior of multi-filament yarns	23
1.1 Introduction	23
1.2 Computational model	23
1.2.1 Kinematic model	23
1.2.2 Load-strain diagram for numerical evaluation of finite n	26
1.2.3 Continuous asymptotic evaluation for infinite n	27
1.3 Parametric studies of properties within the bundle cross-section	28
1.3.1 Scatter of filament lengths	28
1.3.2 Scatter of filament diameters	31
1.3.3 Scatter of filament activation strain (slack)	32
1.3.4 Interaction of filament's length scatter and delayed activation	34
1.3.5 Relation between waviness and delayed activation strain	35
1.4 Random properties over the filament and bundle length	38
1.4.1 Random strength along individual filament	39
1.4.2 Random strength along filaments within the bundle	45
1.4.3 Interaction of random stiffness and strength along the bundle	50
1.5 Conclusion	54
2 Experiment	55
2.1 Introduction	55
2.2 Experiment preparations	55
2.3 Test setup	60
2.4 Measured results	63
3 Results editing	65
3.1 Introduction	65
3.2 Elimination of outliers from the statistics	65
3.3 Impact of jaws on the measured displacements	67
3.4 Conclusion	72
4 Results interpretation	75
4.1 Introduction	75
4.2 Effect of the length on the yarn strength	75
Conclusion	79

Bibliography	81
List of symbols, physical constants and abbreviations	85
List of appendices	I
A Experiment documentation (figures)	III
B Experiment results in detail	VII

LIST OF FIGURES

1	Examples of application of textile-reinforced concrete [22].	19
2	Reinforcing textiles: bi-axial scrim and wrap knit, 3D spacer wrap knit and textile in the matrix [22].	20
3	Different types of concrete reinforcement.	20
1.1	Left: Filaments in the bundle and their elementary characteristics varying over the length. Right: Filament lengths.	24
1.2	Load-strain diagrams of one filament (left) and the whole yarn (right).	26
1.3	Probability functions for random parameter.	28
1.4	Length scatter influence: load-strain diagrams for different $\lambda = \Delta/l$ ratio.	29
1.5	Left: Influence of filament area (diameter) scatter on the load-strain diagram. Right: Filaments in epoxy resin.	31
1.6	Slack influence: load-strain diagrams for different θ_{\max}/ξ ratio.	32
1.7	Load-strain with acting parameters λ, θ and their interactions. Left: length of experiment sample, right: length of crack-bridge.	35
1.8	Wave patterns with corresponding histograms of θ for different lengths l . (histograms are adopted from [7])	36
1.9	AR-glass yarn.	37
1.10	Random strength of chain segments.	39
1.11	Weibull strength distribution PDF (full line) and CDF (dashed line).	41
1.12	Weibull median strength σ_{med} vs. number of segments N in double- logarithmic scale.	42
1.13	Modified median Weibull strength with autocorrelation.	44
1.14	Estimation of bundle maximum tensile force.	46
1.15	Load-strain curve T_ξ of a bundle with n filaments together with curves of filaments q_0 and q_ξ and their mean curve M_ξ (bundle).	47
1.16	Load-strain curves of bundles M_ξ with different number of filaments n as a result of Monte Carlo simulations ($n_{\text{sim}} = 100$). Mean values of the bundle strength \pm std are depicted, as well as the asymptotic response $M_\xi(n \rightarrow \infty)$	48
1.17	Left top: mean size effect curves for different number of filaments within the bundle, curves for $n > 160$ overlap. Left bottom: Values of COV and effective Weibull shape modulus m_{COV} . Right: Yarn efficiency for varying length and number of filaments. Figure adopted from [27].	50
1.18	Effective material stiffness E_i and filament strength over the length. .	51

1.19	Stress-strain diagrams of constitutive law each time with one quantity constant.	51
1.20	Two-parameter randomization by E and σ and their correlation.	52
1.21	Influence of different correlation length on the bundle response for different randomized parameters. Figure adopted from [27].	52
1.22	The bundle response for varying E -modulus with Weibull distribution. Left: case a) with constant $\bar{\sigma}$; case b) with constant $\bar{\xi}$. Figure adopted from [27].	53
2.1	The tested AR-glass yarn on a bobbin.	56
2.2	Specimens' length groups.	56
2.3	Anchoring types: yarn coiled up (left) and poured in anchoring block (right).	57
2.4	A deassembled steel mould.	58
2.5	A steel mould for the production of silicone forms.	58
2.6	Silicone (left) and epoxide (right).	59
2.7	A silicone form.	59
2.8	Special tracks for specimen preparation.	60
2.9	Left: Scheme of the loading device parts with a sketch of series coupling of deformable components. Right: The point of measured vertical displacement.	62
2.10	Unmodified force-displacement curves (all samples).	63
2.11	Unmodified force-displacement curves of different length groups.	64
2.12	Specimens before and after the test.	64
3.1	Relative error of samples and outliers' elimination (marked with crosses). Rel. errors are plotted vs. various parameters.	66
3.2	Force-displacement curves of steel bar; displacements measured on different spots.	68
3.3	Force-displacement curves of double yarns. Experiments performed with jaws before and after servicing. Grey lines represent curves from Fig. 3.2 for comparison.	70
3.4	Force-displacement curves of different length groups obtained directly from experiments. Significant "wave" event with subsequent decrease of stiffness can be observed.	70
3.5	The clamp slack at different force levels (due to different pre-tension of transverse clamp screws).	71
3.6	Calibration curves.	72
3.7	Examples of measured and modified force-displacement curves of different nominal lengths.	73

4.1	Correspondence between the physical experiment and the numerical model.	75
4.2	Yarn strengths vs. yarn lengths of tested sample groups and the size-effect curve as an average \pm std of modified (red) and original (grey) data set.	76
4.3	Estimation of size effect curve parameters.	77
4.4	Explanation of the experimentally obtained curve shape without the effect of autocorrelation of strength.	78
A.1	A steel form with a silicone form.	III
A.2	Freshly cast silicone form (left) and epoxide anchoring blocks (right).	III
A.3	Test machine Zwick/Roell Gruppe Z100.	IV
A.4	Test of a sample of length 1 cm (left) and 2.5 cm (right).	IV
A.5	Test of a sample of length 6 cm (left) and 13 cm (right).	V
A.6	Test of a sample of length 31 cm (left) and 74 cm (right).	V
A.7	Broken samples.	VI
A.8	Self-locking jaws (front) and pneumatic jaws and (rear).	VI

LIST OF TABLES

1.1	AR-glass filament material characteristics used in parametric study. . .	28
1.2	Material parameters used in numerical simulations.	38
1.3	Influence of randomness in material parameters on the measured load-displacement diagrams with increasing length. With the increas- ing length the characteristics increases(+)/decreases(-)/stagnates(·). Adopted from [27].	54
2.1	Characteristics of tested AR-glass yarns.	55
2.2	Average time spent on sample testing.	60
2.3	Number of tested specimens.	61
2.4	Test programme setup.	62
3.1	Date of testing and its ordinal number (comment for Fig. 3.1(b)). . .	66
3.2	Number of specimens used for statistics (after elimination of 37 outliers). .	67
4.1	Final experiment statistics: average, std and CoV of yarn strength. . .	76
B.1	Results of laboratory testing (ordering according to the length group and date of experiment)	VII
B.1	(continued)	VIII
B.1	(continued)	IX
B.1	(continued)	X
B.1	(continued)	XI
B.1	(continued)	XII
B.1	(continued)	XIII
B.1	(continued)	XIV
B.1	(continued)	XV
B.1	(continued)	XVI
B.2	Laboratory conditions: temperature and relative humidity with their extreme values in a certain time period.	XVII

INTRODUCTION

Textile-reinforced concrete is a developing composite material with a high potential of application in civil engineering structures and also in other industrial branches. The material combines a cementitious matrix providing the compressive strength and a tensional reinforcement made by multi-axial fabrics. It has many advantages compared to usual steel-reinforced concrete. The structure reinforced by textile gets thinner, consequently the amount of used concrete is reduced and the structure becomes lighter. The material enables wide shape variability which gives more freedom in the design to engineers and architects.

The textile-reinforced concrete is nowadays applied for façade members, in wastewater treatment systems, water protection wall systems, as integrated formwork elements, for strengthening and rehabilitation of older structures and also the first textile-reinforced pedestrian bridge with span 8.60 m has been built in Germany in 2006 over the Döllnitz river.

The fibers used for the textile reinforcement has to meet several criteria: high fibre tenancy, breaking elongation and modulus of elasticity much higher than the modulus of the concrete matrix, so that the stiffness of building component is not drastically reduced by occurring cracks. The fibers must withstand the chemical action of alkaline medium without loosing its mechanical properties. The most common material of fibers is alkali resistant glass (AR-glass) but carbon, aramid and other (less-suitable) polymers like polypropylene, polyvinyl alcohol, polyethylene and polyacrylnitrile can be used as well.



Fig. 1: Examples of application of textile-reinforced concrete [22].

Filaments are combined to yarns. One yarn composes of several hundreds up to thousands of single filaments. The fineness of the yarn is defined by the unit “tex” (gram per 1000 meters) and depends on the average filament diameter, the fibre material density and the number of filaments. Yarns are subsequently combined into textiles; according to different fabrication process the produced textiles can be, e. g., plane and circular scrims, bi- or multi-axial warp knits or three-dimensional spacer wrap knits.

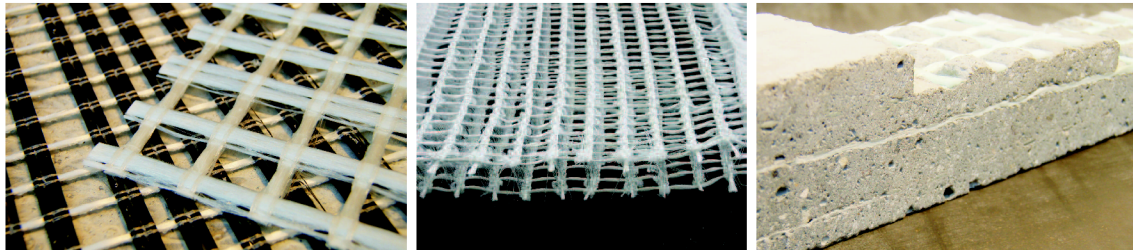


Fig. 2: Reinforcing textiles: bi-axial scrim and wrap knit, 3D spacer wrap knit and textile in the matrix [22].

The matrix of the composite is usually made by fine grained concrete with limited maximum grain size (< 2 mm). The load-bearing behavior of the composite cannot be derived from the qualities of used components, however, the bond between the filaments and matrix has to be taken into account. The better is the anchorage between them, the higher interaction of components is. From this point of view a good cohesion and the good infiltration of matrix within the yarn cross-section is essential. Only the surface of the filaments exposed to the mortar can transmit the load from mortar to the yarn. For the sake of extending the surface, the shape of the yarns is not circular but flat.

Historically, the textile-reinforced concrete developed from fiber-reinforced concrete with short filaments of random orientation by aligning the filaments in the direction of the tensile stresses similarly to classical steel reinforcement, which led to better effectiveness of the reinforcement, increased load-bearing capacity and the cost reduction. The main advantages of the material are high ductility and strain hardening. The yarn reinforcement ensures the bridging of cracks occurred in the

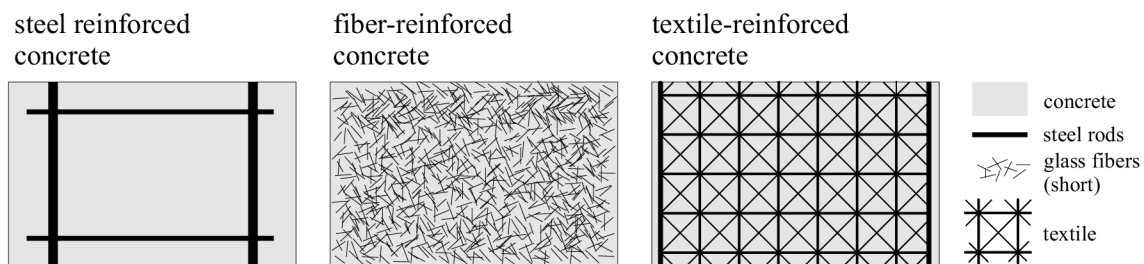


Fig. 3: Different types of concrete reinforcement.

concrete under tension/bending [16]. The increased energy dissipated by multiple cracking of the material provides better safety of the structure.

The material is a subject of intensive research in many institutions [19]. The load-bearing performance and the deformation behavior have been investigated for decades so that the material can be introduced to the actual production in the future and safe structural design and serviceability can be ensured by proper standards.

The scope of presented master thesis is the experimental study of multi-filament yarns made of AR-glass and used for textile-reinforced concrete. The behavior under the tensile loading was investigated by laboratory tests. A high number of specimens (over 300) of six different lengths was tested to obtain statistically significant data which were subsequently corrected and statistically processed. The need of data correction was caused by additional spurious measured deformation of the laboratory loading machine and its components. The deformation behavior of the loading test setup had to be mapped to find the calibration curve serving for the subtraction of these parasite deformations. The numerical model of the multi-filament bundle was introduced for prediction of the yarn performance and for later results interpretation.

The thesis is divided into four chapters. The theoretical background together with the numerical model of a bundle is described in Chapter 1. The chapter defines the computational model of a bundle of n parallel filaments with variable parameters representing possible sources of disorder and inquires into the influence of their randomization on the overall response. These parameters vary from filament to filament within the bundle cross-section (the filament length, diameter, activation strain) and also over the length of each filament (strength, E modulus) for filament's "material points". The second half of the chapter copes also with the dependency of the bundle strength on the number of filaments and their length and the theory of statistical size effect is presented. Numerical simulations are applied for each variable parameter and their mutual interaction and the analytical response of continuous model with infinite number of filaments is presented in parallel.

The following chapters are dedicated to the experiment. Chapter 2 describes the process of the laboratory testing from the design of sample series and their production through the machine setup to the overview of obtained load paths. Experiment results and their accuracy are discussed in Chapter 3. The data set was edited and the outlying results were discarded. Measured deformations distorted by parasite contributions of unstiff loading machine parts were inspected. The estimation of the correction curve and subsequently the yarn deformation adjustment was performed. The last Chapter 4 copes with the edited test data and their interpretation in the sense of their possible application for the identification of the numerical model

parameters.

The final summary of the carried experiment is in the Conclusion. In the Appendix part of the thesis an additional image documentation of the experiment and a complete table of detailed experiment results are presented.

1 BEHAVIOR OF MULTI-FILAMENT YARNS

1.1 Introduction

The yarn structure is a system made by many parallel filaments with random properties. These properties randomly vary over the length of the yarn as well as within each cross-section due to imperfections from the production process. To describe the complex behavior of the bundle, definition and study of each individual random property and its influence on overall performance is essential. Statistical approach is applied as the most convenient way to capture the yarn behavior under tension.

Historically the fundamentals of statistical modeling of multi-filaments yarns was based on the knowledge of probability distributions of extreme values of independent and identically distributed quantities described by Fisher and Trippett (1928, [12]) and by Weibull (1939, [30]), who introduced the weakest-link model. The theory was firstly applied on the mechanical problem by Peirce (1926, [17]). This has been later developed into fiber bundle model (FBM) introduced by Daniels (1945, [9]) and Coleman (1958, [8]) that describes the bundle as a set of parallel fibers, each with strength given by Weibull probability distribution (Phoenix, Harlow, Smith). The further research developed other advanced models of the bundle, where another effects like localization, the effect of a bond between the matrix filaments, non-linear behavior, possible multiple cracking of the filament, load sharing rule, etc. are included. The interaction between patterns can be studied by Monte-Carlo simulations technique.

The presented thesis studied the computational model presented in [7] and [27].

1.2 Computational model

The bundle in this study is modeled as a set of parallel fibers with no interaction among them as the experiments showed neglectable friction between AR-glass filaments over lengths < 50 cm. Each filament is considered independently acting and the response of the whole bundle during displacement-controlled tensile loading can be evaluated in an analytical and numerical approach.

1.2.1 Kinematic model

The deformation–strain relation has to be defined to capture the filament’s kinematics. Especially the response of the very short bundles (corresponding to the length if the crack-bridge ≈ 0.0001 m) are strongly influenced by the length disorder like different length of filaments given by the distance of their clamping points, and other

types of disorder. These effects are expressed by different model parameters. Parameters used for the bundle model can be divided into two groups: those describing the the separate filament and those describing the yarn (a set of filaments).

- Parameters appointed to i -th filament can be used regardless of the composition of the bundle. For alkali resistant (AR-glass), where linear brittle fracture behavior is considered, these parameters are Young's modulus of elasticity E_i , cross-section area A_i and filament strength σ_i . For cases where the filament parameters are randomized within the cross-section, no variability of these parameters over the filament length is considered (parameters are set constant over the length).
- Parameters appointed to the bundle describe the variability of filaments within the bundle. Each of the filament parameters is randomized and expressed by probability distribution function (CDF) – $G_E(E_i)$, $G_A(A_i)$, $G_\sigma(\sigma_i)$. Differences in filament lengths from the nominal length l of the bundle are captured by two extra parameters: parameter λ for the different distance of fixing points of each filament and parameter θ for the different global activation strain of each filament due to waviness of filaments in the bundle. The total length of i -th filament is then $l_{i,\lambda,\theta}$ – see Fig. 1.1 right).

$$l_{i,\lambda,\theta} = (1 + \theta_i)l_{i,\lambda} = (1 + \theta_i)(1 + \lambda_i)l \quad (1.1)$$

where $\lambda_i = (l_{i,\lambda} - l)/l$ is the ratio between extra length of i -th filament to the nominal length of the bundle in the initial state of loading and $\theta_i = (l_{i,\lambda,\theta} - l_{i,\lambda})/l_{i,\lambda}$ is the ratio of filament activation strain (strain of the bundle in state when the i -th filament starts to transmit force). This ratio is also called the filament slack.

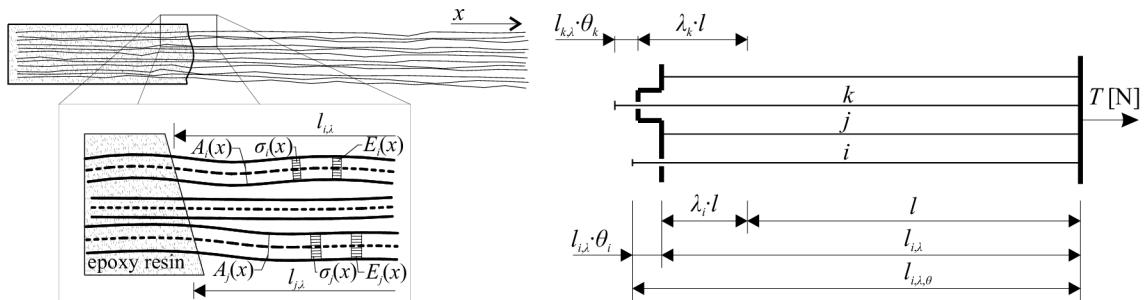


Fig. 1.1: Left: Filaments in the bundle and their elementary characteristics varying over the length. Right: Filament lengths.

Mentioned parameters are implied to the load-strain diagram equation of the i -th filament made of linear-elastic brittle material – Eq. 1.2.

$$q_{\varepsilon,i}(\varepsilon_i) = \begin{cases} 0 & \text{for } \varepsilon_i < 0, \\ E_i A_i \varepsilon_i & \text{for } 0 \leq \varepsilon_i \leq \xi_i, \\ 0 & \text{for } \xi_i < \varepsilon_i \end{cases} \quad (1.2)$$

where ε_i is the strain, $\xi_i = \sigma_i/E_i$ is its critical value (breaking strain) and A is the cross-sectional area of the i -th filament. More convenient form of this relation can be obtained by using the Heaviside (unit step) function: $H(x) = 1$ for $x \geq 0$ and $H(x) = 0$ elsewhere, which zeros the filament stress out of the filament's possible strain interval. The equation 1.2 then becomes:

$$q_{\varepsilon,i}(\varepsilon_i) = E_i A_i \varepsilon_i H(\varepsilon_i) H(\xi_i - \varepsilon_i) \quad (1.3)$$

In order to represent and model the response of the bundle with several parallel fibers of different length, it is convenient to transform the constitutive relation defined as a function of ε (Eq. 1.3) into a common global strain e . The global strain is equal to the strain imposed on the yarn during the tensile displacement-controlled loading. The filament stress can be related to the global bundle strain e by following equivalency: control displacement of the bundle is equivalent to the filament displacement $u(\varepsilon_i) \equiv u(e) = el$. Then according to Eq. 1.1 the local strain in the i -th filament becomes:

$$\varepsilon_i = \frac{u - \theta_i l_{i,\lambda}}{l_{i,\lambda,\theta}} = \frac{el - \theta_i(1 + \lambda_i)l}{l_{i,\lambda,\theta}} = \frac{e - \theta_i(1 + \lambda_i)}{(1 + \theta_i)(1 + \lambda_i)} \quad (1.4)$$

This form expresses the local strain for the actual filament length instead of the nominal length. It should be noted that the nominal length l is arbitrary and the relation between the local strain ε and the global strain e is independent of the choice of l . The i -th filament force related to the control bundle strain e (the constitutive law) can be expressed by substituting Eq. 1.4 into Eq. 1.3:

$$q_{e,i}(e) = E_i A_i \frac{e - \theta_i(1 + \lambda_i)}{(1 + \theta_i)(1 + \lambda_i)} H[e - \theta_i(1 + \lambda_i)] H\left[\xi_i - \frac{e - \theta_i(1 + \lambda_i)}{(1 + \theta_i)(1 + \lambda_i)}\right] \quad (1.5)$$

Global activation strain t_i and global breaking strain x_i of the i -th filament (Fig. 1.2 left) can be obtained from the arguments of Heaviside step functions:

$$\begin{aligned} t_i - \theta_i(1 + \lambda_i) &= 0 \rightarrow t_i = \theta_i(1 + \lambda_i) \\ \xi_i - \frac{x_i - \theta_i(1 + \lambda_i)}{(1 + \theta_i)(1 + \lambda_i)} &= 0 \rightarrow x_i = \theta_i(1 + \lambda_i) + \xi_i(1 + \theta_i)(1 + \lambda_i) \end{aligned} \quad (1.6)$$

1.2.2 Load-strain diagram for numerical evaluation of finite

n

The mechanical model of the bundle with n filaments is now defined. The overall response in form of the load-strain diagram of the bundle during tensile loading can be obtained numerically simply by summing up the contributions of all filaments at each level of global strain.

$$T(e) = \sum_{i=1}^n q_{e,i}(e) \quad (1.7)$$

Each filament is characterized by three significant points: the inception point, when the filament starts to transmit force, the point of maximum transmitted force and the point of rupture, when the transmitted force drops to zero. The last two cases occur at the same strain level, but differ in the transmitted force. Each of these points is expressed by two values (strain and the corresponding force), so for one filament there are only three couples of values completely describing its contribution to overall response. For the whole bundle these values can be separated into three vectors each holding n pairs $[e_j, T_i]$ of bundle strains and corresponding bundle forces: \mathbf{t} , $\mathbf{x}^{(+)}$ and $\mathbf{x}^{(-)}$.

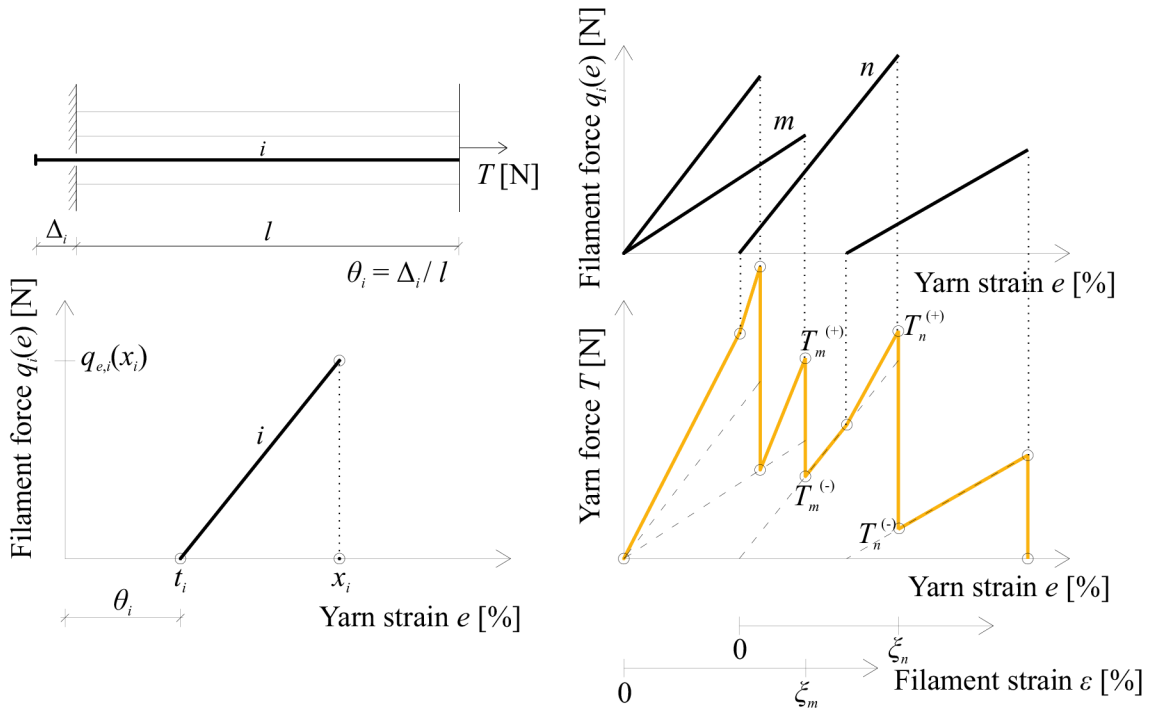


Fig. 1.2: Load-strain diagrams of one filament (left) and the whole yarn (right).

$$\left. \begin{aligned} \mathbf{t} &= [t_j, T_j^{(t)}], & \text{where } T_j^{(t)} &= \sum_{i=1}^n q_{e,i}(t_j) \\ \mathbf{x}^{(+)} &= [x_j, T_j^{(+)}], & \text{where } T_j^{(+)} &= \sum_{i=1}^n q_{e,i}(x_j) \\ \mathbf{x}^{(-)} &= [x_j, T_j^{(-)}], & \text{where } T_j^{(-)} &= T_j^{(+)} - q_{e,i}(x_j) \end{aligned} \right\} j = 1, \dots, n \quad (1.8)$$

The resulting load-strain diagram is obtained by union of these three vectors into one vector $\mathcal{R} = \cup\{\mathbf{t}, \mathbf{x}^{(+)}, \mathbf{x}^{(-)}\}$. Vector \mathcal{R} is sorted in an ascending way according to the yarn strain (first pair member); if two pairs shares the same strain, then the member with higher yarn force comes first (second member). Sorted vector \mathcal{R} contains points of load-strain diagram of the whole bundle, which is piece-wise linear (Fig. 1.2 right), as it was established by simple summation of filaments' contributions. This is only possible if the superposition rule is assumed to be valid.

The evaluation of the bundle tensile response in form of a load-strain diagram contained in \mathcal{R} is a low-demanding and, therefore, a suitable method for analysis with randomized parameters varying both within the bundle cross-section and along the filaments. Random filament parameters introduced in Eq. 1.5, whose influence of variation on the overall bundle response was investigated, are gathered into vector $\boldsymbol{\theta}_i$.

$$q_{e,i}(e) = q_{e,i,\theta}(e; \boldsymbol{\theta}_i) \quad \text{with} \quad \boldsymbol{\theta}_i = \{A_i, E_i, \sigma_i, \theta_i, \lambda_i\} \quad (1.9)$$

In the parametric study the bundle response is investigated for one or more different randomized parameters from the vector $\boldsymbol{\theta}_i$ with defined probability distributions and the qualitative effect is visualized.

1.2.3 Continuous asymptotic evaluation for infinite n

In the practical applications the number of the bundle filaments is very high (several hundreds to thousands). For the high value of filaments n the bundle mean response $M(e)$ can be solved analytically [18] as n -multiple of the mean filament response $\mu(e)$: $M_\theta(e) = n\mu_\theta(e)$:

$$\mu_\theta(e) = \int_{\boldsymbol{\theta}} q_e(e; \boldsymbol{\theta}) dG_\theta(\boldsymbol{\theta}) \quad (1.10)$$

The individual parameters θ_i ($i = 1, \dots, n_v$) of vector $\boldsymbol{\theta}$ are independent and, therefore $dG_\theta(\boldsymbol{\theta}) = dG_1(\theta_1) \times dG_1(\theta_1) \times \dots \times dG_{n_v}(\theta_{n_v})$, where $G_i(\theta_i)$ is the cumulative distribution function of the parameter θ_i . Filament's behavior is governed by the constitutive law (Eq. 1.5).

The introduced models were used for parametric studies of influence of each parameter and its scatter separately. Obtained results helped for qualitative understanding and interpretation of measured data and for clarifying observed phenomena.

1.3 Parametric studies of properties within the bundle cross-section

A parametric study is a suitable method how to clarify the influence of each parameter, its variation and their interaction on the bundle response. The effect of variability in parameters λ , θ and A across the bundle separately and in mutual interaction was investigated in [7]; the effect of varying E , σ over the length and number of filaments n in the bundle was studied in [27]. The filaments' material was AR-glass (Tab. 1.1) which corresponds to material used in experiments.

Tab. 1.1: AR-glass filament material characteristics used in parametric study.

<i>tensile strength</i>	$\sigma = 1.25$ GPa
<i>Young's modulus</i>	$E = 70$ GPa
<i>filament diameter</i>	$D = 26$ μm
<i>breaking strain</i>	$\xi = \sigma/E = 1.768$ %

While demonstrating the effect of randomness of one separate parameter, the other are considered constant (in their mean value – Tab. 1.1). For elementary illustration the bundle is represented by reduced number of filaments $n < 100$ (approx. 100 times less than in real number) and the filament forces are expressed in “scaled” value [cN]. The filament response is calculated according to Eq. 1.3 and the analytical mean solution (Eq. 1.10) is always plotted in diagrams for comparison. The probability density function for random parameter λ and θ are constant – Fig. 1.3.

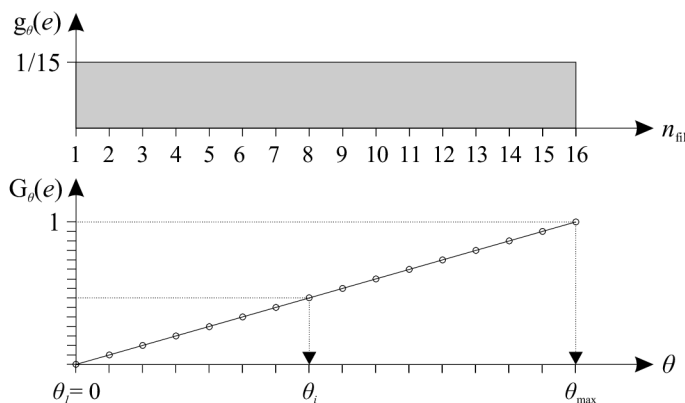


Fig. 1.3: Probability functions for random parameter.

1.3.1 Scatter of filament lengths

In ideal state, all the filaments in the bundle share the same length $l_i = l$. The reality shows that this assumption is not correct and the filament lengths are directly

influenced by the technology of yarn production as well as the specimen preparation. In the experiment presented in this thesis the ends of the specimen are fixed in epoxy resin which can cause two kinds of imperfections. Due to capillary effect the epoxide penetrates through the yarn in the longitudinal direction which causes uneven distance of the fixing points on both sides of the yarn ends or eventually the epoxide doesn't penetrate through the whole yarn cross-section so that the free length of filaments in the middle of the yarn is longer. This unevenness of lengths is expressed by the parameter λ .

In the following parametric study the nominal length of the bundle is equal to the minimum length of filaments in the bundle $l = l_{\min} = \min_{i=1,\dots,n} (l_{i,\lambda})$, $\Delta_{\min} = l - l_{\min} = 0$, the longest filament has length l_{\max} , $\Delta_{\max} = l_{\max} - l$. The difference between the shortest and the longest filament was set $\Delta_{\max} = 2$ mm, which approximately corresponds to 1 mm-unevenness on each side. The distribution of the additional length Δ_i is linear (see the inset of Fig. 1.4) so that λ_i is uniformly distributed among all the filaments such that $\lambda_{i=1,\dots,n} = \lambda_{\max} (i - 1)/(n - 1)$, where $\lambda_{\max} = \Delta_{\max}/l$. The load-strain diagrams were plotted for different nominal lengths ($l = 0.5, 1, 4, 10, 40, 100$ mm) with constant parameters E , A and ξ and zero slack $\theta = 0$.

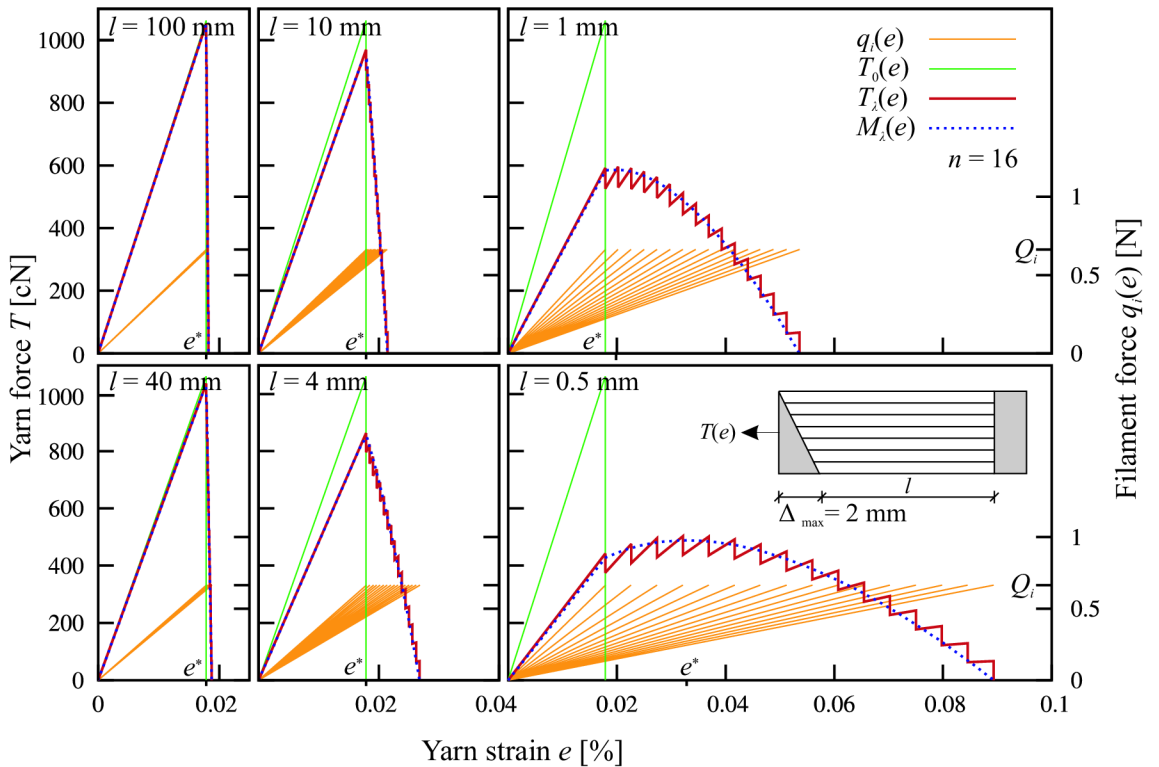


Fig. 1.4: Length scatter influence: load-strain diagrams for different $\lambda = \Delta/l$ ratio.

Fig. 1.4 shows both the numerical and the analytical solutions: the red curve $T_\lambda(e)$ is the numerical solution for $n = 16$ filaments in the bundle, the blue dotted line $M_\lambda(e)$ is the analytical solution according to Eq. 1.11 for infinite number of

filaments. The yellow lines symbolize individual filament load-strain diagrams $q_i(e)$ with the filament strength $Q_i(e)$ and green line $T_0(e)$ is a special case of bundle response for $\lambda = 0$ – the ideal state for $n = 16$.

It is clearly recognizable that the unevenness of filament lengths leads to the reduction of bundle stiffness and consequently to the reduction of the bundle peak load because the maximum tensile strength is not reached in all filaments at the same global strain level. The higher is the λ ratio, the lower is the maximal transmitted tensile force and the more ductile the behavior is. For the very short specimens (l equal to 1 and 0.5 mm) the bundle failure-strain e^* grows, while for longer lengths stays equal to the breaking strain of the filament $e^* = \xi$.

The analytical solution in Eq. 1.11 is obtained from Eq. 1.10, where A , E , $\sigma = \text{const.}$, $\theta = 0$ and λ is uniformly distributed: $\lambda \sim R : g_\lambda = 1/\lambda_{\max} H(\lambda)H(\lambda_{\max} - \lambda)$. The overall response of the bundle is then $M_\theta(e) = n\mu_\theta(e)$.

$$\begin{aligned} \mu_\lambda(e; \lambda) &= \int_\lambda q_e(e; \lambda) dG_\lambda(\lambda) = \frac{EAe}{\lambda_{\max}} \int_0^{\lambda_{\max}} \frac{1}{(1+\lambda)} H[\xi(1+\lambda) - e] d\lambda \\ &= \begin{cases} EAe \ln(1 + \lambda_{\max})/\lambda_{\max} & 0 \leq e \leq \xi \quad \text{lin.} \\ EAe[\ln(1 + \lambda_{\max}) - \ln(e/\xi)]/\lambda_{\max} & e > \xi \quad \text{nonlin.} \end{cases} \quad (1.11) \end{aligned}$$

The stiffness of the bundle is reduced due to the scatter of filament lengths comparing to ideal bundle ($\lambda = 0$) with r_λ ratio:

$$r_\lambda = \ln(1 + \lambda_{\max})/\lambda_{\max} \quad (1.12)$$

The point e^* and the corresponding peak load can be found by differentiation of Eq. 1.11 (as the stationary point). Depending on the value of λ_{\max} this point can lie either on the linear (case I) or on the nonlinear branch of the curve (case II) – see Eqs. 1.13.

$$\begin{aligned} \text{CASE I} & \quad \text{when } \lambda_{\max} \leq [\exp(1) - 1] \approx 1.718 \\ & \quad \quad \quad e^* = \xi \\ & \quad \quad \quad \mu_i(e^*) = EA\xi \ln(1 + \lambda_{\max})/\lambda_{\max} \\ \text{CASE II} & \quad \text{when } \lambda_{\max} > [\exp(1) - 1] \approx 1.718 \\ & \quad \quad \quad e^* = \xi(1 + \lambda_{\max})/\exp(1) \\ & \quad \quad \quad \mu_i(e^*) = EA\xi \ln(1/\lambda_{\max} + 1)/\exp(1) \end{aligned} \quad (1.13)$$

By substituting the nominal length relation into the previous equations an explicit size effect equations can be expressed. We now investigate the case $l = l_{\min}$, $\Delta_{\max} = 2$ mm, with $\lambda_{\max} = \Delta_{\max}/l$. It is important to mention that with different selection of the nominal length a different form of size effect is obtained. For example, with alternative definition $l = l_{\max}$ and $\Delta_{\min} = -2$ mm there would be a linear equation for short bundles and nonlinear for long ones; in diagrams the

shorter yarns would appear stiffer than the long yarns. Despite this fact, the bundle strength does not change with different l definition. On the other hand, the proper definition of l gets its importance when investigating the response of the bundle in a crack-bridge of textile-reinforced concrete, where the energetic considerations must be taken into account for the correct determination of the effective yarn length.

As a conclusion of this parametric study it can be stated that scatter of the filament lengths due to imperfections at epoxy clamping blocks cause reduction of bundle strength, which is more significant for shorter specimens. This effect acts in an opposite way compared to the statistical Weibull size effect. Also introduced more ductile behavior of short yarns contrasts with the diagrams measured in experiments.

1.3.2 Scatter of filament diameters

Another parameter which is a random variable is the cross-section area of each individual filament. Due to technological process of AR-glass filaments production the final diameter ranges approximately from 23 to 29 μm . For the parametric study the mean value $\bar{D} = 26 \mu\text{m}$ with $\text{COV}(D)=10 \%$ was assumed ($\text{std} = 2.6 \mu\text{m}$). The mean bundle response is again obtained from Eq. 1.10 with $E, \xi = \text{const.}, \lambda = \theta = 0$ and filament diameter is defined by its cumulative distribution function $G_D(D)$.

$$\mu_A(e; D) = eEH (\xi - e) \frac{\pi}{4} \int_D D^2 dG_D(D) \quad (1.14)$$

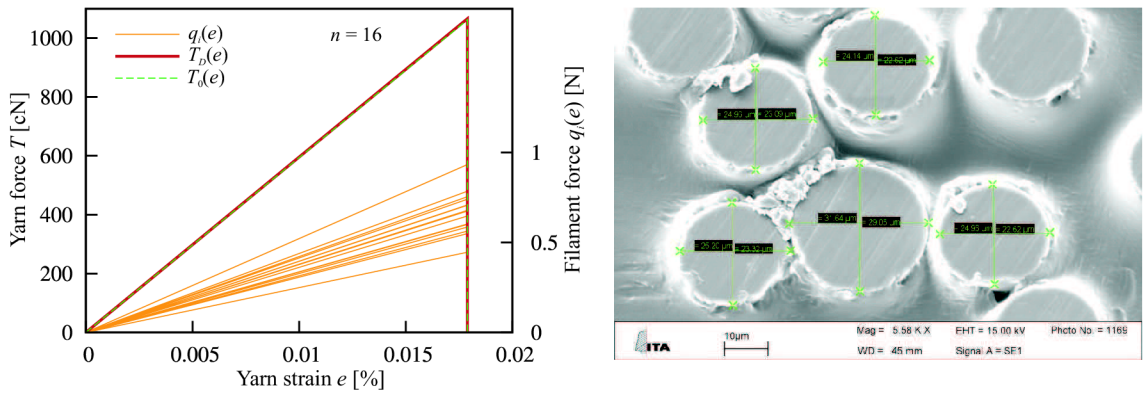


Fig. 1.5: Left: Influence of filament area (diameter) scatter on the load-strain diagram. Right: Filaments in epoxy resin.

The bundle breaks at the filament breaking strain $e^* = \xi$. The difference between the response of a bundle without any scatter of filaments areas and a real bundle can be obtained from the cumulative distribution function $G_D(D)$ as the r_D ratio comparing their mean values:

$$r_D = \frac{\mu_D(e)}{\mu(e)} = \frac{1}{\bar{D}^2} \int_D D^2 dG_D(D) \quad (1.15)$$

If the distribution $G_D(D)$ is assumed to be Gaussian, this ratio has the value of $r_D = (1 + \text{COV}(D)^2)$. When, for example, $\text{COV} = 10\%$ and the mean bundle stiffness is changed just by 1% increment.

This may lead to the conclusion that the overall bundle behavior and its mean response $M_D(e)$ is not significantly changed by scatter of filament diameters (especially compared to $M_0(e)$). Anyway, this introduces the scatter into the peak load.

1.3.3 Scatter of filament activation strain (slack)

During the production process filaments in the yarn are reeled together, which introduces repeating and easily visible wavy pattern. In this pattern, filaments follow different trails and when the experiment sample is prepared, some filaments in the bundle can stay loose while others are directly straight. During tensile loading these straight fibers start immediately transmitting the load, while originally loose fibers are still unloaded (delayed activation effect – slack). This phenomenon can be captured by θ parameter which expresses an additional length of slack fibers.

In the parametric study the nominal length is again set on the length of the shortest filament $l = l_{\min}$. The longest filament in the bundle has then the length $l_{\max} = (1 + \theta_{\max})l$. The ratio $\theta_{\max} = (l_{\max} - l)/l$ is uniformly distributed among all the filaments (analogically to the distribution of λ) over the range $0 \leq \theta_i \leq \theta_{\max}$. Parameters E , A and ξ are considered constant and $\lambda = 0$. The load-strain diagrams in Fig. 1.6 are plotted for three different θ -ratios: $\theta = 2\xi, 1\xi, 0.5\xi$ (ξ is filament breaking strain).

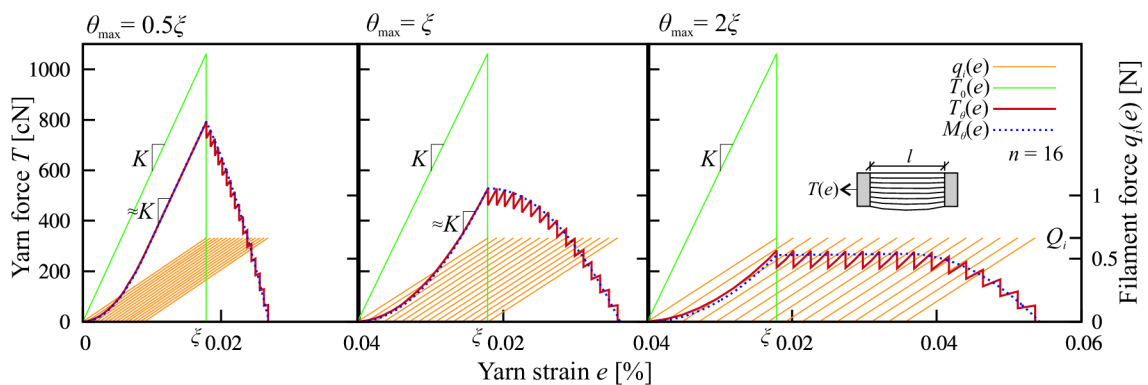


Fig. 1.6: Slack influence: load-strain diagrams for different θ_{\max}/ξ ratio.

Individual filament curves q_i are plotted by yellow lines, the overall numerical bundle response T_θ for $n = 16$ (number of filaments in the bundle) is the sum of filament responses and is marked with red color. The green line T_0 expresses the

ideal bundle diagram for $\theta_{\max} = 0$ and the analytical mean solution $M_\theta(e) = n \cdot \mu_\theta(e)$ is evaluated with the help of Eqs. 1.16 and plotted by blue dot-line.

$$\begin{aligned}
\mu_{\theta,1}(e) &= \frac{EA}{\theta_{\max}} \int_0^e \frac{e-\theta}{1+\theta} d\theta = \frac{EA}{\theta_{\max}} [(e+1) \ln(1+e) - e] \\
&\quad \text{for } e \in \langle 0; \min(\xi, \theta_{\max}) \rangle \\
\mu_{\theta,2,I}(e) &= \frac{EA}{\theta_{\max}} \int_{\frac{e-\xi}{1+\xi}}^e \frac{e-\theta}{1+\theta} d\theta = \frac{EA}{\theta_{\max}} (e+1) \left[\ln(1+\xi) - \frac{\xi}{1+\xi} \right] \\
&\quad \text{for } e \in \langle \min(\xi, \theta_{\max}); \max(\xi, \theta_{\max}) \rangle \quad \wedge \quad \xi < \theta_{\max} \\
\mu_{\theta,2,II}(e) &= \frac{EA}{\theta_{\max}} \int_0^{\theta_{\max}} \frac{e-\theta}{1+\theta} d\theta = \frac{EA}{\theta_{\max}} [(e+1) \ln(1+\theta_{\max}) - \theta_{\max}] \\
&\quad \text{for } e \in \langle \min(\xi, \theta_{\max}); \max(\xi, \theta_{\max}) \rangle \quad \wedge \quad \xi \geq \theta_{\max} \\
\mu_{\theta,3}(e) &= \frac{EA}{\theta_{\max}} \int_{\frac{e-\xi}{1+\xi}}^{\theta_{\max}} \frac{e-\theta}{1+\theta} d\theta = \frac{EA}{\theta_{\max}} \left\{ (e+1) \ln \left[\frac{(1+\theta_{\max})(1+\xi)}{1+e} \right] - \theta_{\max} + \frac{e-\xi}{1+\xi} \right\} \\
&\quad \text{for } e \in \langle \max(\xi, \theta_{\max}); \theta_{\max} + \xi(1+\theta_{\max}) \rangle
\end{aligned} \tag{1.16}$$

In the rendered analytical solution there are three significantly recognizable branches: branch 1 ($\mu_{\theta,1}(e)$) is ascending with gradual increase of stiffness as more filaments get activated; branch 2 is a linear function of yarn strain e , either linearly growing ($\mu_{\theta,2,II}(e)$) with no newly activated or broken filaments (Fig. 1.6 left) or a function close to constant function ($\mu_{\theta,2,I}(e)$) with both activating and breaking filaments (Fig. 1.6 right). Diagram in the middle of Fig. 1.6 misses this branch and after the full activation filaments immediately start breaking – branch 3 ($\mu_{\theta,3}(e)$) expressing the reduction of stiffness.

The maximum load $\mu_\theta(e^*) = \mu_{\theta,3}(e^*)$ is reached in the branch 3 and the corresponding strain e^* is the maximum from values (e_3^*, ξ) , where e_3^* is the stationary point which can be obtained by differentiating the equation for $\mu_{\theta,3}(e)$.

$$\frac{D\mu_{\theta,3}(e)}{De} = 0 \quad \rightarrow \quad e_3^* = (1+\xi)(1+\theta_{\max}) / \exp\left(\frac{\xi}{1+\xi}\right) - 1 \tag{1.17}$$

The size effect formula is obtained by substituting the point e_3^* into $\mu_{\theta,3} \rightarrow \mu_\theta^*$ (peak load) and by taking $\theta_{\max} = \Delta_{\max}/l$ with Δ_{\max} as a given constant. As a length-dependent equation for the peak load $\mu_\theta^*(l; \Delta_{\max})$ is expressed. The resulting formulas are complicated, but the trend of the size effect is following: according to used nominal length definition the curve has different asymptotes. The model used in this parametric study ($l = l_{\min}$) leads to constant strength values for short lengths

and the strength of the long bundles grows linearly to infinity. Another model used in [18] where the nominal length is equal to the longest filament length ($l = l_{\max}$) linearly reaches zero strength value for extremely short yarns ($l \rightarrow 0$), the strength of extremely long bundles is limited by the right asymptote at a constant value.

It may be concluded that the effect of delayed activation caused by waviness of the filament yarns acts against the classical statistical size effect and must be considered in evaluation of experiment data in order to interpret the length-dependent strength correctly.

1.3.4 Interaction of filament's length scatter and delayed activation

To combine the effect of different lengths of filaments due to clamping conditions with their delayed activation, both parameters λ and θ are considered varying over a certain range. The mean bundle response is obtained by double-integration of Eq. 1.10:

$$\begin{aligned} \mu_{\theta,\lambda}(e) &= \int_{\theta} \int_{\lambda} q_e(e; \theta, \lambda) dG_{\theta}(\theta) dG_{\lambda}(\lambda) = \\ &= EA \int_{\theta} \int_{\lambda} \frac{e - \theta(1 + \lambda)}{(1 + \theta)(1 + \lambda)} H \left[\xi - \frac{e - \theta(1 + \lambda)}{(1 + \theta)(1 + \lambda)} \right] H[e - \theta(1 + \lambda)] dG_{\theta}(\theta) dG_{\lambda}(\lambda) \end{aligned} \quad (1.18)$$

Although these two parameters were discussed separately so far, they influence each other in fact. The distribution functions $G_{\lambda}(\lambda)$ and $G_{\theta}(\theta)$ interact due to chosen definition of strain (Eq. 1.4). It means that the effect of the same θ_{\max} is different for various values of λ_{\max} , the extra length due to slack is influenced by the extra length of filaments due to λ parameter, which can be formulated as: $\Delta_{\theta} = \theta l (1 + \lambda)$.

Development of stiffness during the tensile loading can be seen in Fig. 1.7, where curves for $M_0(e)$, $M_{\lambda}(e)$, $M_{\theta}(e)$ and $M_{\lambda,\theta}(e)$ are plotted for comparison. Additional length ratios are uniformly distributed so that $G_{\lambda}(\lambda)$ and $G_{\theta}(\theta)$ are linear. The scatter of λ reduces the stiffness with r_{λ} factor (Eq. 1.12). After reducing the stiffness of $M_{\theta}(e)$ with this factor, it can be seen, that it does not correspond to the real stiffness of the $M_{\lambda,\theta}(e)$ curve, which would be overestimated. Especially for very short lengths corresponding to the crack-bridges, the evaluation of $\mu_{\lambda,\theta}(e)$ gets important.

The curves for sample of dimensions $l = 30$ mm, $\lambda_{\max} = 2/30$ and $\theta_{\max} = 0.009$ corresponding to laboratory experiments is in Fig. 1.7(left); a situation close to the crack-bridge is in the same Fig. (right): $\lambda_{\max} = 1.2$ (the longest filament

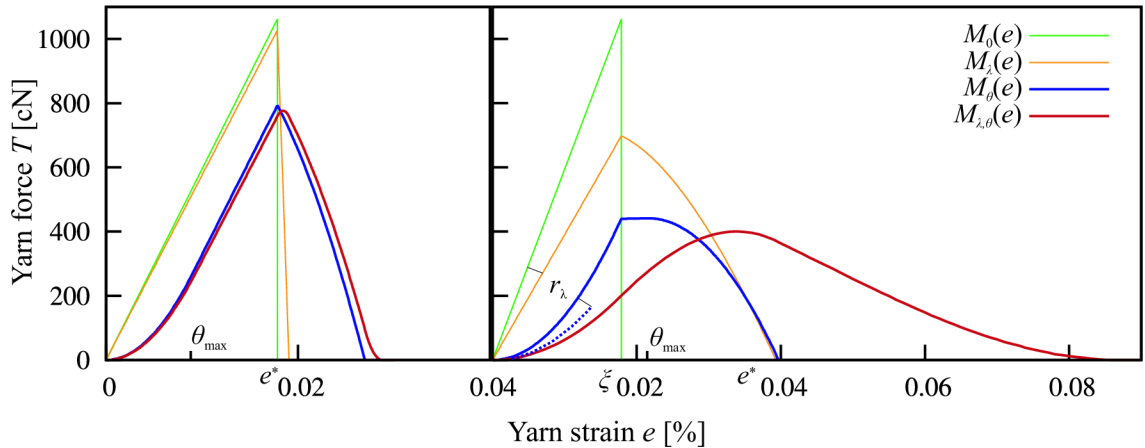


Fig. 1.7: Load-strain with acting parameters λ , θ and their interactions. Left: length of experiment sample, right: length of crack-bridge.

is 2.2 times longer than the shortest one) and $\theta_{\max} = 1.2\xi = 0.0214$. For the laboratory testing the reduction of stiffness due to varying λ can be neglected, while for the crack-bridge situation it is significant. Also the maximum transmitted load is reduced and the corresponding strain e^* grew – it can be approximated as $e^* = (1 + \lambda_{\max}/2) \cdot \max(\xi, \theta_{\max})$.

1.3.5 Relation between waviness and delayed activation strain

There is a direct correspondence between filament delayed activation and its waviness. We can observe several wave patterns on the bundle, that are caused either due to production technology or during the preparation of experimental samples. It is useful to describe particular kinds of waviness to classify its influence on the delayed activation of filaments with respect to the changing nominal length. Basically there are two limit cases: (I) the differences of filament lengths Δ_θ in the bundle grow linearly with growing nominal length l – this leads into length-independent delayed activation θ_{\max} ; and case (II) with growing nominal length l the length differences decrease $\theta_{\max} \rightarrow 0$. The study dealt with four basic types of bundle waviness (Fig. 1.8) and their length-dependence of the slack ratio.

Wave patterns (a) and (b) are introduced during the yarn production, pattern (c) appears due to inaccuracy in the test sample preparation and type (d) arises during the reeling of yarn on the bobbins.

The geometry of the filament is defined by the wave function $w(x, \alpha)$ with parameter $\alpha \in \langle 0, 1 \rangle$ defining the filament's position in the bundle. Total length of the

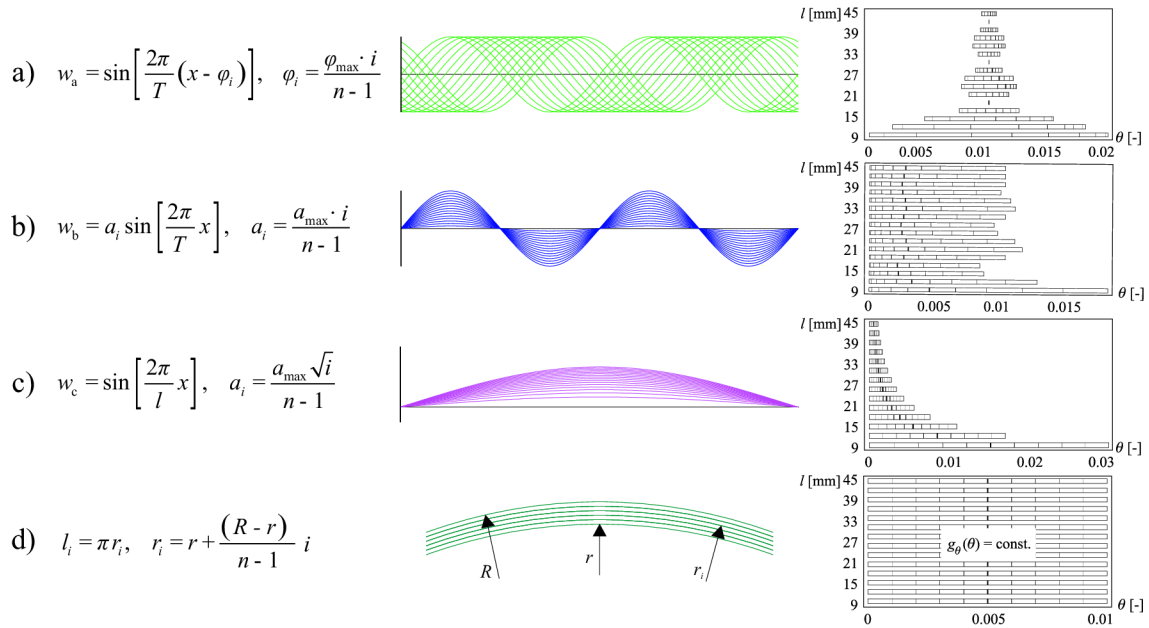


Fig. 1.8: Wave patterns with corresponding histograms of θ for different lengths l . (histograms are adopted from [7])

i -th filament can be calculated as the integral:

$$l_i = \int_0^l \sqrt{1 + w(x, \alpha)'^2} dx \quad (1.19)$$

The filament activation strain is then $\theta_i = (l_i - l) / l$ (considering $\lambda=0$). Histograms of parameter θ_i with respect to nominal length l show the length-dependency for each of considered wave pattern. (Histogram horizontal bars are divided into 10 segments each representing 10 % fraction of θ_i for given nominal length.) No interactions between filaments is assumed so that the strain formulation in Eq. 1.4 is valid.

The wave pattern (a) consists of periodic (sinusoidal) waves of equal amplitude shifted mutually in x -direction by φ_i . The resulting θ scatter oscillates around the common average value (approx. 1.1 %), the variation subsequently decreases with growing nominal length (limit case (II)). The second pattern (b) is formed by non-shifted waves with the same length but different amplitudes. The distribution of amplitudes a_i among filaments is uniform, majority of the filaments get activated at small e strains (in the beginning of loading) and with the growing nominal length the distribution of θ stabilizes and becomes length-independent (limit case (I)). Case (c) is a single-wave pattern of length l created during samples preparation. Filaments in this pattern have different amplitudes but the distribution is not uniform – it contains higher fraction of filaments with larger amplitudes. The considered distribution leads to uniform activation density function, which gets reduced to al-

most zero value with longer lengths l and the effect of delayed activation disappears (limit case (II)). The waves in case (d) are caused by coiling the yarn onto a bobbin. All the filaments share the same length which leads to uniform delayed activation density. This distribution does not change with growing l – it means it is length-independent (limit case (I)). With the increasing nominal length linearly grow the length-differences of filaments.

The aim of this geometrical classification was to find and validate the proper delayed activation density for different sample-lengths and find the domination wave-pattern (Fig. 1.9).

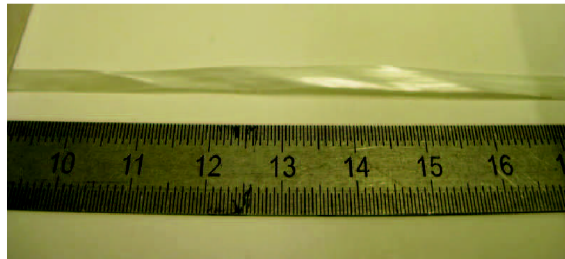


Fig. 1.9: AR-glass yarn.

1.4 Random properties over the filament and bundle length

The previous section was focused on the influence of randomization of parameters of individual parameters in the bundle on the total response. These parameters were: cross-section area, uneven length and delayed activation (slack) of individual filaments due to their waviness. The stiffness and the strength of the bundle were evaluated, compared to the ideal bundle and their length-dependency was investigated. Both of these two characteristics got reduced due to the variation of input parameters as well as both of them showed decreasing trend with diminishing length – it means in an opposite manner compared to the classical statistical size effect [30, 10, 3]. All the parameters were randomized within the cross-section and stayed constant for the whole length of the filament. It is useful to investigate the effect of spatial variation of the stiffness parameter E and the strength parameter σ .

In the following section, parameters (strength σ and Young's modulus E) are randomized along the filament and their spatial distribution as well as the auto-correlation is considered. The strength distribution randomness was considered as a stationary random process and a method Latin Hypercube Sampling (LHS), which is a type of Monte Carlo simulation method, was used.

The reference parameters are in calculations considered either I) as random and follow Weibullian PDF with given mean value, std and COV or, II) as constant and are represented with their mean value. For ideal bundle with no variation of parameters (constant values) is the response equal to $T_0(e) = M_0(e) = nEAeH(\xi - e)$ as a function of bundle strain e . Filaments diameter is taken as a constant $D = 26 \mu\text{m}$, other values of used parameters and their statistical moments are in Tab. 1.2. These values were obtained from former laboratory tests on AR-glass multi-filaments bundles.

Tab. 1.2: Material parameters used in numerical simulations.

	Tensile strength σ	Young's modulus E	Breaking strain $\xi = \sigma / \bar{E}$
Mean value	$\bar{\sigma} = 1.25 \text{ GPa}$	$\bar{E} = 70 \text{ GPa}$	$\bar{\xi}_{ \bar{E}} = 1.786 \%$
Standard deviation	$\text{std}_{\sigma} = 0.3125 \text{ GPa}$	$\text{std}_E = 10.5 \text{ GPa}$	$\text{std}_{\xi} = 0.4464 \%$
COV	0.25	0.15	0.25
<i>Weibull distribution:</i>			
Shape parameter	$m_{\sigma} = 4.5422$	$m_E = 7.9069$	$m_{\xi} = 4.5422$
Scale parameter	$s_{\sigma} = 1.369 \text{ GPa}$	$m_E = 74.373 \text{ GPa}$	$m_{\xi} = 1.9557 \%$

1.4.1 Random strength along individual filament

Considering the cross-section of the bundle, the material properties are randomized over the filaments $i \in \langle 1, \dots, n \rangle$, while for length randomization the variability of strength and stiffness is simulated for material points of each filament \mathcal{M}_j , $j \in \langle 1, \dots, p \rangle$. It is necessary to account for the distance-dependent autocorrelation of two material points in the spatial randomization of properties (over the length of the filament). The filament strength is dictated by the minimal strength over the length (the weakest-link model). To find the strength minima, investigation of the lower tail of the strength probability distribution is of big importance.

There are two basic approaches of the spatial randomization of strength:

- The filament is modeled as a chain of a finite number of segments (random variables), each of which represents a part of the filament with a given length and have random strength from the same probability distribution. The strengths of segments are identically distributed and independent – IID (with no dependence). This model leads to Weibull integral for the failure probability P_f (Eq. 1.28).
- The filament strength is randomized as one-dimensional random field (random process) with given autocorrelation distance. This approach takes into account a distance over which the fluctuation of a random parameter is correlated. This distance is a constant (autocorrelation length) and does not depend on the field (filament) length.

Spatial strength randomization using IDD

Classical Weibull theory of statistical size effect

The definition of classical Weibull integral for strength of structures described in [30, 3, 20] can be derived from illustrative example of in series coupled segments (chain model). Each segment of the chain is independent of others and its strength is a random variable with a given probability distribution function. If the CDF is identical for all segments of the chain, then we call segments as independent and identically distributed (IID). All the segments share the same loading σ (due to a common force F).



Fig. 1.10: Random strength of chain segments.

The probability of failure of any segment is $P_1(\sigma)$ is equal to the strength CDF. The probability of survival of one segment is the complement $1 - P_1(\sigma)$. The prob-

ability of survival of the whole chain is $1 - P_f$ and is given by condition that all the segments must survive (the collapse of one segment means the collapse of the whole chain). For independent segments, the survival probability is the product of survival probabilities of individual segments linked in a series:

$$1 - P_f = \underbrace{(1 - P_1)(1 - P_1)\dots(1 - P_1)}_{N\text{-times}} = (1 - P_1)^N \quad (1.20)$$

By taking the logarithm of the equation, we obtain:

$$\ln(1 - P_f) = N \ln(1 - P_1) \quad (1.21)$$

As the probability of chain failure P_f is a very low number in practical situations, the expression can be simplified by substitution $\ln(1 - P_1) \approx -P_1$, which leads to approximation:

$$P_f(\sigma) = 1 - e^{-NP_1(\sigma)} \quad (1.22)$$

$$P_f(\sigma) = 1 - \exp\left[-\frac{V}{V_r}P_1(\sigma)\right] \quad (1.23)$$

where $P_1(\sigma)$ is the probability distribution of failure of a representative volume V_r for a given stress level σ . Representative volume is a part of the total volume V of structure (chain) that is considered independent of other parts. The number of independent chain segments is then $N = V/V_r$.

Now the function of concentration $c(\sigma) = P_1(\sigma)/V_r$ is introduced (representing the density (concentration) of the failure probability of structure. Weibull defined an empirical relation for this function (in its simplified, two-parametric version) as:

$$c(\sigma) = \frac{1}{V_r} \left\langle \frac{\sigma}{\sigma_0} \right\rangle^m \quad (1.24)$$

with m as the shape parameter and σ_0 as the scale parameter of Weibull distribution. The fraction in Malacuya brackets is the positive part of stress (tension) $\langle \bullet \rangle = \max(\bullet, 0)$. After substituting the function of concentration into Eq. 1.23, we obtain:

$$P_f(\sigma) = 1 - \exp\left[-\frac{V}{V_r} \left\langle \frac{\sigma}{\sigma_0} \right\rangle^m\right] \quad (1.25)$$

The behavior of Weibull probability distribution is demonstrated for increasing number of chain segments in Fig. 1.11. The random strength of each segment is given by Weibull PDF and CDF as:

$$\begin{aligned} F_1(\sigma; s, m) &= 1 - \exp[-(\sigma/s)^m] \\ f_1(\sigma; s, m) &= \begin{cases} (m/s) (\sigma/s)^{m-1} \exp[-(\sigma/s)^m] & \sigma \geq 0; s, m > 0 \\ 0 & \sigma < 0 \end{cases} \end{aligned} \quad (1.26)$$

Using Eq. 1.20 we can express the CDF and PDF of Weibull distribution for N number of elements:

$$\begin{aligned} F_N &= 1 - [1 - F_1(\sigma; s, m)]^N \\ f_N &= \frac{\partial F_N}{\partial \sigma} = N \cdot f_1(\sigma; s, m) [1 - F_1(\sigma; s, m)]^{N-1} \end{aligned} \quad (1.27)$$

Graphs of probability density (full line) and cumulative distribution function (dash line) are plotted in Fig. 1.11 for different N . The trend of decreasing mean value and the standard deviation with increasing number of elements can be observed.

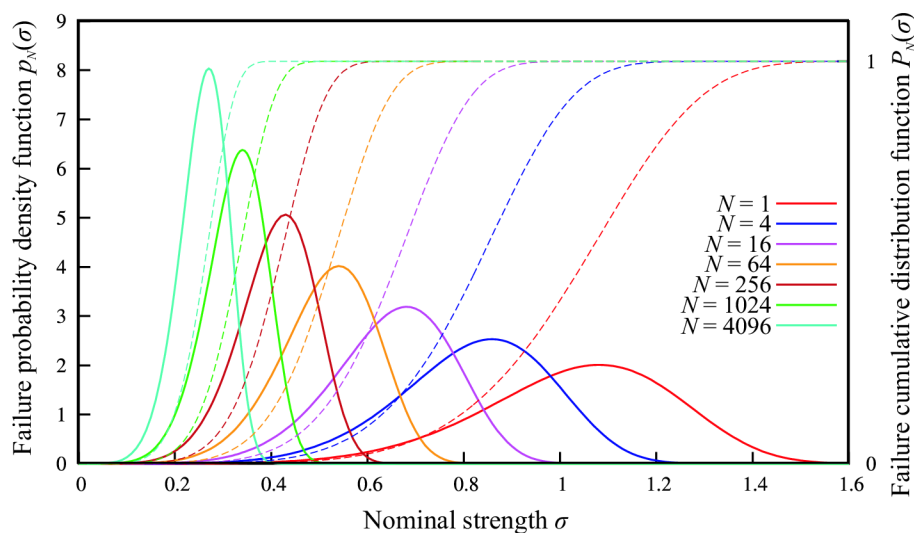


Fig. 1.11: Weibull strength distribution PDF (full line) and CDF (dashed line).

This reduction of strength can be even more clearly shown in the double logarithmic plot of strength as a function of number of segments. For chosen level of failure probability $P_f = 0.5$ (median strength) the size effect curve is presented in Fig. 1.12. In logarithmic coordinates, the curve appears as a straight line with a slope given by the shape parameter $(-1/m)$.

Filament strength randomization

The Weibull integral for the filament strength using the weakest-link model together with Weibull probability distribution expresses the failure probability P_f at the stress level σ as:

$$P_f(\sigma) = 1 - \exp \left[- \int_l \left\langle \frac{\sigma}{s_0} \right\rangle^m \frac{dl}{l_0} \right] \quad (1.28)$$

For a given parameter m of the Weibull distribution (shape parameter) there is

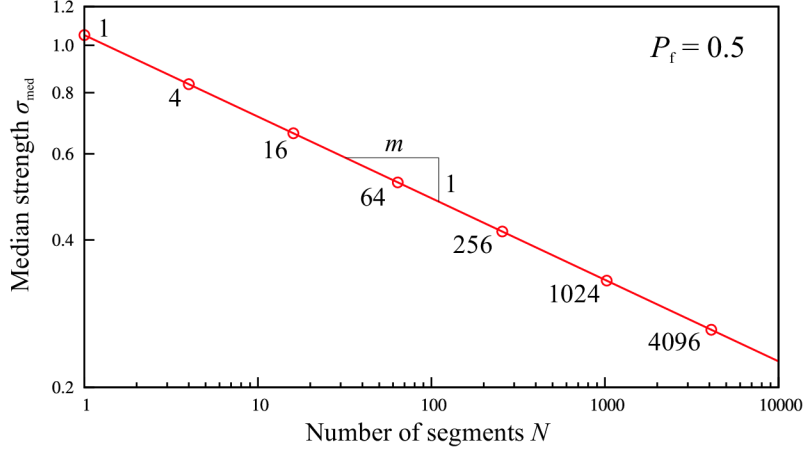


Fig. 1.12: Weibull median strength σ_{med} vs. number of segments N in double-logarithmic scale.

a length l_0 and corresponding parameter s_0 (scale parameter). As noted in [27], the length l_0 (or the representative volume V_r) should be better called “reference”. This is because in the classical Weibull theory, the choice of l_0 and the associated parameters m and s_0 is arbitrary and can be recalculated from a strength distribution of any length. The Weibull theory represents a typical self-similar behavior that lacks any characteristics dimensions. That is why the dependence of the median strength is a power law. Since σ (tensile strength) of the filament is positive and constant, Weibull integral can be rewritten as $-\ln(1 - P_f) = l/l_0 (\sigma/s_0)^m$. The expression for strength with certain failure probability P_f as a function of the length is obtained:

$$\sigma(l) = s_0 [-\ln(1 - P_f)]^{1/m} \left(\frac{l_0}{l}\right)^{1/m} \quad (1.29)$$

In the double-logarithmic scale of l vs. σ is this size-effect relation represented as a straight line with slope $-1/m$ passing the point $[l_0, s_0]$.

To obtain the mean strength, the function from Eq. 1.29 must be integrated over the range of P_f :

$$\bar{\sigma}(l) = s_0 \Gamma\left(1 + \frac{1}{m}\right) \left(\frac{l_0}{l}\right)^{1/m} \quad (1.30)$$

where Γ is the Gamma function.

The variation coefficient (COV) of the strength distribution has the direct correspondence with the shape parameter m with no dependency on the length and can be evaluated as:

$$\text{COV} = \sqrt{\frac{\Gamma(1 + 2/m)}{\Gamma^2(1 + 1/m)} - 1} \quad (1.31)$$

The reference length l_0 is an arbitrarily chosen length with no relation to the total length. To obtain the same size effect $\sigma(l)$ and the same failure probability P_f for differently chosen reference lengths (l_1) the scale parameter s has to be recalculated:

$$\frac{s_1}{s_0} = \left(\frac{l_1}{l_0}\right)^{-1/m} \quad (1.32)$$

The simulation process of finding the filament strength is following:

1. The filament is divided into $p = l/l_0$ nonoverlapping segments, each of which has the reference length l_0 with the random strength σ_j governed by the same probabilistic distribution.
2. The filament strength is equal to the minimum from strength of segments (the weakest-link model).
3. The mean filament response is estimated by repeating steps 1) and 2) n_{sim} -times (number of simulations) and calculating the average of strength minima.
4. This process is performed for different filament lengths to see the size effect.

By changing the reference length, it is possible to run the simulation even for extremely short filaments (the scale parameter has to be adjusted according to Eq. 1.32). The problem of the theory is that for reference length $l_1 \rightarrow 0$ the scale parameter $s_1 \rightarrow \infty$ as well as the filament strength $\sigma \rightarrow \infty$ – it means that theoretically, very short filaments would have unlimited strength (see Eq. 1.32). This fact is in contradiction with reality and another model has to be used. It is obvious that spatial distribution of strength along the filament can not be modeled with infinitesimally small reference length and has to be taken into account.

Spatial strength randomization using stationary random field

The spatial distribution of strength can be modeled in a form of random field, where the autocorrelation is included. Any used random field in following calculations is stationary homogeneous and ergodic with autocorrelation function:

$$R_{aa}(\Delta d) = \exp \left[- \left(\frac{|\Delta d|}{l_\rho} \right)^r \right] \quad (1.33)$$

where l_ρ is called *correlation length* and has a positive value. The shorter is the Δd distance, the stronger statistical correlation is applied. The function is called *squared exponential* or *bell-shaped* or *Gaussian autocorrelation function*, if the parameter $r = 2$.

More about advanced simulation techniques of random fields, their efficiency and accuracy can be found in [23, 25, 29, 28].

The process of numerical simulations is the same as in the case of IID randomization, however, the autocorrelation of strength is accounted for. As mentioned above, the final strength of the bundle is obviously the global minimum value of random strength process. To find this value, very dense field of discretization points has to be generated, which makes this method very demanding on computational equipment. This problem has been overcome by investigating the asymptotic behavior [27, 26].

If the spatial material autocorrelation is taken into account, the mean size effect follows the full line in Fig. 1.13: for filament lengths $l \gg l_\rho$ the mean strength tends to the classical Weibull theory with no autocorrelation influence (right asymptote), while for very short fibers $l \ll l_\rho$ is the strength limited by the length-independent mean value (left asymptote).

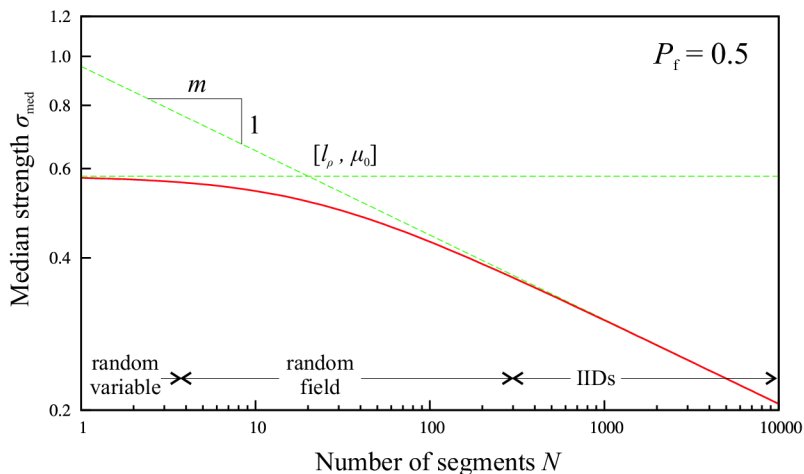


Fig. 1.13: Modified median Weibull strength with autocorrelation.

The transitional zone can be covered by a smooth function representing the transition between the left and right asymptotes intersecting in $[l_\rho, \mu_0]$. This approach makes the simulation process unnecessary [2, 4]. For this approach the filament is discretized and randomized according to chain model with IID segments of l_0 length. For filament lengths larger than $l > l_0$ (which is considered as known value for given material) is the mean strength obtained from Eq. 1.30 – classical Weibull size effect. The strength of shorter filaments $l < l_0$ has the value of μ_0 equal to the mean strength value of filament of zero length. This value is also the mean strength value for lengths $l = l_0$. The length l_0 is a coordinate of intersection of mentioned asymptotes. In this approximation mean strengths of extremely short and long fibers are described with good accuracy, while the values for filaments of $l \approx l_0$ are overestimated.

A better approximation of the transitional zone is found through modifying Eq. 1.29, where the length-dependent function $f(l)$ is introduced replacing $(l_0/l)^{1/m}$ member in:

$$\sigma(l) = s_0[-\ln(1 - P_f)]^{1/m} f(l) = s(l) [-\ln(1 - P_f)]^{1/m} \quad (1.34)$$

with $s(l) = s_0 f(l)$ implying that the length dependence of strength is associated with scale parameter s . If we rewrite the equation to express P_f we can see that the function $f(l)$ effects only the scale parameter s , while the shape parameter m remains unaffected: $\text{CDF} = P_f = 1 - \exp[-\sigma/(s_0 f(l))]^m$. The value of coefficient of variation stays unchanged as well, as it depends only on the m parameter, not on length l . The mean size effect can be formulated analogically to Eq. 1.30 as:

$$\bar{\sigma}(l) = s_0 \Gamma(1 + 1/m) f(l) = s(l) \Gamma(1 + 1/m) \quad (1.35)$$

Three zones of size effect are distinguished in Fig. 1.13 – the mean strength is simulated by: single random variable ($l/l_\rho \rightarrow 0$), autocorrelated random process ($l/l_\rho \approx 1$) and a set of IID random variables ($l/l_\rho \rightarrow \infty$).

The used length-dependent function $f(l)$ was found intuitively by asymptotic matching to interpolate between the two asymptotes within the transitional zone. Simulations performed in [27] showed that the numerically obtained mean of minima occurred in between two suggested equations:

$$f(l) = \left(\frac{1}{l_\rho} + \frac{l_\rho}{l_\rho + l} \right)^{-1/m} \quad \text{or} \quad (1.36)$$

$$f(l) = \left(\frac{l_\rho}{l_\rho + l} \right)^{1/m} \quad (1.37)$$

Some researches believe that another possible method how to mimic the effect of the spatial variability of strength is by averaging the stresses between neighboring material points, which introduces the dependence between sampling points of IID strength randomization. This model is called *non-local Weibull integral* [5, 1]. However, in the case of filament tensile loading it is impossible to use this model, as the stress level is equal for all material points of chain and no averaging of stress is meaningful.

1.4.2 Random strength along filaments within the bundle

Having investigated the single filament behavior, it can be proceeded to the evaluation of the total bundle response. Both of formerly mentioned models (simulation

of IID random variables and the random process method) were used to randomize the set of n filaments in parallel arrangement. In the following definitions, the distribution of normalized bundle strength $Q_n^* = \sup [T(e)/n]$ is considered.

Daniel's numerical recursion

The classical model of a bundle was formulated by Daniels [9]. The bundle composes of a set of n independent parallel linear-brittle fibers equally sharing the tensile loading. All the filaments $i \in \langle 1, \dots, n \rangle$ also share the identical strength function distribution $F_X(x) = F_{(i)}(x) = P_{(i)}(X \leq x)$ and all the other parameters are considered constant. The maximum filament tensile strength $Q_{(i)}(\alpha) = X_{(i)} = A\sigma_{(i)}(\alpha)$ is randomized independently for each filament (α denotes the random nature of quantity). The set of $Q_{(i)}$ of the bundle is ordered in an ascending manner ($Q_{(i)} \leq Q_{(i+1)}$) and the marginal distribution function of $Q_{(i)}$ is obtained as $f_X(x)$ (PDF) and $F_X(x)$ (CDF) [14]:

$$f_{(i)}(x) = i \binom{n}{i} [F_X(x)]^{i-1} [1 - F_X(x)]^{n-i} f_X(x) \quad (1.38)$$

And the bundle maximum tensile force (see Fig. 1.14):

$$Q_n^* = \max_{1 \leq i \leq n} \left(Q_i \frac{n-i+1}{n} \right) \quad (1.39)$$

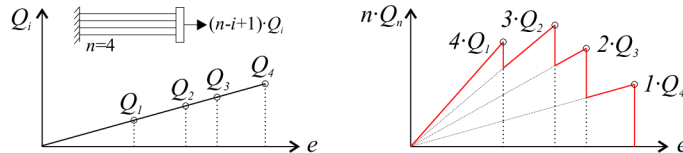


Fig. 1.14: Estimation of bundle maximum tensile force.

The yarn load is expressed through the load per filament: $Q_n = T(e)/n$. Since we are interested in the bundle strength, we look for the maximum force Q_n^* and its distribution function G_n . Assuming that the filament strength is independent and identically distributed random variable with the known distribution function F_X , the CDF distribution of the maximum tensile filament force is [9]:

$$G_n(x) = P(Q_n^* \leq x) = \sum_{i=1}^n (-1)^{i+1} \binom{n}{i} [F_X(x)]^i G_{n-i} \left(\frac{nx}{n-i} \right) \quad (1.40)$$

which is a recursive function where the lowest terms are defined as $G_0(x) \equiv 1$ and $G_1(x) = F_X(x)$ (CDF of a bundle with one filament is equal to CDF of filament strength).

The main disadvantage of this analytical solution is that Daniels' recursive formula is extremely computationally demanding and with the growing number of filaments occurring in practise exceeds common computational facilities. Then the only possibility how to map the bundle size effect are numerical stochastic simulations of Monte Carlo type. The results of both methods are perfectly matching as shown in [27]: the mean bundle strength drops with increasing number of filaments and the response in its shape is getting closer to the asymptotic load-strain curve (for $n \rightarrow \infty$). The bundle strength distribution asymptotically changes from Weibull to Gaussian for increasing number of filaments n .

Fig. 1.15 shows the response of one bundle with three different numbers of filaments. The overall bundle response T_ξ is given as simple summation of filament strength contributions q_ξ (superposition rule). The analytic curve $M_\xi = n \cdot \mu_\xi$ for $n \rightarrow \infty$ and the response of the ideal filament q_0 (with strength equal to the mean value) are plotted for comparison.

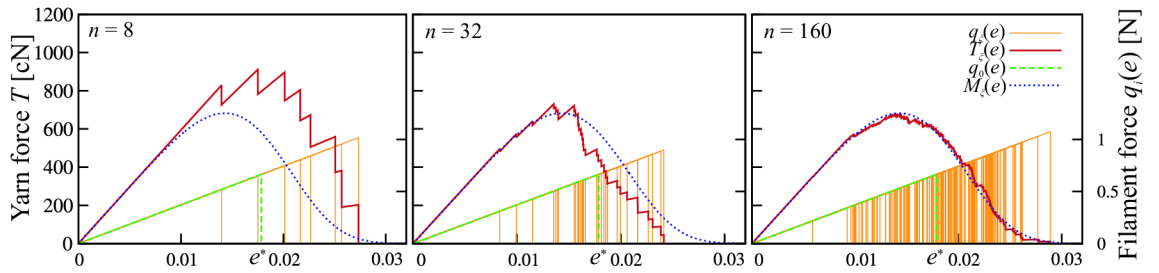


Fig. 1.15: Load-strain curve T_ξ of a bundle with n filaments together with curves of filaments q_0 and q_ξ and their mean curve M_ξ (bundle).

The numerical solution of the bundle response M_ξ was run for $n_{\text{sim}} = 100$ -times for four different $n = 1, 8, 31, 160$ of filaments. The obtained peak load values were statistically processed and the mean strength value with the corresponding std are marked in Fig. 1.16 with a red circle. The mean value decreases for increasing number of filaments as well as the value of std and the response becomes less scattered and gets closer to the asymptotic curve μ_ξ .

Asymptotic bundle response

The fact that with $n \rightarrow \infty$ the strength distribution converges to the normal distribution is used to verify the asymptotic behavior of stochastic simulations (assuming filament strength as IID random variable). According to the central limit theorem for positive constants μ_σ^* (mean value) and γ_σ^* (standard deviation) is: $(\sqrt{n}(Q_n^* - \mu_\sigma^*)/\gamma_\sigma^*)$ tends to a normal random variable with mean value equal to 0 and standard deviation equal to 1 (standard normal distribution). The approximation of the bundle strength for large n reads [9]:

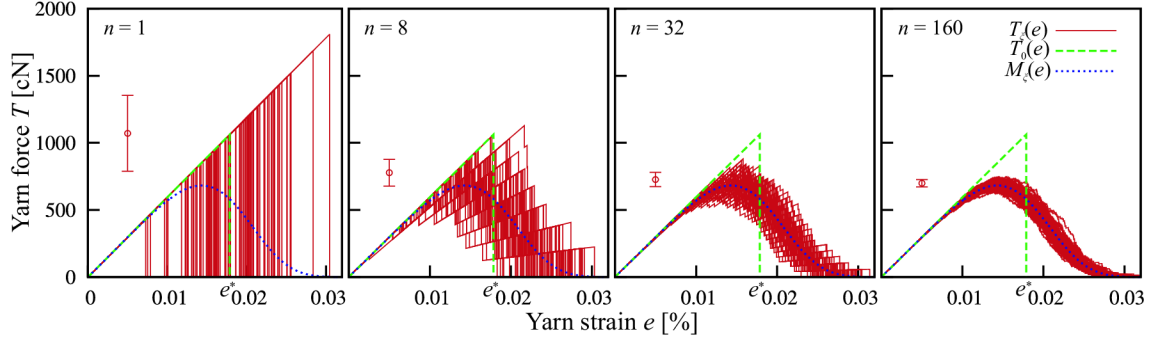


Fig. 1.16: Load-strain curves of bundles M_ξ with different number of filaments n as a result of Monte Carlo simulations ($n_{\text{sim}} = 100$). Mean values of the bundle strength \pm std are depicted, as well as the asymptotic response $M_\xi(n \rightarrow \infty)$.

$$G_n(x) = P(Q_n^* \leq x) \approx \Phi\left(\frac{x - \mu_\sigma^*}{\gamma_\sigma^*} \sqrt{n}\right) \quad (1.41)$$

with Φ symbolizing the normal cumulative distribution with the following parameters:

$$\begin{aligned} \text{mean value} & \quad \mu_\sigma^* = E[Q_n^*] = e^* [1 - F(e^*)] \\ \text{variance} & \quad (\gamma_\sigma^*)^2/n = D[Q_n^*] = (e^*)^2 F(e^*) [1 - F(e^*)] \end{aligned}$$

The assumption is valid only under the following conditions: the value e^* maximizes the function $\mu(e) = e[1 - F(e)]$ and is unique and positive; $\lim_{e \rightarrow \infty} \mu(e) = 0$, then $\mu_\sigma^* = \mu(e^*) = \sup[\mu(e)]$; $e \geq 0$ and the yarn stiffness is $EA = 1$.

The problem of random filament limit strength σ can be transformed into the problem of filament random breaking strain ξ [18], as $\sigma = E\xi$ (for constant stiffness $E = \text{const}$). The linear relation between these two quantities implies that: $\mu(e) = \mu_\sigma(e) = \mu_\xi(e)$, which is the normalized asymptotic mean bundle load-strain function ($n \rightarrow \infty$):

$$\begin{aligned} \mu_\xi(e) &= \int_0^\infty q(e, \xi) f_\xi(\xi) d\xi = EAe \int_0^\infty H(\xi - e) f_\xi(\xi) d\xi = EAe \int_{\xi=e}^\infty f_\xi(\xi) d\xi = \\ &= EAe [1 - F_\xi(e)] \end{aligned} \quad (1.42)$$

where the constitutive law is given by Eq. 1.3 and $f_\xi(e)$, $F_\xi(e)$ is PDF, resp. CDF of filament breaking strain ξ .

If the random strain is considered to follow Weibull distribution with parameters s (scale) and m (shape), then CDF of ξ is:

$$\begin{aligned} F_\xi(e; s, m) &= 1 - \exp[-(e/s)^m] \\ \mu_\sigma(e) &= EAe \exp[-(e/s)^m] \end{aligned} \quad (1.43)$$

The strain corresponding to the peak load e^* can be found by derivation of the stress function. By substituting this value into stress equation, the maximum load μ^* is found, as well as the standard deviation γ^* .

$$\begin{aligned} \frac{d\mu_\sigma(e)}{de} = 0 &\quad \rightarrow \quad e^* = m^{-1/m} s \\ \mu_\sigma^* = \mu(e^*) &= EA m^{-1/m} s \cdot \exp(-m^{-1}) \\ \gamma_\sigma^* &= EA s m^{-1/m} \sqrt{\exp(-m^{-1}) [1 - \exp(-m^{-1})]} \end{aligned} \quad (1.44)$$

Concerning the asymptotic behavior, the transition to normal distribution is valid for the central part of the distribution (close to the mean value). The left tail has to keep the Weibull distribution, as the minimum strength cannot be less than zero. However, the importance of the left tail can be neglected as the distance from the central part of the distribution measured in multiples of the standard deviation is large with large n .

Size effect of a bundle with variable number of filaments

As observed in simulations in [27], the shape of mean size effect curve – MSEC (in double logarithmic scale of yarn strength vs. length) remains the same even for growing number of filaments n in the bundle. The curve is just shifted downwards (the mean strength of $l \rightarrow 0$ bundle decreases), but the slope of right asymptote (given by parameter m), as well as the intersection point of asymptotes (with x -coordinate equal to correlation length l_ρ) is kept. The drop-trend of bundle strength efficiency ($\mu_{\sigma,n}^*/\mu_{\sigma,0}^*$) with growing number of n is significant mainly for $n < 160$; with higher number of filaments the mean strength ratio stabilizes on a certain value (Fig. 1.17 top left; figure adopted from [27]).

The bundle strength as a function of its length is according to Eq. 1.34 associated with the scale parameter of Weibull distribution $s_\xi(l) = s_\xi f(l)$, subsequently $F_\xi(e; s_\xi(l), m_\xi)$ (Eq. 1.43). To obtain the mean load-strain equation, the length-dependent distribution of breaking strain is substituted into Eq. 1.42:

$$\mu_\xi(e, l) = EAe \exp \left[- \left(\frac{e}{s_\xi f(l)} \right)^m \right] \quad (1.45)$$

The peak load $\mu_\xi^*(e, l)$ is found analogically to previous section as load corresponding to the stationary point e^* , as well as the mean size effect function for maximum load:

$$\begin{aligned} \frac{d\mu_\xi(e, l)}{de} = 0 &\quad \rightarrow \quad e^*(l) = [f(l) m]^{-1/m} s_\xi \\ \mu_\xi^*(l) = \mu_\xi(e^*, l) &= EA m^{-1/m} s_\xi \exp(-m^{-1}) f(l) = \mu_\sigma^* f(l) \end{aligned} \quad (1.46)$$

The analytical solution or numerical simulations can be used to evaluate both effects separately (number of filaments and length), or they can be composed together and the combined size effect can be plotted as a 3D surface (Fig. 1.17 right). For higher number of filaments ($n \rightarrow \infty$) the change of z -coordinate becomes constant and the surface can be expressed as a single curve – the mean strength is asymptotically independent of the number of parallel filaments.

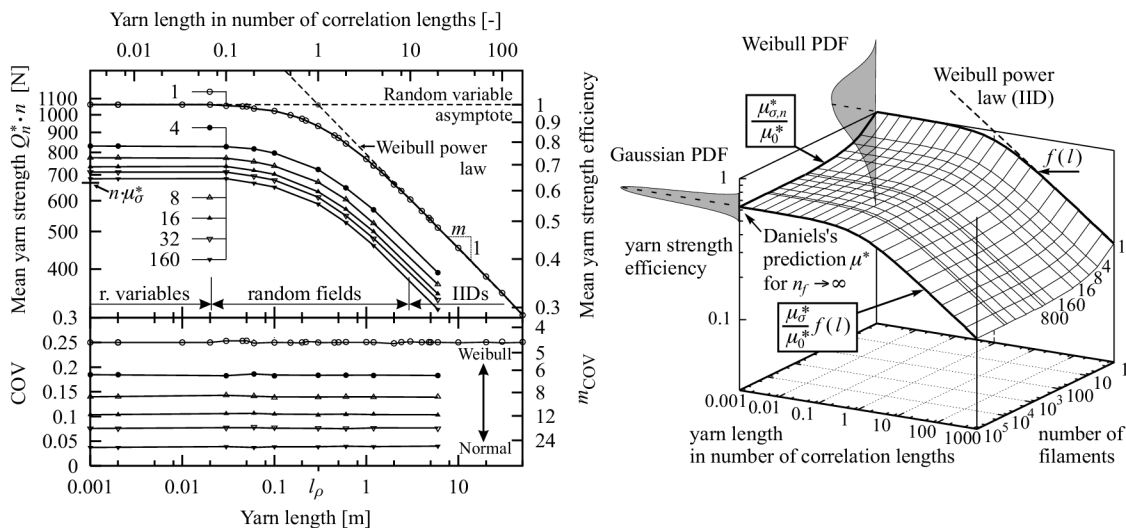


Fig. 1.17: Left top: mean size effect curves for different number of filaments within the bundle, curves for $n > 160$ overlap. Left bottom: Values of COV and effective Weibull shape modulus m_{COV} . Right: Yarn efficiency for varying length and number of filaments. Figure adopted from [27].

The value of COV is independent of the yarn length (\rightarrow the inclination of size effect curve in double logarithmic scale) – even for the autocorrelated model, however, the value changes for different number of filaments within the bundle. (COV of a bundle with certain n filaments is constant for variation of bundle length, but is different from the COV of a bundle with different n .) This is caused by the reduction of std with growing n – the rate of reduction is $1/\sqrt{n}$. From this, new COV (new slope of the size effect curve) could be evaluated with value $m_{\text{COV}} > m$ (less steep slope of the size effect curve) – Fig. 1.17 left bottom. The influence of changing COV with varying n is not covered by the model.

1.4.3 Interaction of random stiffness and strength along the bundle

Another random variable of the bundle model can be the Young's modulus of elasticity E , that is responsible for the filament stiffness.

Random E -modulus and strength along a single filament

The fluctuation of $E(x)$ modulus over the length of the filaments is modeled as autocorrelated random process. The effective modulus of i -th filament E_i can be calculated from a set of p random values (each assigned to one material point of the filament) by static condensation of all E_j (for springs in series coupling):

$$E_i = p \left(\sum_{j=1}^p E_{i,j}^{-1} \right)^{-1} \quad (1.47)$$

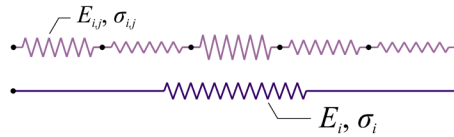


Fig. 1.18: Effective material stiffness E_i and filament strength over the length.

For very short filaments ($l \ll l_\rho$) the random process has almost constant value over the length and the E modulus is given by a single random variable with distribution function $G_E(E)$. On the other hand for very long filaments ($l \gg l_\rho$) the parameter scatter gets insignificant and the effective stiffness converges to the limit value E_∞ with low standard deviation.

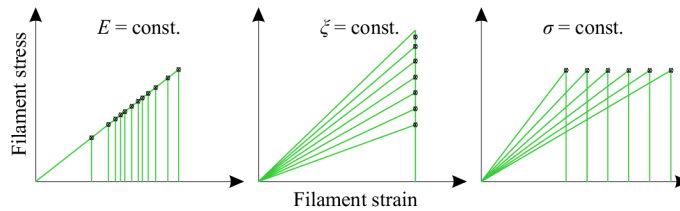


Fig. 1.19: Stress-strain diagrams of constitutive law each time with one quantity constant.

The point of break is given not only by elasticity modulus E , but all three quantities of the constitutive law $\sigma = E \cdot \xi$ (Hook's law) interact. The randomization of the constitutive law can be visualized for three limiting cases – each for one variable kept constant – Fig. 1.19. The resulting stress-strain curves show the one-parameter randomization. This concept does not correspond to real situation, as any material parameter is not ever a constant value. The two-parameters' randomization is shown in Fig. 1.20 for different correlation coefficients between distributions of strength σ and E -modulus. Uncorrelated, positively and negatively correlated cases are depicted. Unfortunately there is no significant evidence for any of these cases. Due to this fact the $\sigma - E$ relation is for further computations considered uncorrelated.

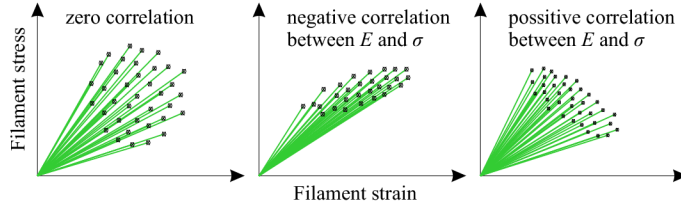


Fig. 1.20: Two-parameter randomization by E and σ and their correlation.

One-parameter randomization of the constitutive law along the bundle

Numerical simulations of the influence of varying parameter E and σ were run in order to map the bundle response. Random parameters were simulated by one-dimensional autocorrelated random field according to Eq. 1.33 for three different autocorrelation lengths, resp. l/l_ρ ratio. These varying parameters were applied to a bundle model with 16 filaments (illustrative example).

To simulate the bundle behavior, 16-variate Gaussian random process was generated (16 mutually uncorrelated random fields) in p material points of discretization for three autocorrelation lengths l_ρ . Fifty realizations of one random process (representing n_{sim} simulations of one filament) are plotted in the first row of Fig. 1.21 (figure adopted from [27]). Left scale shows the values of random strength, while the right one is for E -modulus.

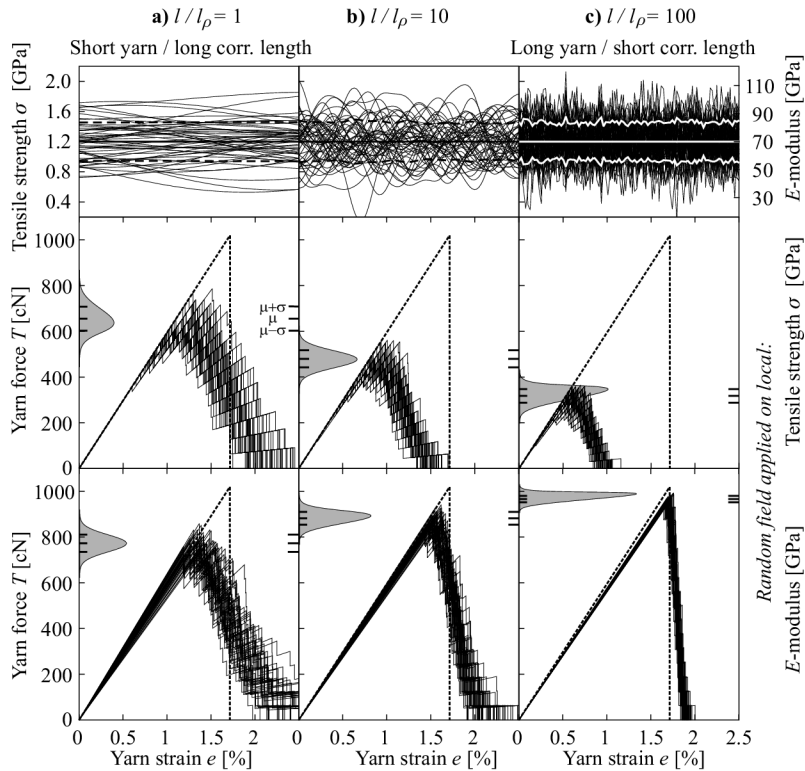


Fig. 1.21: Influence of different correlation length on the bundle response for different randomized parameters. Figure adopted from [27].

The second row of Fig. 1.21 shows the bundle response for varying tensile strength σ . The probability density function of the peak values together with the marked mean value and standard deviation are situated on the left y -axis of the graph. It can be observed that with increasing filament length l the tensile strength is reduced and the response become less scattered (reduction of std).

The same effect of scatter reduction can be seen in the simulations of E -fluctuation (the third row of Fig. 1.21). The std gets reduced with increasing length, but oppositely to the random σ simulations – the mean value increases for longer lengths (opposite size effect). The reason to this phenomenon is that the filaments do not reach their peak load at the same time, which is more significant for short specimens.

The stiffness variation of the very short specimens $l/l_p \rightarrow 0$ was studied on the model with condensed stiffness $E_{i,j} = E_{(i)}$ – one random value for each filament. Numerical solution was again used for a bundle with 16 filaments, the random E follows the Weibull distribution function $G_E(E)$ with parameters specified in Tab. 1.2. Analytical solution for infinite $n \rightarrow \infty$ was obtained from Eq. 1.10 for two different cases: a) constant tensile strength of filaments $\bar{\sigma}$ and b) constant breaking strain $\bar{\xi}$. The equation is adjusted as:

$$\begin{aligned} \mu_{E|\bar{\sigma}}(e) &= Ae \int_0^{\infty} EH (\bar{\sigma}/E - e) dG_E(E) \\ \mu_{E|\bar{\xi}}(e) &= AeH (\bar{\xi} - e) \int_0^{\infty} E dG_E(E) = \bar{E}AeH (\bar{\xi} - e) \end{aligned} \quad (1.48)$$

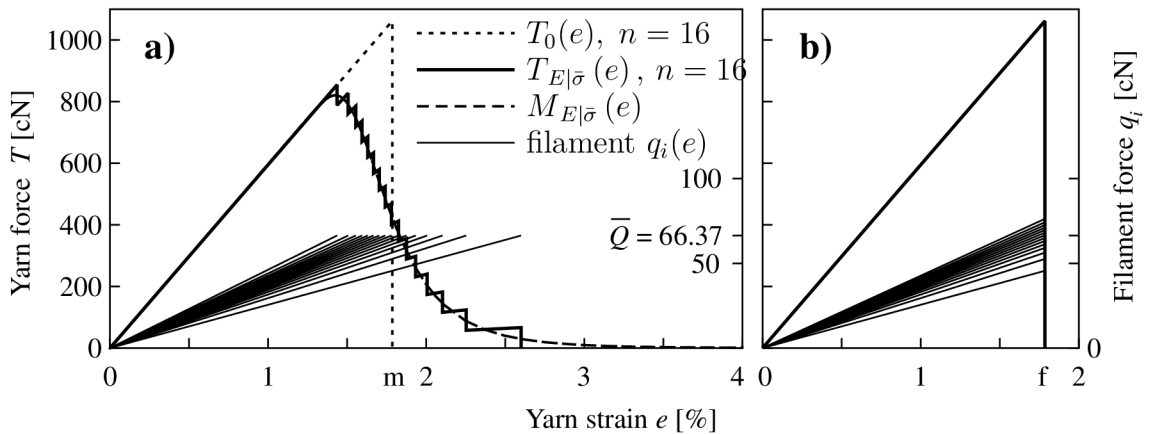


Fig. 1.22: The bundle response for varying E -modulus with Weibull distribution. Left: case a) with constant $\bar{\sigma}$; case b) with constant $\bar{\xi}$. Figure adopted from [27].

The case b) is equivalent to the response of the bundle with varying cross-section area. The mean bundle response is equal to the response of a perfect bundle $M_{E|\bar{\xi}}(e) = T_0(e)$.

Two-parameter randomization of the constitutive law along the bundle

In the real bundle the randomness of E -modulus and the randomness of σ (or ξ) act simultaneously. To describe this complex behavior we can simulate the response by numerical methods. Both random fields are uncorrelated (see Fig. 1.20 left) and filaments don't interact. The analytical solution for the very short and very long bundles (asymptotic behavior) can be obtained for $n \rightarrow \infty$. The solution for very short bundles, where the random field reduces into random variable with given CDF, can be integrated:

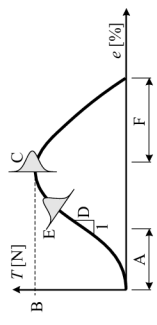
$$\mu_{\sigma,E}(e) = \int_0^{\infty} \int_0^{\infty} q(e, \sigma, E) dG_E(E) dG_{\sigma}(\sigma) = Ae \int_0^{\infty} \int_0^{\infty} H\left(\frac{\sigma}{E} - e\right) E DG_E(E) dG_{\sigma}(\sigma) \quad (1.49)$$

For very long bundles the variation of E can be considered as homogenized parameter over the filament length, the breaking stress can be substituted by the breaking strain (see Fig. 1.19 left) and the mean response is given by Eq. 1.42. If the ξ distribution is given by Weibull equation, then: $G_{\xi}(\xi) = F_X(\xi; s_{\xi}, m_{\xi})$, $\xi = \sigma/E_{\infty}$, and then it can be written as $\mu_{\xi,E}(e) = AE_{\infty}e \exp[-(e/s_{\xi})^{m_{\xi}}]$.

1.5 Conclusion

The computational model will be compared with results obtained by physical experiment on multi-filament glass yarns of different lengths. By knowing the force-displacement diagrams from tensile tests of statistically significant set of samples, it could be possible to identify the model parameters and their distributions, their interaction and their influence on the bundle response with the increasing length, so that the numerical model could fit the real yarn behavior.

Tab. 1.3: Influence of randomness in material parameters on the measured load-displacement diagrams with increasing length. With the increasing length the characteristics increases(+)/decreases(-)/stagnates(.). Adopted from [27].



	<i>Fixed distribution of:</i>	l_{λ}	A	l_{θ}	$m, s_{\xi}, f(l)$	E_j
A(l):	evolution of initial stiffness	.	.	-	.	.
B(l):	mean peak load	+	.	+	-	+
C(l):	scatter of peak load	.	.	-	-	-
D(l):	mean stiffness	+	.	+	.	.
E(l):	scatter of stiffness	-	.	-	.	-
F(l):	post-peak range	-	.	-	-	-

2 EXPERIMENT

2.1 Introduction

The main scope of this master thesis was to perform an experiment with a high number of tensile tests of glass-filament yarns. The task was to observe and subsequently to describe their behavior with special focus on the statistical size effect. To obtain statistically significant results, a high number of experiment realizations was performed.

The shape of samples and the production technology was inspired by the experiments run previously at RWTH Aachen University ([6] and other) with regards to the equipment of and possibilities of experimental laboratory of the Department of Structural Mechanics, Faculty of Civil Engineering, Brno University of Technology.

2.2 Experiment preparations

The material selected for the tensile tests was the AR-glass yarn produced by Saint Gobain Vetrotex with brand name Cem-FIL Direktroving LTR 5325, 2400 tex (Fig. 2.1). The fineness of the yarn is represented by the “tex” unit describing the weight of the yarn in grams per kilometer. The basic characteristics of the yarn are in the Tab. 2.1:

Tab. 2.1: Characteristics of tested AR-glass yarns.

<i>nominal fineness</i>	2400 tex (=g · km ⁻¹)
<i>glass density</i>	$\gamma = 2.678 \text{ g} \cdot \text{cm}^{-3}$
<i>total yarn area</i>	$A = \text{tex}/(1000 \cdot \gamma) = 0.8962 \text{ mm}^2$
<i>number of filaments</i>	$n \approx 1600$
<i>filament area</i>	$A_1 = A/n \approx 560.12 \text{ }\mu\text{m}^2$
<i>filament diameter</i>	$d_1 = (4A_1/\pi)^{1/2} \approx 26.7 \text{ }\mu\text{m}$

Specimen series design

The experiment was focused on the observation of effect of the size (resp. length) on the yarn strength. Consequently, a wide range of yarn lengths was desired with emphasis on production of the longest possible specimen length, so that the behavior in this region can be mapped. Laboratory equipment enabled the maximum free length of the specimen 740 mm (the length of the jaws (holders), the anchoring blocks plus the expected elongation length has to be taken into account). The



Fig. 2.1: The tested AR-glass yarn on a bobbin.

shortest length of the specimen was due to technology reasons set 10 mm. Between these two values of maximum and minimum length, six length groups were suggested with equal distribution of their logarithms. As the size effect curve is visualized in the double-logarithmic scale, the specimens length groups were chosen so that the obtained peak-loads would be captured using equidistant spacing – see Fig. 2.2.

<i>group nr.</i>	1	2	3	4	5	6
<i>nominal length L_{nom}</i>	1 cm	2.5 cm	6 cm	13 cm	31 cm	74 cm

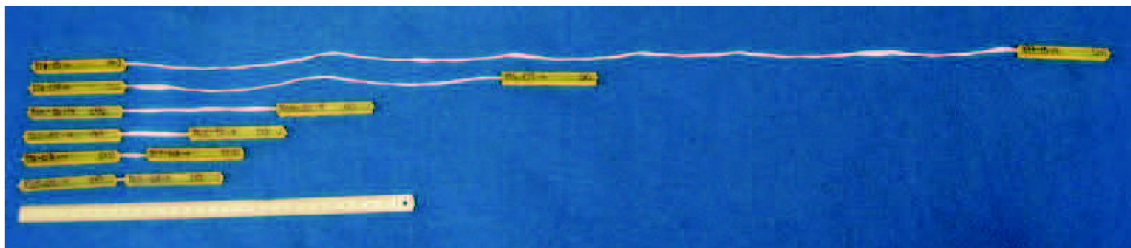


Fig. 2.2: Specimens' length groups.

The minimum number of samples in each of the length groups was, with regards to statistical significance, taken as 30 pieces.

The most problematic part of tensile testing was to deal with the anchoring of glass yarns into the machine. Basically, there are two ways how to create bundle supports: endings can be either directly coiled up on a cylinder or poured into anchoring blocks and clamped (Fig. 2.3). The former one is effortless but with the problem how to determine the real free length of the yarn, as the tension stress is gradually transmitted from the cylindrical support to the yarn. On the contrary the

latter form of support has the free length relatively clear, but it is very laborious and time-consuming to create the specimens. (Direct clamping of yarns is not possible, as the yarn is made of fragile material that would crush at the support point due to lateral compression in clamps.)

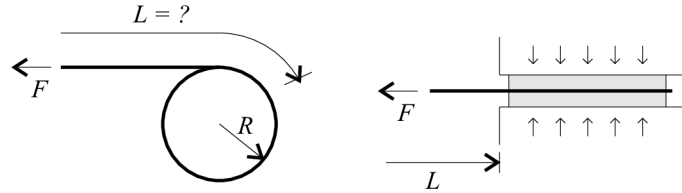


Fig. 2.3: Anchoring types: yarn coiled up (left) and poured in anchoring block (right).

As the testing machine is equipped with self-locking holders, yarn endings were poured into 75 mm long anchoring blocks made of epoxy. Special silicon forms had to be made for the purpose of pouring these epoxy blocks.

Specimen manufacturing

Production process of epoxy anchoring blocks was the most time-demanding part. Moreover, before epoxy pouring itself, a steel mould for production of silicon forms had to be set up.

This steel mould consisted of 4 bounding members (2 steel bars $120 \times 14 \times 14 \text{ mm}^3$ and 2 steel bars $70 \times 14 \times 14 \text{ mm}^3$), 5 steel blocks ($75 \times 8 \times 8 \text{ mm}^3$) substituting five future epoxy blocks, the chipboard base and 8 screws enabling the mould to be dismantled – see Fig. 2.4. To localize the future position of the yarn, short mini-rods were put into holes drilled through the shorter side steel members (trenching on to the silicone form in short length of about 1 mm). (The initial intention why these mini-rods were introduced was the protection of the furrow cut in silicone form for placing the glass yarn. The round ending of the furrow would provide the protection against tear during the repeated shuck of the epoxy resins. This idea had to be rejected because the round hole caused the outflow of the epoxy from the form to the yarn. Due to this reason the rods were inserted to the mould in a short length from the outside.) Once the steel mould was manufactured, preparation of the silicone form could be performed – see Fig. 2.5.

The used silicone was a two-component matter produced by Alpina company with commercial name Koraform 50 (Fig. 2.6 left). The components are mixed in a weight ratio 10:1 (comp. A (beige color) : comp. B (colorless)); to produce one form $80+8 \text{ g}$ of silicone was used. Both components are very dense liquids and the mixing process had to be slow, so that no voids and bubbles were developed. The setting time was 24 hours. After that time the mini-rods were pulled out, steel mould

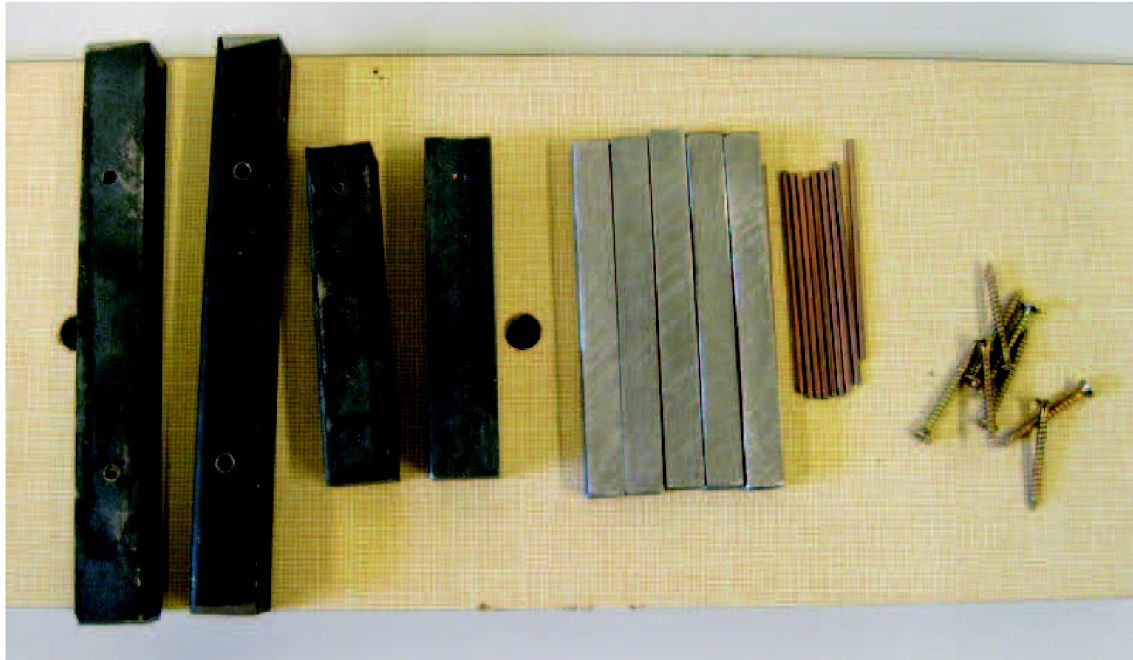


Fig. 2.4: A deassembled steel mould.



Fig. 2.5: A steel mould for the production of silicone forms.

was dismantled and the hardened silicone form was carefully taken out. Edges of the form were neaten by scissors and the furrows for placing the yarn were cut by knife. A finished silicone form is in Fig. 2.7. The total number of poured silicone forms was 21. Manufacturing of one silicone form takes about one hour.

Finished silicone forms were placed in special holder-tracks that enabled keeping the required free length of the samples – Fig. 2.8. Five yarns of the same length were stretched between two silicone forms and the yarn ends were poured into epoxy – Fig. 2.6 right – product of bacuplast Feserverbundtechnik GmbH with commercial name EP 210-2 (resin, colorless) and EPH 412-2 (hardener, orange). The weight mixing ratio of epoxy resin was 10:4 (comp. A (resin) : comp. B. (hardener)), to pour off anchoring blocks for 5 specimens, approx. 65 g(= 46.4 + 18.6) of epoxy was



Fig. 2.6: Silicone (left) and epoxide (right).

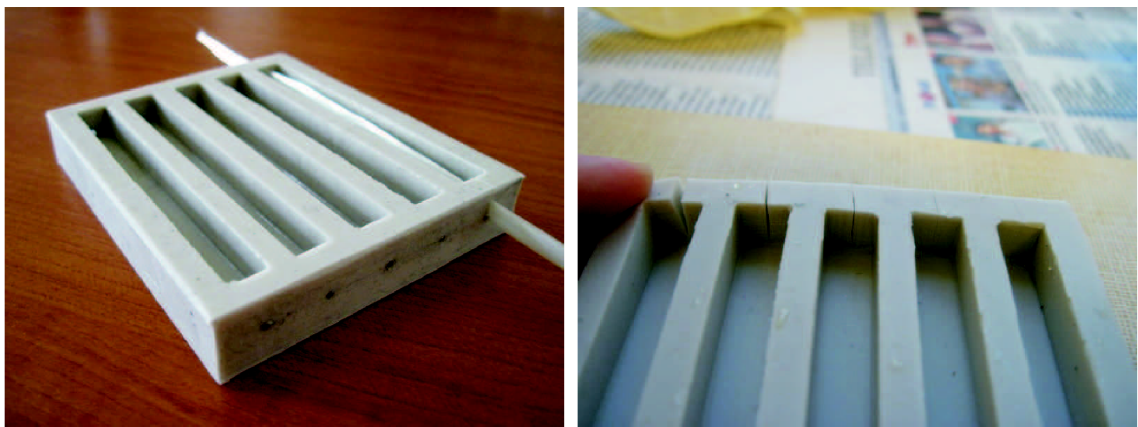


Fig. 2.7: A silicone form.

needed. The hardening time of resin was 24 hours. After one day specimens were shucked out, properly labeled and edges were ground down.

The production of the experiment samples was extremely time-consuming and run over several weeks (Tab. 2.2). The most problematic part was to deal with the problem of epoxide rising into the yarn starting from the epoxide blocks. Without any treatment the epoxide rose even several centimeters along the yarn. When the form ends were greased, the length had just slightly reduced. The problem was finally solved by strong greasing of the yarn by vaseline: in the width of 5 mm at both yarn edges (the part which goes through the sides of the form) was the yarn perfectly greased through the whole cross-section. With this treatment, the capillary effect was prevented and the length of penetration of epoxide into the free length of the yarn was reduced to zero. It should be noted, that this procedure necessitates a precise work, so that the desired free length is kept: the specimen is not either shorter due to the the capillarity of the epoxide, nor longer due to the opposite effect, when the vaseline rises through the yarn and the epoxide cannot penetrate through the whole cross-section of the anchoring block.



Fig. 2.8: Special tracks for specimen preparation.

Tab. 2.2: Average time spent on sample testing.

<i>Time consumed on preparation of 1 specimen</i>	~ 60 min
<i>Test time of 1 specimen</i>	~ 10 min

The total number of tested samples was 317 pieces. An overview of the particular sample series (label Pxx) according to different days of production is presented in Tab. 2.3, where also the numbers of tested samples with different nominal lengths are displayed at the bottom. There are samples of more length groups in most of the series, so that the possible deviation of created samples could not affect just one length group. The final number of samples used for experiment evaluation was reduced because of significant imperfections caused during the production process (some samples were discarded from the statistics). All the specimens were stored together in the same conditions.

2.3 Test setup

Equipment

Tensile tests were performed using the testing machine Z100 Zwick/Roell Gruppe equipped by two load cells measuring the force (20 kN and 2.5 kN) and mechanical

Tab. 2.3: Number of tested specimens.

Series nr.	Date of production	1 cm	2.5 cm	6 cm	13 cm	31 cm	74 cm	sum
P01	11.8.2011						5	5
P02	25.8.2011	5			5	5	5	20
P03	13.9.2011	5	5	5	5	5	5	30
P04	14.9.2011	4	5	5	10	5	5	34
P05	15.9.2011	5	5	9	5	5	5	34
P06	20.9.2011	5	5	5	5	4	5	29
P07	21.9.2011		5			5		10
P08	22.9.2011	5	4		5		5	19
P09	23.9.2011	4		5	2	10	5	26
P10	24.9.2011		5	5	5			15
P11	29.9.2011	5		4			5	14
P12	30.9.2011		5	5	5			15
P13	5.10.2011	5				5	5	15
P14	20.10.2011	5	5	5				15
P15	21.10.2011						5	5
P16	22.10.2011				5	4		9
P17	24.10.2011	5	4				5	14
P18	25.10.2011				3	5		8
<i>Number of specimens</i>		53	48	48	55	53	60	317

tensile clamps (jaws) of combined type (self-locking with pre-stressing screws) – Fig. A.3. The displacement was measured at the top edge of the upper jaw by deflection extensometer (Fig. 2.9). The test was controlled by the machine software.

Testing schedule

The testing of specimens was performed in nine days. To avoid some effects that could influence the results and degrade the experiment statistics, mixed sets of samples were tested in 9 different days. Samples of different length and different age (from different series) were present in each set. Also the local conditions in the laboratory (temperature and relative humidity) were recorded during the testing period and are a part of the testing protocol (contracted version in Tab. B.2).

Testing methodology

Before the tests were started, all the connections between the machine parts (parts connecting the machine cross-head and the sample) were tighten: steel piece was

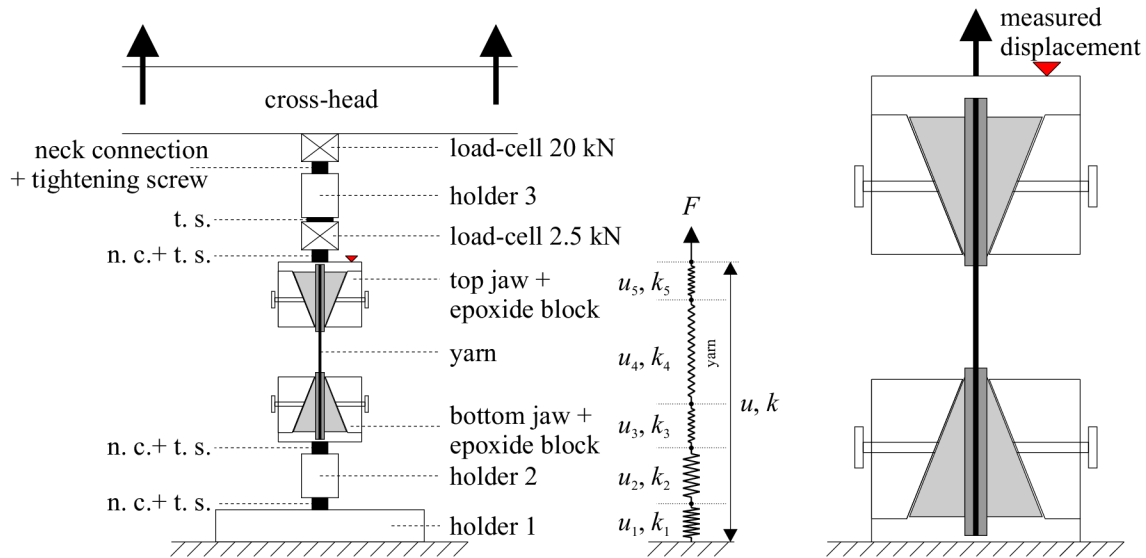


Fig. 2.9: Left: Scheme of the loading device parts with a sketch of series coupling of deformable components. Right: The point of measured vertical displacement.

inserted into jaws and loaded by tension force 2000 N. All the connection screws were tightened by hand and the steel piece was unloaded and removed. Such a procedure prestresses all the connections which eliminates the portion of spurious deformations.

The test program was created for each length group of samples. Parameters of the program were set according to Tab. 2.4. Samples were loaded by displacement-increments of the cross-head of the constant rate and the reaction force was measured by the load-cell. The test speed was chosen to correspond to 1.1 % elongation of the nominal length per minute. After the measured force dropped by 5 % of the current maximum, the test speed switched to a lower value, so that the unloading path was recorded and the failure was not catastrophic (this was important especially for short lengths).

Tab. 2.4: Test programme setup.

<i>Length group nr.</i>		1	2	3	4	5	6
<i>start position</i>	[mm]	10.5	25	60	130	310	740
<i>pre-load</i>	[N]	5	5	5	5	5	5
<i>test speed</i>	[mm/min]	0.11	0.28	0.66	1.43	3.41	8.14
<i>test speed after 5% reduction of F_{\max}</i>	[mm/min]	0.05	0.15	0.40	1.20	2.00	8.14

Each sample was investigated before the tensile test: the length of the sample was measured by slide caliper, each epoxy block was checked (the length of epoxide that penetrated into the free length was eventually measured and recorded) and other additional features were noted (unequal waviness, more filaments broken before

the test,...). The test was started by setting the force to zero. The sample was inserted into the jaws in the vertical position and transverse screws on the jaws were tighten by hand. The prescribed pre-load was applied (5 N) and the program called for clamping the extensometer. After that the sample started to be loaded with given test speed (which was reduced after the peak load) until the failure. The extensometer was unclamped, the broken sample removed and the machine returned the cross-head into its initial position.

2.4 Measured results

Data (displacement, force, time,...) were continuously recorded and saved during the test. Force-displacement curves obtained from experiment are plotted in Fig. 2.10. Different colors represent different length groups of samples. “Raw” curves plotted in the figure are obtained directly from experimental device without any modification. Examples of samples before and after the tensile test is in Fig. 2.12. Due to imperfect stiffness of the machine, the measured curves (displacements) have to be edited. The following chapter deals with the test curves adjustment.

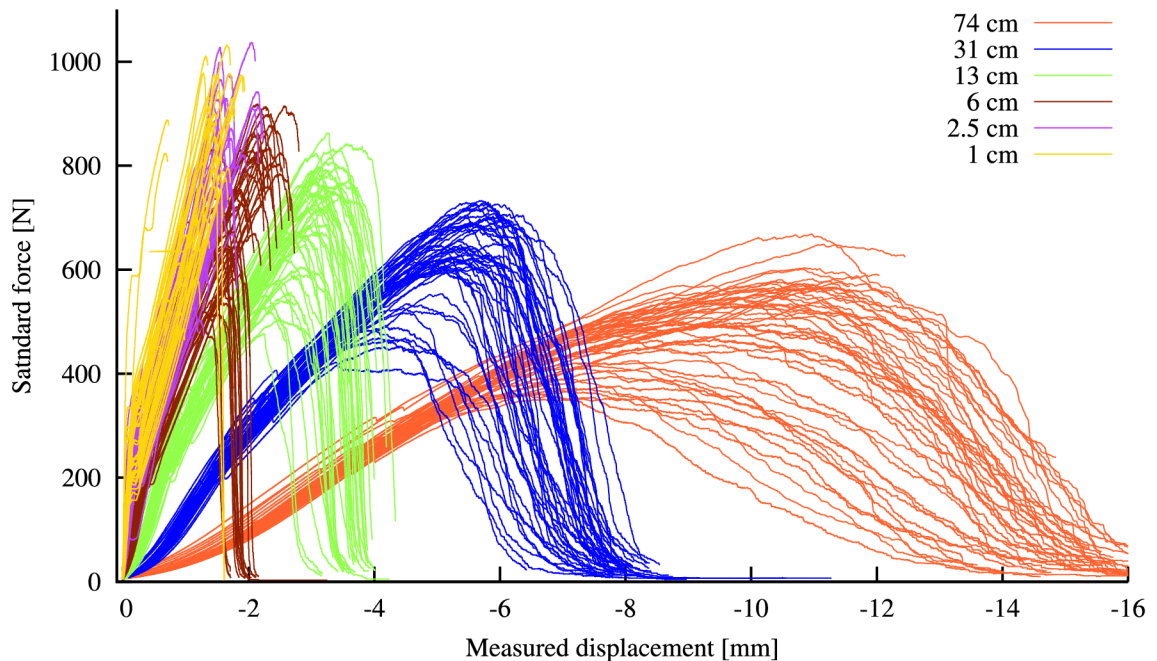


Fig. 2.10: Unmodified force-displacement curves (all samples).

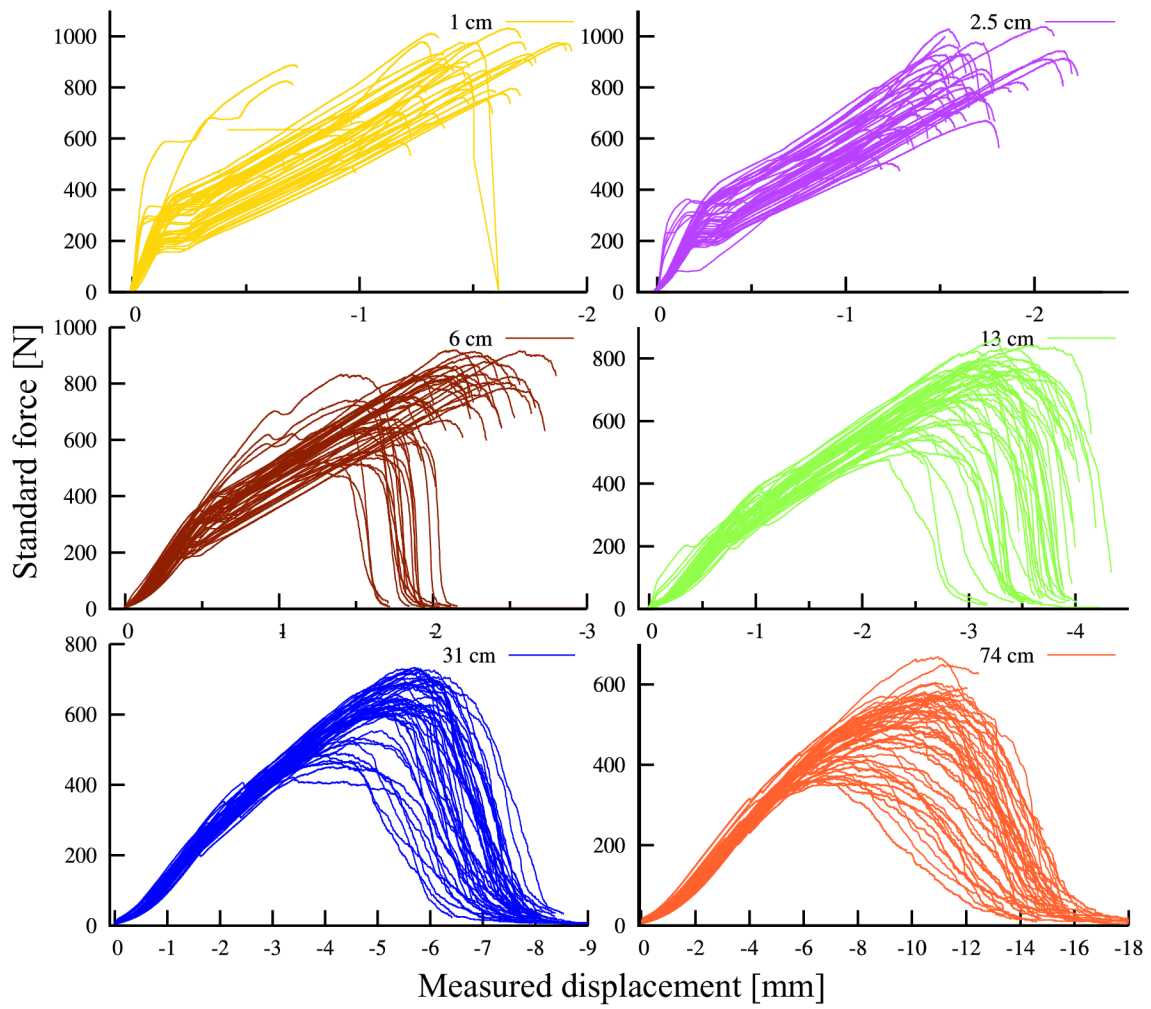


Fig. 2.11: Unmodified force-displacement curves of different length groups.

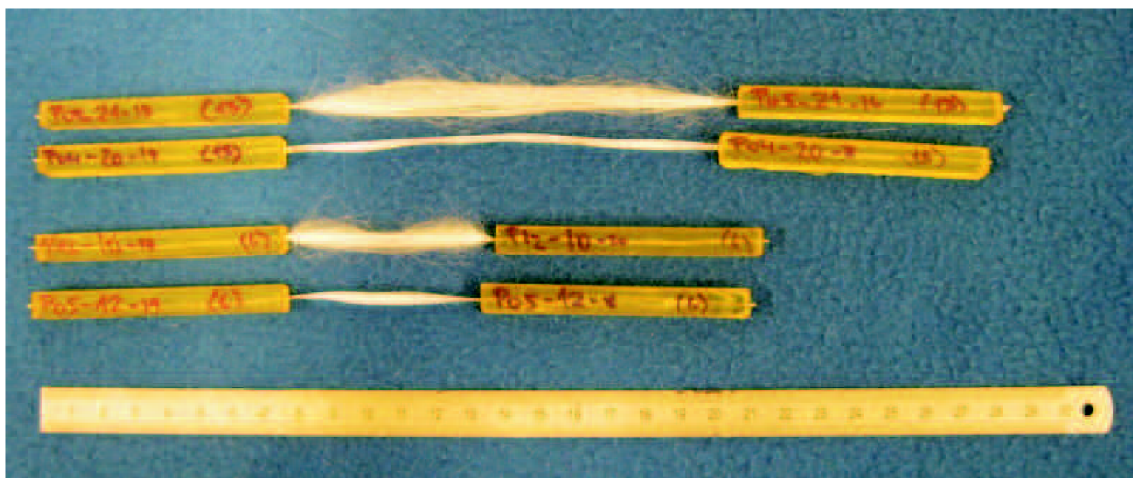


Fig. 2.12: Specimens before and after the test.

3 RESULTS EDITING

3.1 Introduction

Before it could be proceeded to evaluation of experimentally obtained results, some modifications of the data set had to be made. Firstly, the number of samples was reduced by elimination of samples either with strength value extremely differing from the average, or due to serious imperfections caused in the production. Elimination criteria of outliers are described in this chapter. Furthermore, also the displacements measured during the tensile loading embodied some harmful patterns. Identification of these patterns and adjustment of the obtained force-displacement curves is also discussed in this chapter.

3.2 Elimination of outliers from the statistics

To obtain a set of statistical data not influenced by any unintentional effects (such as the sample damage, epoxide penetration into the yarn, etc.), some extreme values and values corresponding to samples obviously unmatching with the others (in some feature) were set aside. The only objective information obtained from the test is the maximum force. Therefore, identification of outliers was only possible by exploiting this information. A direct usage of F_{\max} can not be used because the data exhibit a significant dependence on the length L (Fig. 4.2). Therefore, the average effect of length must be filtered out from the data. It was conjectured that the COV is not dependent on L . The following formula was used to calculate the relative error of each of the sample maximal load $F_{\max,i}$:

$$\text{rel.error} = \frac{F_{\max,i} - \mu_F}{\mu_F} \quad (3.1)$$

where μ is an average of F_{\max} for a corresponding sample nominal length L_{nom} (length group). The values of the relative error were plotted in graphs (Fig. 3.1) vs. different criteria – sample age, date of testing, nominal length and sample series (samples produced in one day). It was decided that samples with absolute value of relative error exceeding 0.35 were marked as outliers and discarded from the data set used for further statistical processing. In addition, according to visual check of samples before testing, the whole series P01 and P02 were also discarded.

This decision can be supported by graph (d), where the significant trend of growing average series strength is clearly visible. This trend was caused by the fact, that the sample production procedure was continuously improved as more experience

and skills were acquired. The first series contained a lot of imperfections because there was no prior practice with the sample production.

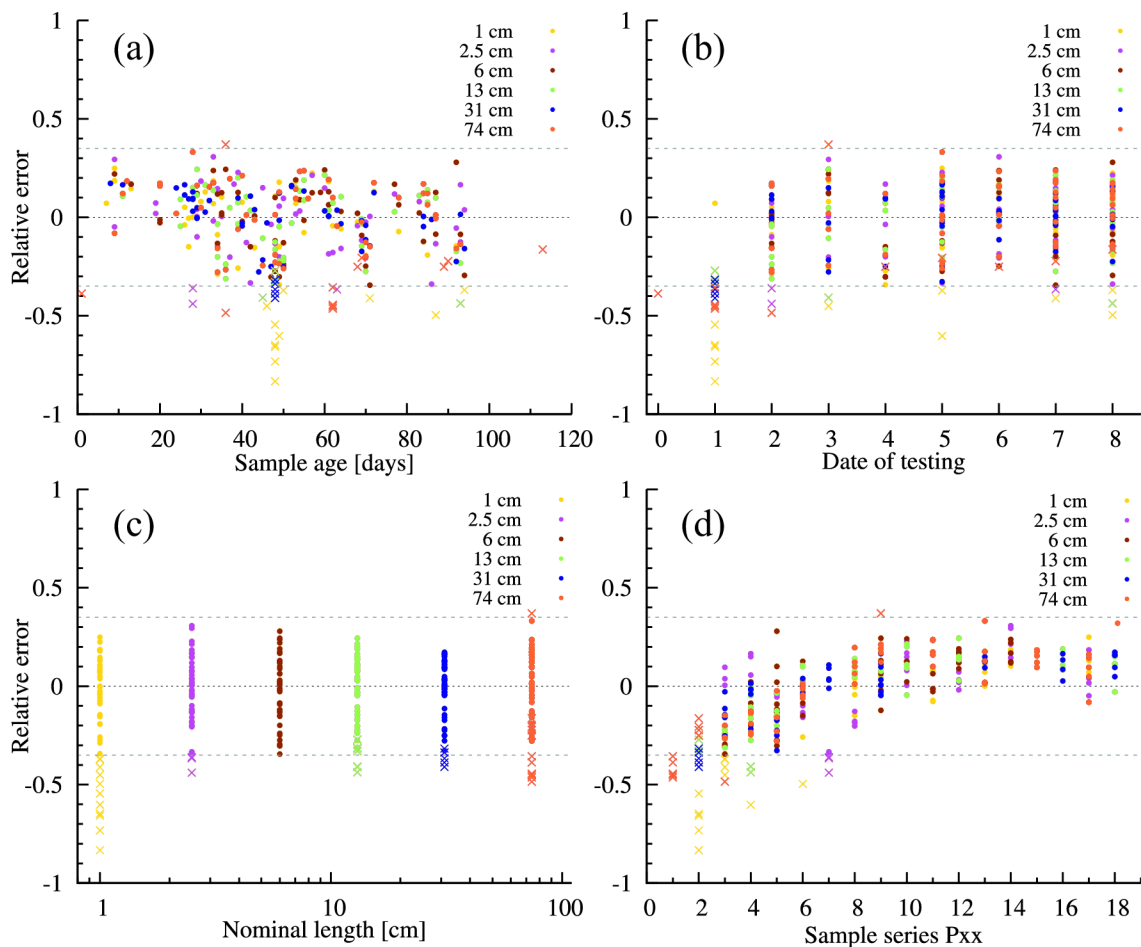


Fig. 3.1: Relative error of samples and outliers' elimination (marked with crosses). Rel. errors are plotted vs. various parameters.

Tab. 3.1: Date of testing and its ordinal number (comment for Fig. 3.1(b)).

0	12.8.2011	3	29.10.2011	6	22.11.2011
1	12.10.2011	4	1.11.2011	7	23.11.2011
2	19.10.2011	5	2.11.2011	8	16.12.2011

From the other three plots it can be seen that there is no correlation between the relative error of strength and sample age (the time between the date of testing and the day of production of the sample) – graph (a), date of testing (b) or nominal length (c). The drop of values in graph (b) in the first two test dates (nr. 0 and 1) was caused by testing of samples from the series P01 and P02. These imperfect samples were purposely used to learn and to verify the correct test software setup and testing procedure. In other testing days, groups of mixed samples (from different series) were used to reduce the potential impact of changing laboratory conditions

during the days. The ordering number (used as the x -axis in graph (b)) and their corresponding dates of testing are overviewed in Tab. 3.1.

The number of filtered samples (outliers) was 38; the final number of samples accepted for the statistical processing was 279, their overview is in Tab. 3.2.

Tab. 3.2: Number of specimens used for statistics (after elimination of 37 outliers).

Series nr.	Date of production	1 cm	2.5 cm	6 cm	13 cm	31 cm	74 cm	sum
P03	13.9.2011	1	5	5	5	5	4	25
P04	14.9.2011	3	5	5	8	5	5	31
P05	15.9.2011	5	5	9	5	5	5	34
P06	20.9.2011	4	5	5	5	4	5	28
P07	21.9.2011		2			5		7
P08	22.9.2011	5	4		5		5	19
P09	23.9.2011	4		5	2	10	4	25
P10	24.9.2011		5	5	5			15
P11	29.9.2011	5		4			5	14
P12	30.9.2011		5	5	5			15
P13	5.10.2011	5				5	5	15
P14	20.10.2011	5	5	5				15
P15	21.10.2011						5	5
P16	22.10.2011				5	4		9
P17	24.10.2011	5	4				5	14
P18	25.10.2011				3	5		8
<i>Number of specimens</i>		42	45	48	48	48	48	279

3.3 Impact of jaws on the measured displacements

While the force reaction induced by displacement loading can be measured without any errors, the objective measurement of sample deformation is much more challenging. The correct way to get this data, is to measure directly the sample elongation with any kind of extensometer. The problem is that common types of contact extensometers cannot be used for the yarn experiment, because it is impossible to connect the device to the sample. The measurement could be improved by installation of two displacement-meters on the inner edges of epoxide blocks, whose differences of measured values would correspond mostly to the yarn deformation (if the epoxide would not deform). However, the loading machine disposes of only one

INC modul (incremental card) and there was only one extensometer available. In the presented experiment, the deflection extensometer was placed on the upper side of the top jaw (see Fig. 2.9 right), which caused inaccuracy of measured displacements. Furthermore, the unstiff behavior of jaws developed other additional displacement distortion.

By placing the extensometer on the mentioned position the read deformation does not belong only to the yarn elongation. It is a sum of deformations of all the device parts under the extensometer – see Fig. 2.9 left. These parts are: two steel holders connected with neck connection and tightened by screw (k_1, k_2) and the bottom and top jaws (k_3, k_5) holding the sample – all these components can be modeled as a set of in series coupled springs with unknown stiffness. The springs representing jaws contain also the tensile stiffness of the epoxy anchoring blocks and their deformation, as well as the events taking place on the contact between them). From the measured u (deformation) and k (stiffness) of the whole set, it is desirable to eliminate the contribution of machine equipment and get only the u_{yarn} and k_{yarn} .

If the stiffness of the machine equipment causing the additional spurious deformation is found, it could be simply subtracted from the measured deformation and the resulting difference would belong directly to the yarn elongation. The stiffness of the machine (the calibration curve) was sought by different additional experiments.

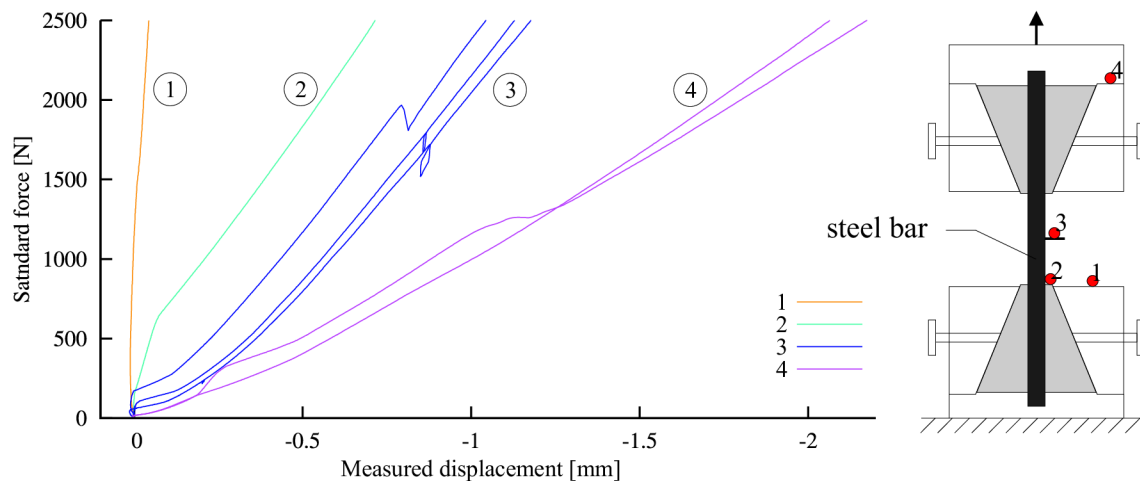


Fig. 3.2: Force-displacement curves of steel bar; displacements measured on different spots.

Firstly, the stiffness of the machine assembly was looked for by loading a very stiff material. If the sample deformation under the tensile loading can be considered as zero, the whole measured displacement can be attributed to the machine and its equipment. This was realized by using a flat steel bar as an experiment specimen. The steel was loaded up to $F_{\text{max}} = 2500$ N (keeping the load within the elastic region) and the extensometer was placed stepwisely on four different positions (levels) of

the assembly, so that the decrease of stiffness can be observed and assigned to appropriate part – see Fig. 3.2.

The yellow curve representing the deformation of two bottom holders and the stiff part of the bottom jaw (point 1) signalizes that these components can be considered as perfectly stiff. By placing the extensometer on the wedge of the bottom jaw (point 2) the bi-linear behavior of the jaws appeared. In a certain moment the stiffness suddenly dropped and the loading continued with a new decreased (but again constant) value of stiffness (linear force-displacement curve). In the next step the deformation was recorded with an extensometer placed in the middle of the steel specimen (point 3) on a special small cantilever fixed to the steel bar. Apparently, a new effect was introduced in the beginning phase of the test. Comparing to the line 2, the initial stiffness was lower and its value gradually grew until it reached a constant value of stiffness (corresponding to the decreased value in previous case) – curves (cyan and blue) continued as parallel lines. This effect of gradual stiffness growth can be assigned to some events taking place on the specimen-jaw contact. Even though there was a pre-load applied, jaws (the wedge) appeared to be slipping on the sample surface until it definitely transversely bit into the steel. The straight branch of the curve was disturbed by other event visible on all three realizations (blue lines) on almost the same displacement value. It can be most likely linked with some kind of slip either on the steel-jaw contact or inside the jaw construction. The last two violet curves were obtained by reading the deformation from the top of the upper jaw, where the default point of measurement was situated – point 4. Compared to the blue curves the approximately half value of stiffness can be observed, which is an obvious fact, as both of the jaws were inspected.

From this experiment, an evident unstiff behavior of used jaws was demonstrated. Anyway, in the case of loading the yarn with epoxy anchoring blocks, another parasite deformations can be expected. To investigate the additional deformation of the epoxide a stiff wire and a string of free length about 2 mm were anchored into two resin blocks and loaded. Unfortunately the tests were not successful, because the cohesion between the steel and the epoxide was not efficient and the wire (string) started to slide out of the block. Subsequently, other approach was chosen – the calibration curves were sought by testing directly the AR-glass yarns. To keep the yarn deformation as small as possible, two yarns (instead of one) poured into one sample of very short free length ($l \approx 4$ mm) were used.

These double-yarns were loaded until the break and the deformation was read on the default spot. The corresponding force-displacement curves (blue and violet) are plotted in Fig. 3.3. Grey curves belong to the steel bar testing from Fig. 3.2, they are plotted here for the purpose of comparison of the stiffness. The bi-linear trend was again significant, but the transition between the original and the decreased stiffness

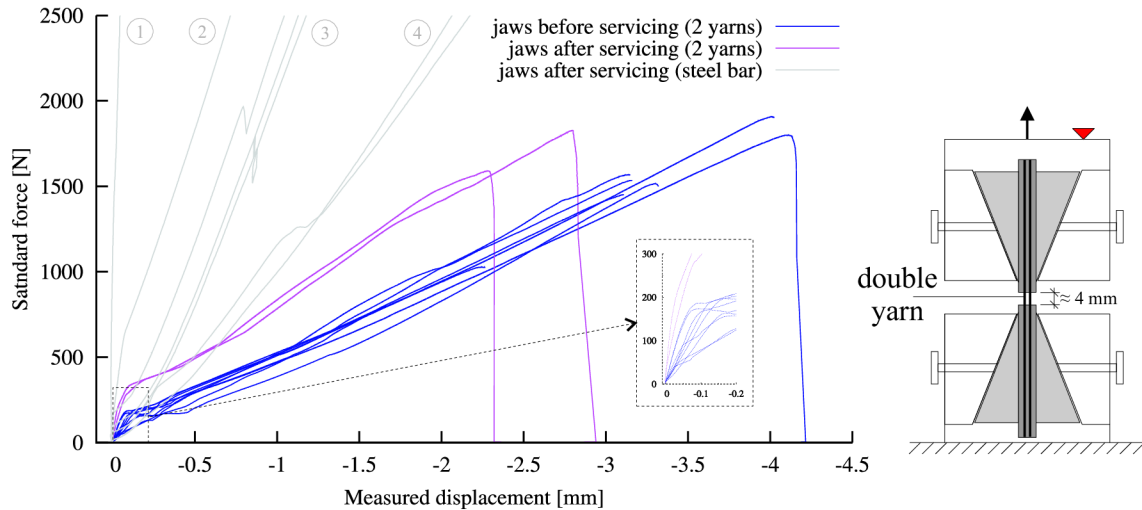


Fig. 3.3: Force-displacement curves of double yarns. Experiments performed with jaws before and after servicing. Grey lines represent curves from Fig. 3.2 for comparison.

was not so strict, but appeared as a “wave” – at a certain force level there was a sudden growth in deformation (about 0.15 mm) and afterwards the curve continued with changed (lower) tangent. The origin of this event will be now discussed.

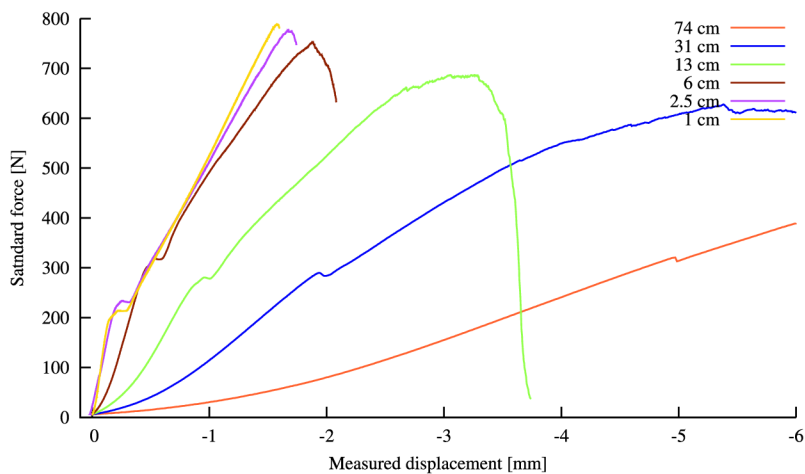


Fig. 3.4: Force-displacement curves of different length groups obtained directly from experiments. Significant “wave” event with subsequent decrease of stiffness can be observed.

During the actual testing of the experimental single yarn samples of different nominal lengths this “wave” event was present in all the tests done before the jaws servicing. The examples of curves (each representing one nominal length group) can be seen in Fig. 3.4.

The position of the wave had the direct conjunction with the force applied on the transverse screws pre-stressing the jaw wedge. While most of the samples were

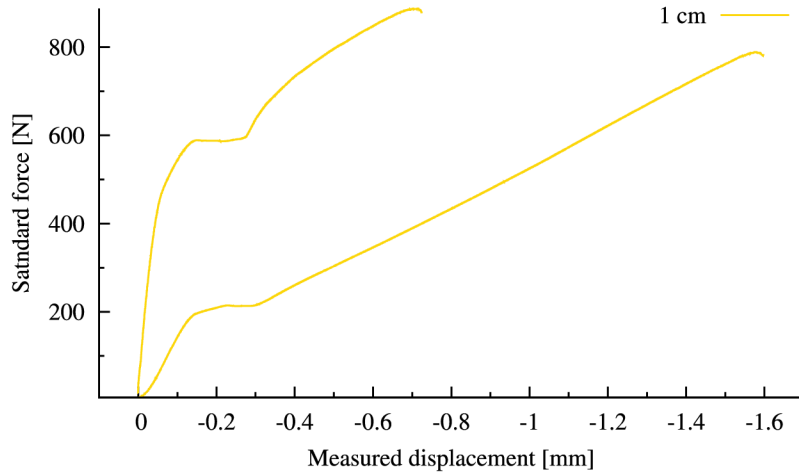


Fig. 3.5: The clamp slack at different force levels (due to different pre-tension of transverse clamp screws).

tested by one person and the wave appear on the force level varying between 200–400 kN, when the transverse screws were tighten strongly, the wave shifted to the force with much higher value (600–700 kN) – see Fig. 3.5. In cases of both curves the length of the wave (the slipped displacement) is approximately equal.

The harmful influence on the displacement measurement was caused by the inner construction of the used jaws. The problem was consulted with the Zwick/Roell representative for several times and the jaws were taken to be checked in the company domicile in Ulm, Germany. Afterwards the test on double yarns was repeated – see the violet curves in Fig. 3.3. Unfortunately the problem with bi-linear behavior was not solved, only the wave temporarily disappeared (appeared again after several new tests).

The bi-linear calibration curve appeared to be complicated to define, as the point of stiffness drop occurred in the varying positions. Furthermore, the initial stiffness had a wide range of values – see the zoomed view in Fig. 3.3. Due to this reasons first branch of the diagram, as well as the wave event were cut off and the calibration curve was defined as a line representing only the second linear branch with a slope calculated as an average value from corresponding obtained curves from Fig. 3.2 and 3.3 measured on the top side of upper jaw. Both types of samples (steel bar and double yarns) were used to find four different calibration curves: for both of the sample types the curve with a zero and a non-zero y -intercept member. Curves were plotted in Fig. 3.6. The orange and the violet curve correspond do the double-yarn calibration samples, the blue and the green lines were defined from the slope of curves from steel bar test (with the extensometer placed on the point 4).

The correction of the force-displacement curves was made by subtracting the calibration curve from the second branch of the curve – the initial steeper part and

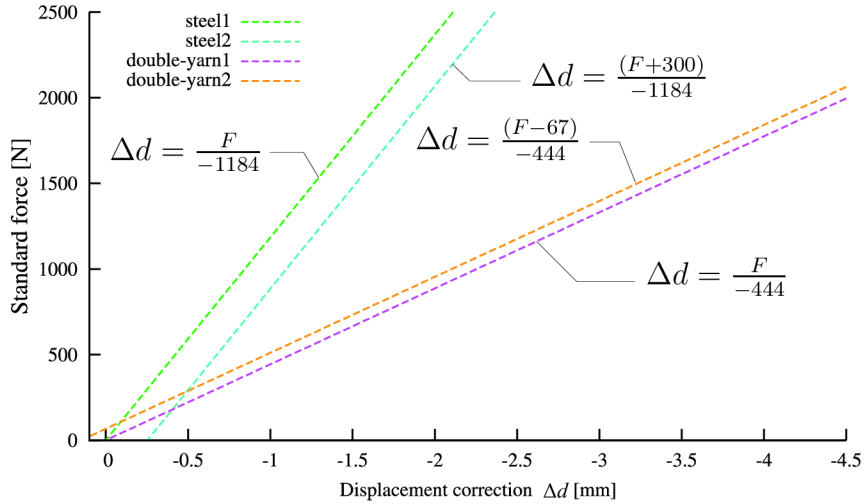


Fig. 3.6: Calibration curves.

the wave were cut off. The result of this type of diagrams correction can be seen in Fig. 3.7. From the plotted graphs (of three random samples with the nominal length 1 cm, resp. 2.5 cm and two of length 6 cm) the fact that this displacement reduction is not correct is obvious. Evidently, the parasite deformations were not extracted from the measured data and the machine unstiff components cannot be substituted by one-spring linear model because they do not behave in a linear manner. Its behavior is close to the bi-linear with unknown parameters, however, in some cases, the searched force-displacement correction curve is even more complicated. Due to this fact, despite the previous experience with load-displacement curves correction [13, 24, 15] the effort to correct the yarn diagrams was not successful.

3.4 Conclusion

It had to be concluded that it is not possible to obtain any credible information about the yarn deformation with this type of experiment setup because there are too many additional deformations which were not identified and quantified. This fact was unfortunately not obvious before because the laboratory equipment is new and any similar experiments were not realized here before. The strength of the yarns with its value less than 1 kN belongs to the region where the jaws show non-linear force-displacement behavior. The company Zwick/Roell admitted that this behavior cannot be suppressed because it is given by the mechanical construction of jaws. They proposed the usage of other type of clamping system – the pneumatic jaws were lent to the laboratory of Department of Structural Mechanics. These jaws can be used in the future to find more information and edit the past experiment results. Other way how to get the correct yarn deformation is to use other type of extensometer – e.g., non-contact optical device.

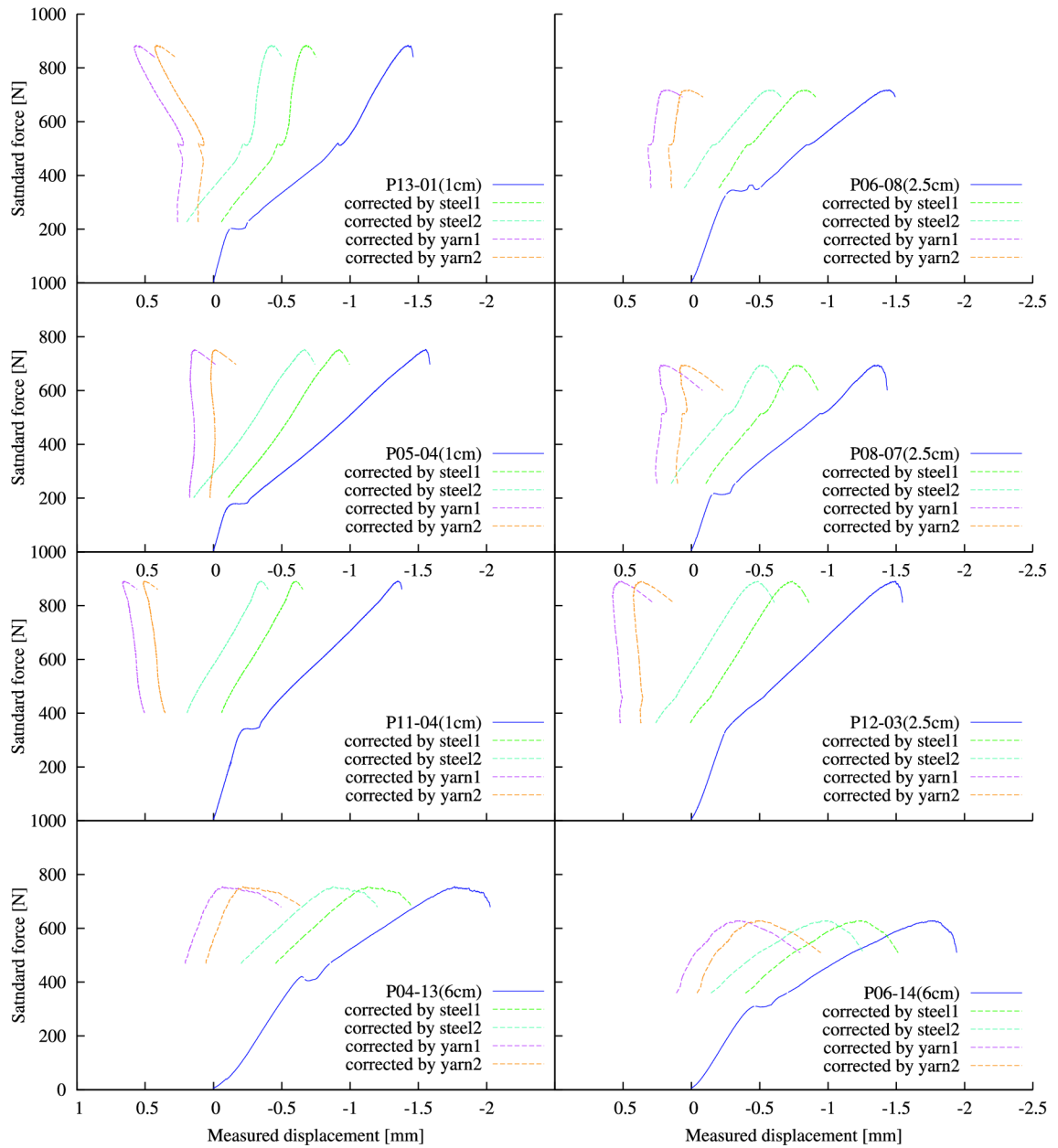


Fig. 3.7: Examples of measured and modified force-displacement curves of different nominal lengths.

4 RESULTS INTERPRETATION

4.1 Introduction

Knowing the correct load-displacement diagrams of tested samples it could be proceeded to put this information together with the numerical model from the Chapter 1. If we knew the yarn strain during the loading, the model could be fitted to the real sample performance and the significance of the included sources of randomness could be quantified. Based on the specimen loading paths the model parameters (ξ , λ , θ) with their probability distributions could be estimated and the correspondence between the experiment and model results verified.

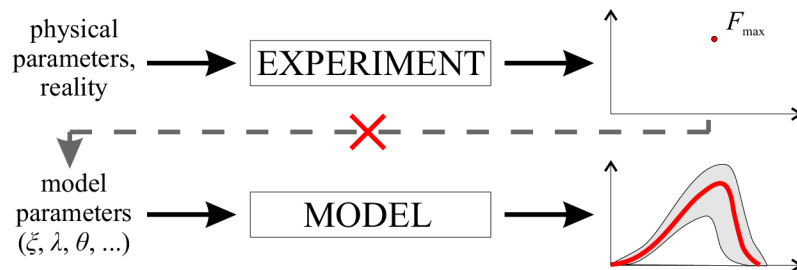


Fig. 4.1: Correspondence between the physical experiment and the numerical model.

As mentioned in the previous chapter, the gathered information about specimen deformation under the tensile loading is unreliable and the attempts to extract these data from the measured displacements were unsuccessful. Due to this fact the potential model parameters identification had to be abandoned (Fig. 4.1) and the evaluation of the experiments reduced to the statistical processing of maximum sample strength with respect to its length (statistical size effect).

4.2 Effect of the length on the yarn strength

The most significant effect of the obtained data set was the strength reduction with the length extension. For each of the length groups, an average value of strength F_{\max} , its standard deviation and a coefficient of variation were calculated. Obtained values together with the average sample free length L and the number of samples used for the statistics n_{sam} are overviewed in Tab. 4.1. The effect of decreasing average and std of the strength with the increasing sample length can be observed. The value of CoV can be considered as stagnating in the range close to 15 %. The number of samples after the elimination of outliers exceeds required 30 pieces in each length group (279 in a total sum) and the obtained data can be considered as a statistically representative set with a high significance.

Tab. 4.1: Final experiment statistics: average, std and CoV of yarn strength.

<i>Length group</i> <i>nr.</i>	<i>L</i> avr [mm]	F_{\max}			n_{sam} [-]
		avr [N]	std [N]	COV [%]	
1	9.2	824.8	126.3	15.32	42
2	23.9	795.7	121.3	15.24	45
3	58.8	737.9	122.9	16.66	48
4	128.5	693.2	101.2	14.60	48
5	308.4	625.4	81.0	12.94	48
6	738.5	498.6	78.6	15.77	48

The graph with the samples' peak loads in a double-logarithmic scale is in Fig. 4.2. The plotted points represent individual experiments, their color is assigned to the production series. Samples with relative error of strength exceeding ± 0.35 as well as the whole series P01 and P02 are marked with a cross (outliers), the border lines separating the outliers from the accepted values (rel. error = ± 0.35) are marked with dash line. The average of each length group strength (marked with a circle \pm std) defines the size-effect curve. The red color represents the modified (reduced) data set while the light grey shows the trend of the original complete set of samples. The fact that these two curves do not notably differ from each other confirms the claim of statistically sufficient number of samples.

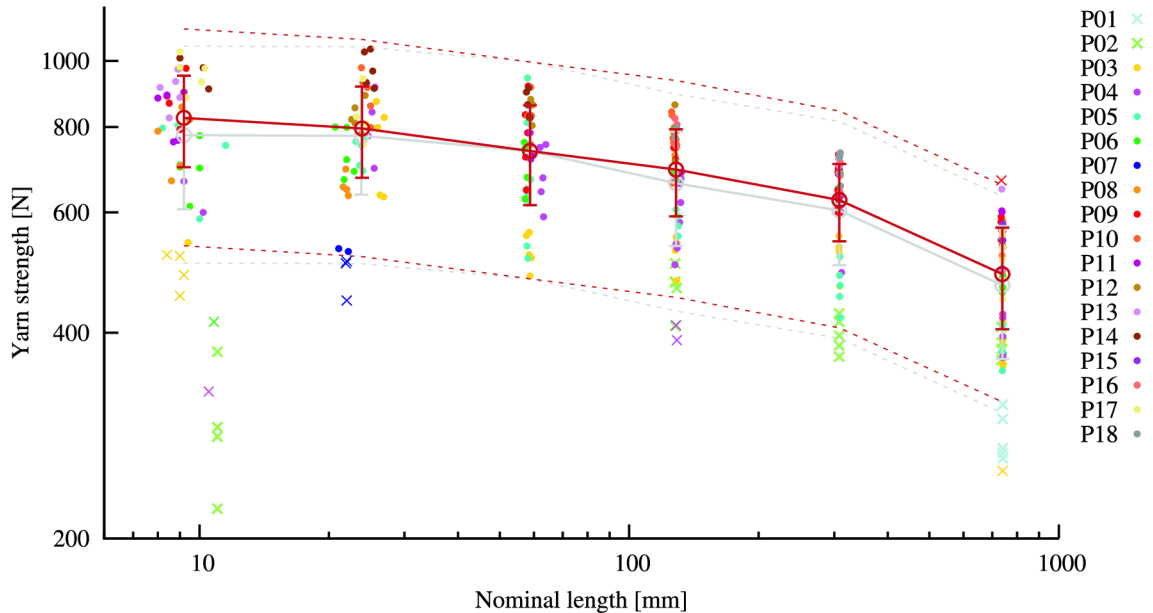


Fig. 4.2: Yarn strengths vs. yarn lengths of tested sample groups and the size-effect curve as an average \pm std of modified (red) and original (grey) data set.

Now, the curve can be fitted with the modified Weibull size-effect function with

the included autocorrelation length (Eq. 1.37). Two different curve-fits can be seen in Fig. 4.3. The parameters l_ρ (autocorrelation length) defining the point of asymptotes' intersection, the strength value c of the left asymptote and m (the shape parameter of Weibullian distribution) governing the slope of the right asymptote in a double-logarithmic scale were chosen intuitively.

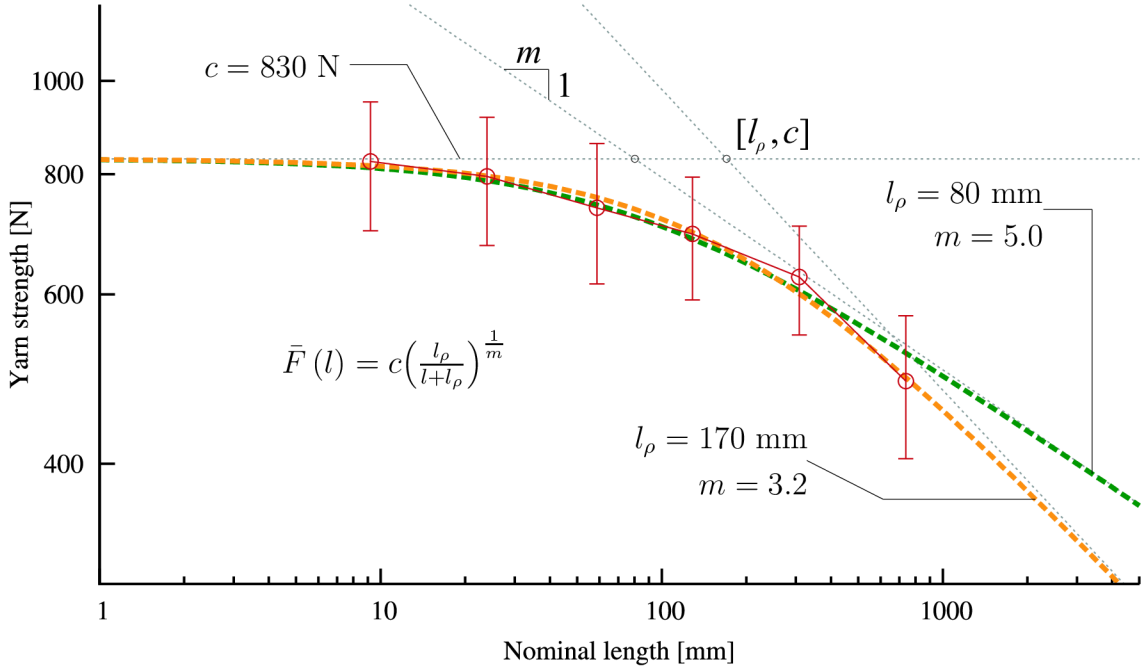


Fig. 4.3: Estimation of size effect curve parameters.

The green curve with parameters $m = 5.0$ and $l_\rho = 80$ mm seems to correspond to the shape of the measured curve for lengths $L < 150$ mm but overestimates the strength of samples over 500 mm. On the other hand, the yellow curve with $m = 3.2$ and $l_\rho = 170$ mm describes the last part of the obtained red curve for longer samples with a good accuracy, but slightly overestimates the strength of samples with the length $L \approx l_\rho$. What more, the value of $m = 3.2$, which corresponds to $\text{CoV} = 34\%$ appeared to be unrealistic. (The common value of $m \in \langle 4 - 6 \rangle$ is mentioned in the literature [27].) The CoV of the green fitted line is 23 %, which looks more reasonable.

Anyway, the estimation of these size-effect parameters is just an assumption. The other explanation of the shape of the curve could be acquired with the help of the computational model parameters (Fig. 4.4). If there is no strength autocorrelation of the material, or the autocorrelation length is much lower, the strength dependency on the yarn length would be expressed by a line in a double-logarithmic scale (classical Weibull size-effect). The strength of shorter samples could be reduced by the influence of uneven filament length or by the effect of scatter in the

filament activation strain (see Tab. 1.3). Furthermore, the other unpredictable effects can also cause the strength reduction of shorter samples (e.g., damage caused during the production and manipulation with the sample). Unfortunately, because the true deformation diagrams of the yarn are not available, there is no information supporting any of mentioned trends.

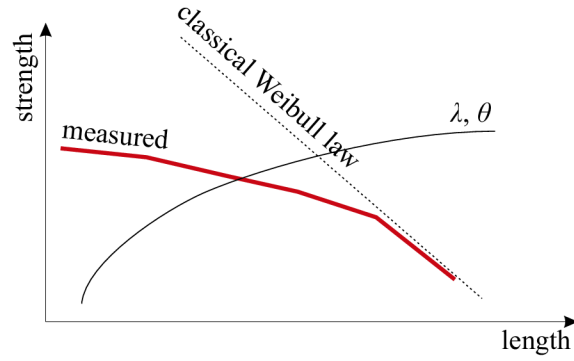


Fig. 4.4: Explanation of the experimentally obtained curve shape without the effect of autocorrelation of strength.

The assumption of the presence of other unpredicted influence can be supported by the fact that the CoV of the strength has a high value. According to the knowledge of the behavior of the bundle model with an infinite number of filaments n it could be expected that the value of CoV was much lower (proportional to the inverse of square root of n). If the value of the shape parameter for one filament is $m = 5.0$ ($\text{CoV}_1 = 23\%$) the value of CoV for a bundle with $n = 2400$ should be $\text{CoV}_{2400} = \text{CoV}_1 / \sqrt{2400} \approx 0.5\%$ which contrasts with the experimentally measured value.

CONCLUSION

The master's study presents the results of extensive experimental work on multi-filament yarns. The yarn is composed of several hundreds to thousands filaments with diameter measured in tens of micrometers and made of alkali-resistant glass. The textiles knitted from these yarns are used as a reinforcement for the so-called textile reinforced concrete. The textile reinforced concrete is an innovative and developing composite material with a high potential of application not only in civil engineering structures. It combines the characteristics of a cementitious matrix providing the compressive strength with tensile resistance of the textile reinforcement. These textiles had developed from the fiber-reinforced concrete (with a randomly oriented short fibers reinforcement) by aggregation and orientation of filaments in the direction of the tension, which led to better efficiency of the reinforcement. The main advantages of this material are the thickness (and subsequently the weight) reduction of the concrete members compared to the common steel-reinforcement system and the ductile response on load of the structure.

The experiment was focused on the yarn response under the tensile loading. The yarns were anchored in an epoxy resin blocks and loaded by the testing machine in the experimental laboratory of the Department of Structural Mechanics, Brno University of Technology. More than 300 specimens of six different nominal lengths (from 1 cm to 74 cm) were tested to obtain data with a high statistical significance. The measured values of the samples' force-deformation dependency (load-displacement curves) were examined and statistically processed. Firstly, samples marked as outliers were eliminated from the data set and the tendency of displacement correction has followed. The need of displacement adjustment was caused by the fact that measured values of deformation did not completely belong to the yarn sample, but also the loading machine and its unstiff components contributed to the measured displacement. This parasite deformations had to be subtracted from the measured values to obtain the true load-displacement curves of the samples.

For the prediction and for the further evaluation of the carried experiment, the numerical model adopted from [7, 27] was presented. The yarn is modeled as a bundle composed of many filaments with a zero-friction among them and with random parameters representing different types of disorder sources. Some parameters are assigned to the certain filament within the bundle cross-section, the other vary over the single filament's length. The influence of the individual parameter randomization and their mutual interaction was modeled and the qualitative bundle response was demonstrated. Furthermore, the effect of the bundle length as well as the effect of the number of filaments on the bundle strength was also described in terms of the classical statistical Weibull size-effect theory and its modification introducing

the spatial autocorrelation of the material characteristics. In parallel, the analytical behavior of the bundle with an infinite number of fibers is presented to be compared with results of the numerical simulations.

By knowing the true load-displacement diagrams from the experiment, the parameters of the computational model and their distribution could be identified so that the model would fit the reality. Unfortunately, this intention was not fulfilled as the test-curves' adjustment was not successful due to the fact that the elimination of the spurious deformation was too complicated to manage. The loading machine and its components (especially the used types of jaws) exhibited strongly non-linear behavior under the tensile loading. The stiffness of the loading device was investigated by a series of complementary tests. However, the linear calibration curves established on the basis of these tests were not correct and suitable for the results' adjustment. Consequently, the only objective information obtained from the experiment were the bundle strengths (maximal load value) and the statistical evaluation had to be reduced to processing of these data.

The strength of each yarn was plotted versus its length in a double-logarithmic scale. The obtained size-effect curve was intuitively fitted by the equation of modified Weibull size effect with the spatial strength autocorrelation. Although those two curves matches each other with a good accuracy, it should be stated that the sample strength could be influenced also by other effects, e.g., effects of parameters discussed in the theoretical part of the thesis (model parameters as unequal length of the filaments or the individual activation strain of each filament in the bundle), with a friction among filaments of the longer lengths or with other unpredictable factors (as the local conditions changing in time or the human factor). Without knowing the correct load-deformation curves, these statements are only hypothetical.

Anyway, the obtained experience should be exploited for a new future testing. With a better test equipment (non-contact extensometer or two contact extensometers, pneumatic jaws), a correct displacement measurement can be expected and a potential correction of already carried experiment could be possible. Furthermore, the investigation of interaction between the yarn and the concrete matrix can be tested, e.g., by the fragmentation tests [11, 21].

It is hardly possible to predict the result of an experiment without any previous experience. This type of material research requires the perfect knowledge of the test equipment and its setup, as the method itself and the used device strongly influence the final result. The information about material obtained from an experiment should be always treated within the context of used method and local conditions. The fact that the experiment result do not have to prove the real physical material characteristics should be kept in mind. Anyway, the experimental testing remains an important method in analyzing and explaining the nature of reality.

BIBLIOGRAPHY

- [1] Bažant, Z. P.; Novák, D.: Probabilistic nonlocal theory for quasi-brittle fracture initiation and size effect I: Theory. *Journal of Engineering Mechanics, ASCE*, volume 126, nr. 2, 2000: pages 166–174.
- [2] Bažant, Z. P.; Pang, S. D.; Vořechovský, M.; et al.: Statistical size effect in quasibrittle materials: Computation and extreme value theory. In *5th Int. Conference FraMCoS – Fracture Mechanics of Concrete and Concrete Structures, held in Vail, Colorado, USA*, volume 1, edited by V. C. Li; K. J. Willam; C. K. Y. Leung; S. L. Billington, Ia-FraMCoS, 2004, ISBN 0 87031 135 2, pages 189–196.
- [3] Bažant, Z. P.; Planas, J.: *Fracture and Size Effect in Concrete and Other Quasibrittle Materials*. CRC Press, Boca Raton and London, 1998.
- [4] Bažant, Z. P.; Vořechovský, M.; Novák, D.: Asymptotic Prediction of Energetic-Statistical Size Effect from Deterministic Finite Element Solutions. *Journal of Engineering Mechanics (ASCE)*, volume 133, nr. 2, 2007: pages 153–162, ISSN 0733-9399.
- [5] Bažant, Z. P.; Xi, Y.: Statistical size effect in quasibrittle structures. II. Nonlocal theory. *Journal of Engineering Mechanics, ASCE*, volume 117, nr. 11, 1991: pages 2623–2640.
- [6] Chudoba, R.; Vořechovský, M.; Eckers, V.; et al.: Effect of twist, fineness, loading rate and length on tensile behavior of multifilament yarns (a multivariate study). *Textile Research Journal (Sage)*, volume 77, nr. 11, 2007: pages 880–891, ISSN 0040-5175.
- [7] Chudoba, R.; Vořechovský, M.; Konrad, M.: Stochastic modeling of multifilament yarns I: Random properties within the cross-section and size effect. *International Journal of Solids and Structures (Elsevier)*, volume 43, nr. 3-4, 2006: pages 413–434, ISSN 0020-7683.
- [8] Coleman, B.: On the strength of classical fibres and fibre bundles. *Journal of the Mechanics and Physics of Solids*, volume 7, 1958: pages 60–70.
- [9] Daniels, H.: The maximum of Gaussian process whose mean path has a maximum, with an application to the strength of bundles of fibres. *Advances in Applied Probability*, volume 21, 1945: pages 315–333.

- [10] Epstein, B.: Statistical aspect of fracture problems. *Journal of Applied Physics*, volume 19, 1948: pages 140–147.
- [11] Feih, s.; Wonsyl, K.; Minzari, D.; et al.: Testing procedure for the single fiber fragmentation test. Technical report, Riso National Laboratory, Roskilde, Denmark, 2004.
- [12] Fisher, R. A.; Tippett, L. H. C.: Limiting forms of the frequency distribution of the largest and smallest member of a sample. *Proc., Cambridge Philosophical Society*, volume 24, 1928: pages 180–190.
- [13] Frantík, P.: *GTDiPS dokumentace*. Vysoké učení technické v Brně, 2008.
- [14] Gumbel, E.: *Statistics of Extremes*. Columbia University Press, New York, 1958.
- [15] Kaděrová, J.: *Testování statistického vlivu velikosti pomocí čtyřbodového ohybu*. Master thesis, Institute of Structural Mechanics, Faculty of Civil Engineering, Brno University of Technology, 2009.
- [16] Konrad, M.; Jeřábek, J.; Vořechovský, M.; et al.: Evaluation of mean performance of cracks bridged by multi-filament yarns. In *EURO-C 2006 Computational Modelling of Concrete Structures, held in Mayrhofen, Austria*, edited by Meschke; de Borst; Mang; Bičanič, London, UK: Taylor & Francis Group, 2006, ISBN 0 415 39749 9, pages 873–880.
- [17] Peirce, F.: Tensile test for cotton yarns v. The weakest link theorems on the strength of long and composite specimens. *Journal of Textile Institute*, volume 17, 1926: pages T355–T368.
- [18] Phoenix, S.; Taylor, H.: The asymptotic strength distribution of a general fiber bundle. *Advances in Applied Probability*, volume 5, 1973: pages 200–216.
- [19] RILEM: Textile Reinforced Concrete. State-of-the-Art Report 36, RILEM Technical Committee, Aachen, Germany, 2006.
- [20] Teplý, B.; Novák, D.: *Spolehlivost stavebních konstrukcí*. Akad. Nakl. CERM, Brno, 2004.
- [21] Tripathi, D.; Jones, F. R.: Single fibre fragmentation test for assessing adhesion in fibre reinforced composites. *Journal of Materials Science*, 1998.
- [22] <http://www.textil-beton.de>: Textone - business network for fiber- and textile-reinforced concrete. January 2012.

- [23] Vořechovský, M.: Comparison of stability and accuracy of numerical simulation methods for simulation of statistics of extremes. *Probabilistic Engineering Mechanics (Elsevier)*, 2004: pg. under preparation, ISSN 0266-8920.
- [24] Vořechovský, M.: Korekce zatěžovacích drah na netuhých lisech. In *Směřování kateder/ústavu STM stavebních fakult ČR a SR 2005/2006*, edited by J. Pejchalová; J. Kala; Z. Keršner, Mikulov, Czech Republic: Brno University of Technology, Fac. of Civil Engrg., Institute of Struct. Mech., 2006, ISBN 80-214-3248-9, pages 93–97.
- [25] Vořechovský, M.: Simulation of simply cross correlated random fields by series expansion methods. *Structural safety (Elsevier)*, volume 30, nr. 4, 2008: pages 337–363, ISSN 0167-4730.
- [26] Vořechovský, M.: Incorporation of statistical length scale into Weibull strength theory for composites. *Composite Structures*, volume 92, nr. 9, 2010: pages 2027—2034, ISSN 0263-8223.
- [27] Vořechovský, M.; Chudoba, R.: Stochastic modeling of multi-filament yarns: II. Random properties over the length and size effect. *International Journal of Solids and Structures (Elsevier)*, volume 43, nr. 3-4, 2006: pages 435–458, ISSN 0020-7683.
- [28] Vořechovský, M.; Novák, D.: Efficient Random Fields Simulation for Stochastic FEM Analyses. In *2nd M.I.T. Conference on Computational Fluid and Solid Mechanics, held in Cambridge, USA*, edited by K. J. Bathe, Oxford, UK: Elsevier Science Ltd., 2003, ISBN 0-08-044046-0, pages 2383–2386.
- [29] Vořechovský, M.; Novák, D.: Correlation control in small sample Monte Carlo type simulations I: A Simulated Annealing approach. *Probabilistic Engineering Mechanics (Elsevier)*, volume 24, nr. 3, 2009: pages 452–462, ISSN 0266-8920.
- [30] Weibull, W.: The phenomenon of rupture in solids. *Royal Swedish Institute of Engineering Research (Ingenioersvetenskaps Akad. Handl.)*, Stockholm, volume 153, 1939: pages 1–55.

LIST OF SYMBOLS, PHYSICAL CONSTANTS AND ABBREVIATIONS

A	cross-section area
AR-glass	alkali resistant glass
CDF	cumulative distribution function
COV	coefficient of variation
D	filament diameter
$D[\dots]$	variance (dispersion)
E	Young's modulus of elasticity
$G_i(\theta_i)$	cumulative distribution function of a random parameter
F_{\max}	maximal load
$H(\cdot)$	Heaviside (unit step) function
L	length of sample
L_{nom}	nominal length
MSEC	mean size effect curve
P_f	probability of failure
PDF	probability density function
Q_n^*	maximum tensile force of n -filament yarn normalized by n
$\mathcal{R}_{\rightarrow\rightarrow}$	autocorrelation function
$T^{(+)}, T^{(-)}$	yarn force at the breaking strain before and after filament rupture
avr	average
e	bundle/yarn strain
$f(l)$	length effect due to the spatially varying strength
l	nominal length of the test specimen
l_ρ	autocorrelation length

m	Weibull modulus (shape parameter)
n	number of filament in the bundle
n_{sam}	number of samples
n_{sim}	number of simulations
nr.	number
p	number of material points used to discretize a filament in the bundle
$q_{e,i}(e), q_{\varepsilon,i}(\varepsilon_i)$	global and local representation of the constitutive law
s	scale parameter of Weibull distribution
std	standard deviation
\mathcal{M}	set of material points if i -th filament
\mathcal{R}	set of points representing the bundle load-strain diagram
Γ	Gamma function
γ_σ	standard deviation of strength distribution
α	random nature
ε	filament strain
θ	filament activation strain - slack
λ	ratio of extra filament length to the nominal length
$\mu_\theta(e), \mu_0(e)$	mean load/strain function of the filament with and without imperfections
ξ	filament breaking strain
σ	stress, strength

LIST OF APPENDICES

A Experiment documentation (figures)	III
B Experiment results in detail	VII

A EXPERIMENT DOCUMENTATION (FIGURES)

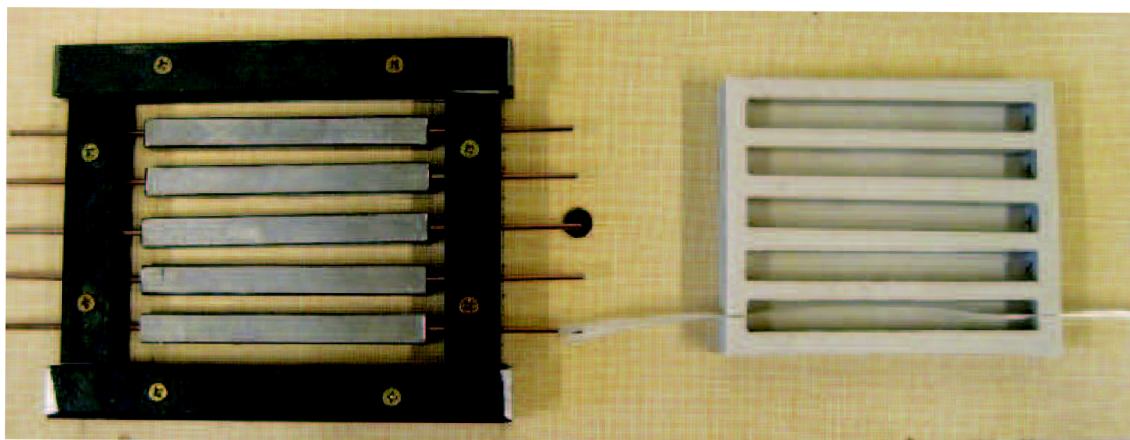


Fig. A.1: A steel form with a silicone form.

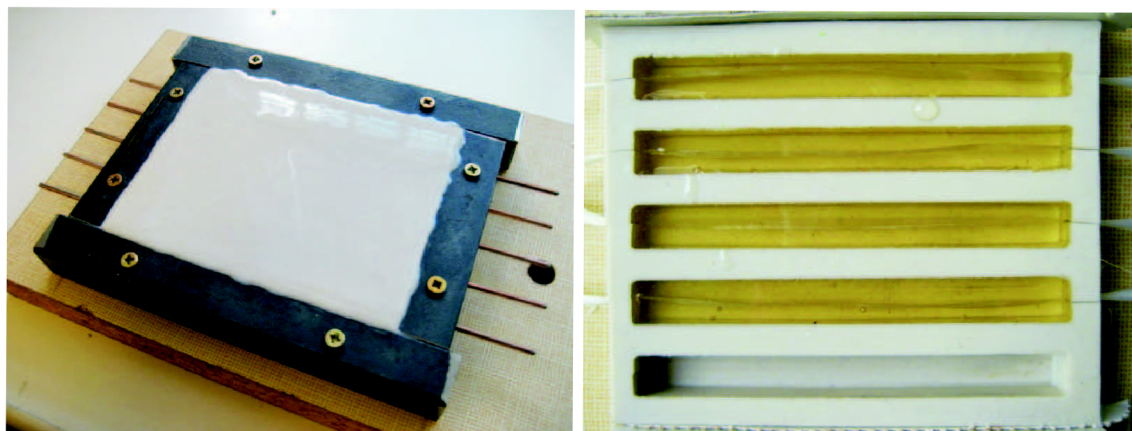


Fig. A.2: Freshly cast silicone form (left) and epoxide anchoring blocks (right).

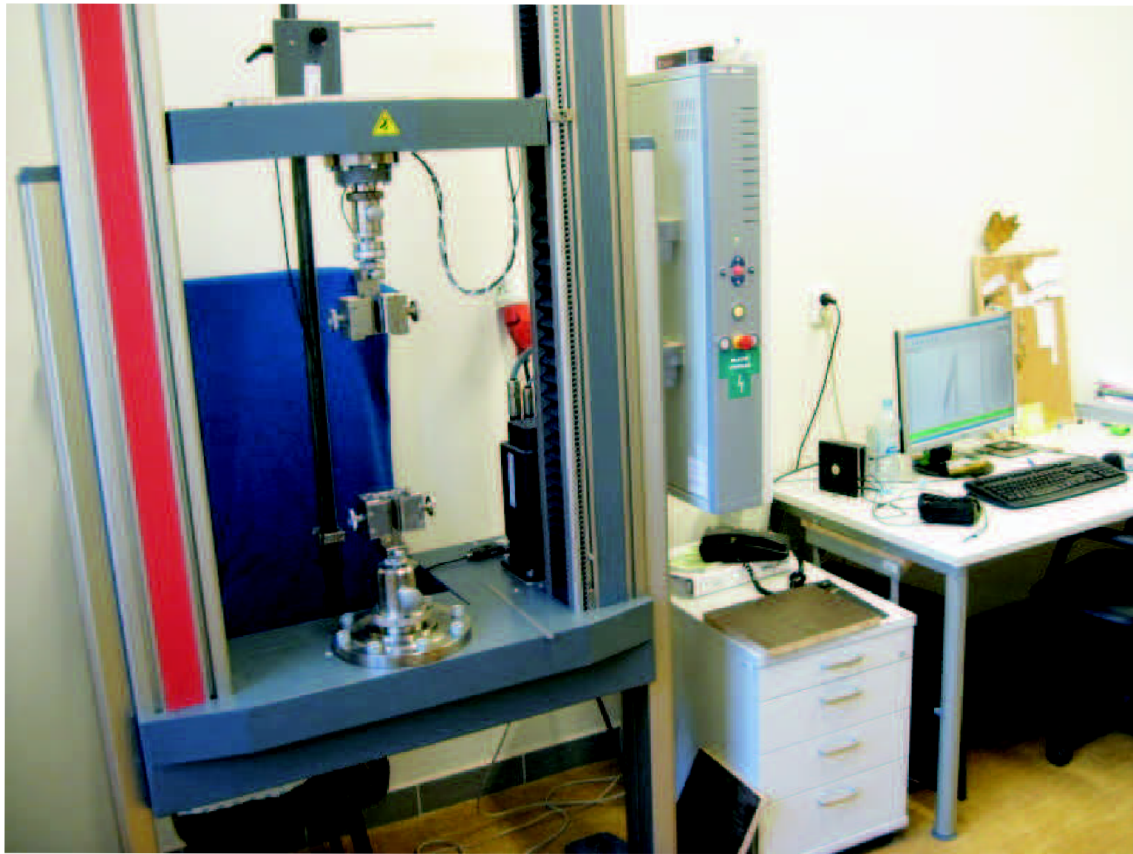


Fig. A.3: Test machine Zwick/Roell Gruppe Z100.

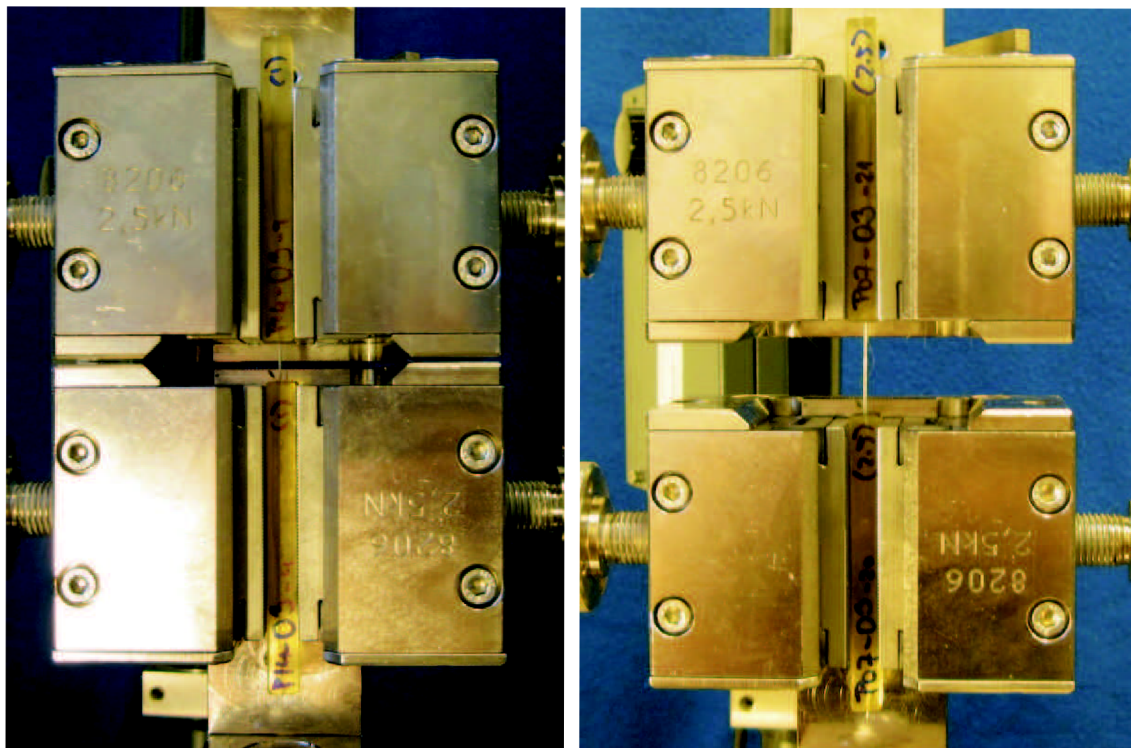


Fig. A.4: Test of a sample of length 1 cm (left) and 2.5 cm (right).

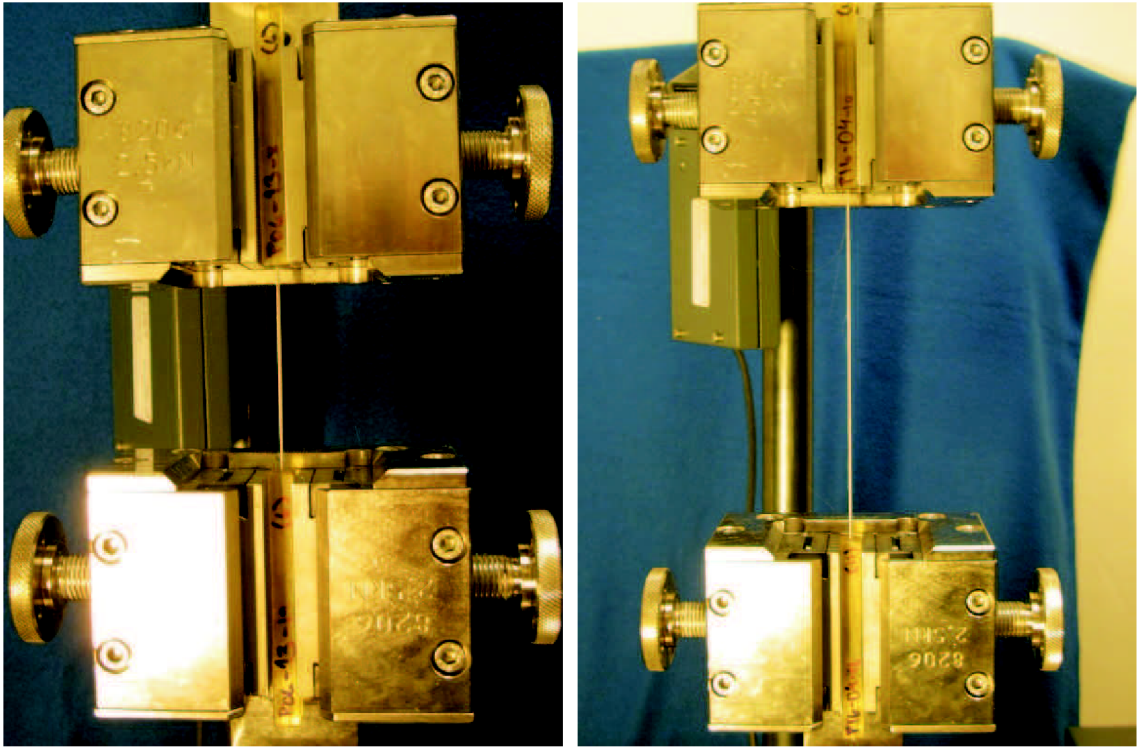


Fig. A.5: Test of a sample of length 6 cm (left) and 13 cm (right).

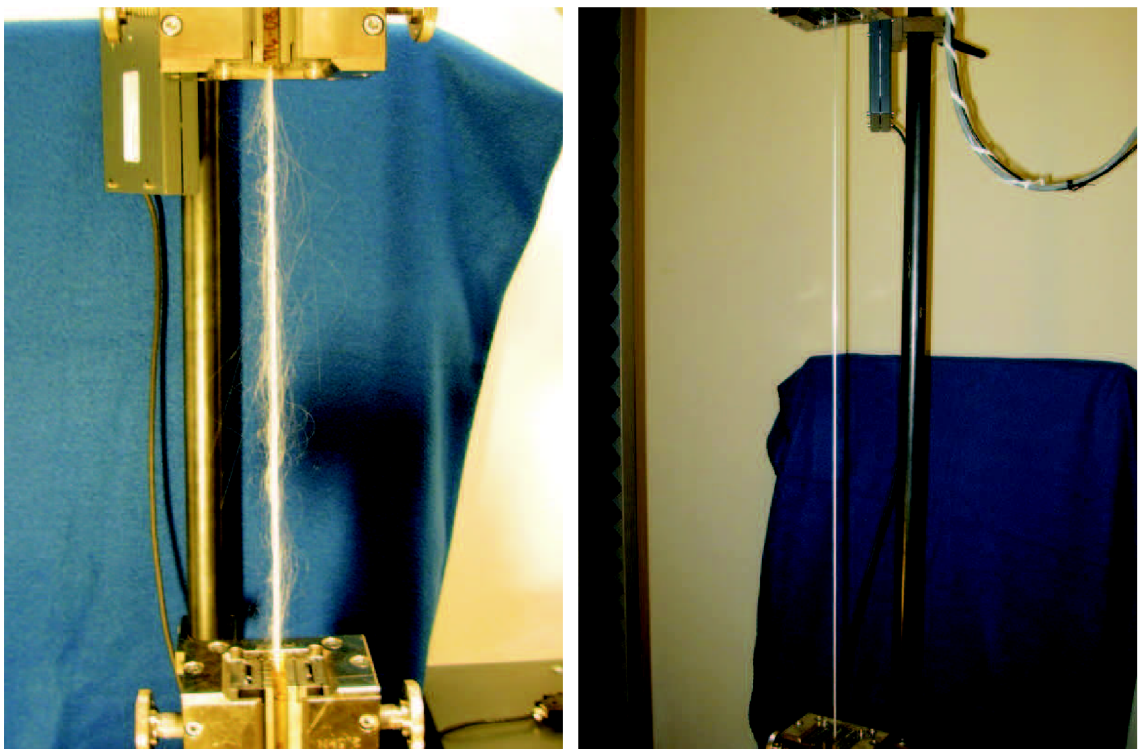


Fig. A.6: Test of a sample of length 31 cm (left) and 74 cm (right).



Fig. A.7: Broken samples.

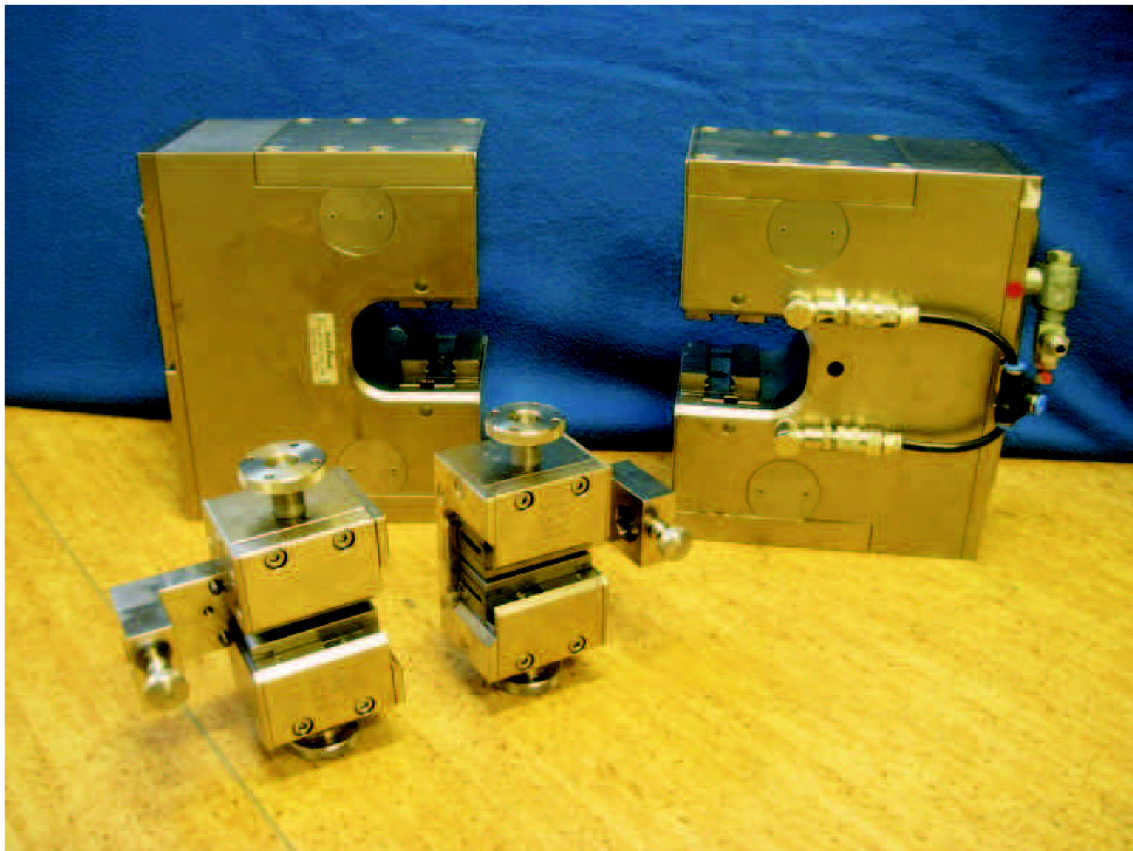


Fig. A.8: Self-locking jaws (front) and pneumatic jaws and (rear).

B EXPERIMENT RESULTS IN DETAIL

Tab. B.1: Results of laboratory testing (ordering according to the length group and date of experiment)

Specimen number	Length L [mm]	Breaking force F_{\max} [N]	Deformation dL at F_{\max} [mm]	Date of experiment	Date of production	Age [day]
<i>LENGTH GROUP nr. 1: $l \sim 10$ mm</i>						
P13-01	9.0	884	1.42	12.10.2011	5.10.2011	7
P05-04	11.5	752	1.56	19.10.2011	15.9.2011	34
P05-05	10.0	587	1.18	19.10.2011	15.9.2011	34
P08-02	9.5	821	1.46	19.10.2011	22.9.2011	27
P08-04	9.0	702	1.16	19.10.2011	22.9.2011	27
P09-01	9.0	793	1.46	19.10.2011	23.9.2011	26
P09-02	8.5	867	1.55	19.10.2011	23.9.2011	26
P03-02	9.0	453	0.58	29.10.2011	13.9.2011	46
P06-01	9.5	612	0.90	29.10.2011	20.9.2011	39
P11-04	8.4	891	1.35	29.10.2011	29.9.2011	30
P14-02	9.0	977	1.51	29.10.2011	20.10.2011	9
P03-01	9.4	542	0.73	1.11.2011	13.9.2011	49
P04-04	10.2	600	0.95	1.11.2011	14.9.2011	48
P11-03	8.0	882	1.38	1.11.2011	29.9.2011	33
P03-04	9.0	518	0.62	2.11.2011	13.9.2011	50
P04-03	9.0	702	0.97	2.11.2011	14.9.2011	49
P06-02	9.0	699	1.32	2.11.2011	20.9.2011	43
P06-03	10.0	697	0.94	2.11.2011	20.9.2011	43
P09-03	8.4	888	0.71	2.11.2011	23.9.2011	40
P13-04	8.5	825	0.67	2.11.2011	5.10.2011	28
P14-01	9.2	945	1.52	2.11.2011	20.10.2011	13
P17-02	9.0	978	1.28	2.11.2011	24.10.2011	9
P17-03	9.0	1030	1.65	2.11.2011	24.10.2011	9
P05-02	8.9	805	1.27	22.11.2011	15.9.2011	68
P08-05	9.1	856	1.47	22.11.2011	22.9.2011	61
P11-05	9.2	900	1.47	22.11.2011	29.9.2011	54
P13-03	8.1	914	1.36	22.11.2011	5.10.2011	48
P14-04	10.2	977	1.70	22.11.2011	20.10.2011	33
P03-05	9.2	486	0.85	23.11.2011	13.9.2011	71

Tab. B.1: (continued)

Specimen number	Length L [mm]	Breaking force F_{\max} [N]	Deformation dL at F_{\max} [mm]	Date of experiment	Date of production	Age [day]
P04-02	9.2	666	1.35	23.11.2011	14.9.2011	70
P05-03	8.2	797	1.67	23.11.2011	15.9.2011	69
P06-04	10.0	777	1.63	23.11.2011	20.9.2011	64
P08-03	8.0	789	1.58	23.11.2011	22.9.2011	62
P09-05	9.3	975	1.88	23.11.2011	23.9.2011	61
P11-02	8.7	761	1.45	23.11.2011	29.9.2011	55
P13-05	8.9	972	1.90	23.11.2011	5.10.2011	49
P14-05	10.5	909	1.72	24.11.2011	20.10.2011	35
P17-04	10.1	931	1.75	24.11.2011	24.10.2011	31
P03-03	8.4	520	0.59	16.12.2011	13.9.2011	94
P05-01	9.0	705	1.16	16.12.2011	15.9.2011	92
P08-01	8.6	667	1.00	16.12.2011	22.9.2011	85
P11-01	8.9	765	1.25	16.12.2011	29.9.2011	78
P13-02	8.8	933	1.35	16.12.2011	5.10.2011	72
P14-03	9.0	1010	1.31	16.12.2011	20.10.2011	57
P17-01	9.3	883	1.37	16.12.2011	24.10.2011	53
P17-05	10.3	975	1.44	16.12.2011	24.10.2011	53
<i>LENGTH GROUP nr. 2: $l \sim 25$ mm</i>						
P06-08	22.0	717	1.45	19.10.2011	20.9.2011	29
P06-09	22.0	799	1.51	19.10.2011	20.9.2011	29
P07-01	22.0	509	1.02	19.10.2011	21.9.2011	28
P07-05	22.0	446	0.90	19.10.2011	21.9.2011	28
P12-04	23.0	811	1.59	19.10.2011	30.9.2011	19
P12-05	23.0	853	1.70	19.10.2011	30.9.2011	19
P04-08	25.6	915	1.44	29.10.2011	14.9.2011	45
P08-02	22.2	635	1.12	29.10.2011	22.9.2011	37
P10-05	25.0	799	1.37	29.10.2011	24.9.2011	35
P14-09	24.2	1030	1.55	29.10.2011	20.10.2011	9
P03-06	26.3	636	1.25	1.11.2011	13.9.2011	49
P05-06	24.2	767	1.47	1.11.2011	15.9.2011	47
P10-04	24.0	930	1.62	1.11.2011	24.9.2011	38

Tab. B.1: (continued)

Specimen number	Length L [mm]	Breaking force F_{\max} [N]	Deformation dL at F_{\max} [mm]	Date of experiment	Date of production	Age [day]
P03-07	25.8	872	1.72	2.11.2011	13.9.2011	50
P04-06	25.2	841	1.55	2.11.2011	14.9.2011	49
P05-08	24.0	690	1.52	2.11.2011	15.9.2011	48
P06-07	20.7	800	1.65	2.11.2011	20.9.2011	43
P07-02	21.1	531	1.12	2.11.2011	21.9.2011	42
P08-07	21.9	694	1.34	2.11.2011	22.9.2011	41
P10-02	23.8	977	1.69	2.11.2011	24.9.2011	39
P12-01	23.8	781	1.69	2.11.2011	30.9.2011	33
P14-07	24.4	930	1.65	2.11.2011	20.10.2011	13
P17-10	24.1	757	1.67	2.11.2011	24.10.2011	9
P03-10	26.8	632	1.29	22.11.2011	13.9.2011	70
P05-07	23.1	762	1.53	22.11.2011	15.9.2011	68
P08-06	22.0	648	1.31	22.11.2011	22.9.2011	61
P14-10	25.0	1040	2.05	22.11.2011	20.10.2011	33
P17-07	23.2	828	1.50	22.11.2011	24.10.2011	29
P03-09	26.0	799	1.83	23.11.2011	13.9.2011	71
P04-09	24.7	776	1.67	23.11.2011	14.9.2011	70
P05-09	23.6	703	1.57	23.11.2011	15.9.2011	69
P06-06	21.7	670	1.74	23.11.2011	20.9.2011	64
P07-04	21.9	505	1.21	23.11.2011	21.9.2011	63
P08-09	21.6	654	1.46	23.11.2011	22.9.2011	62
P10-01	24.6	914	2.14	23.11.2011	24.9.2011	60
P12-02	22.6	821	1.92	23.11.2011	30.9.2011	54
P14-06	25.5	911	2.05	23.11.2011	20.10.2011	34
P17-06	24.0	942	2.14	23.11.2011	24.10.2011	30
P03-08	26.9	826	1.38	16.12.2011	13.9.2011	94
P04-07	24.5	927	1.53	16.12.2011	14.9.2011	93
P05-10	23.8	752	1.32	16.12.2011	15.9.2011	92
P06-10	22.9	689	1.21	16.12.2011	20.9.2011	87
P07-03	22.2	526	0.88	16.12.2011	21.9.2011	86
P10-03	25.0	859	1.46	16.12.2011	24.9.2011	83
P12-03	24.3	890	1.49	16.12.2011	30.9.2011	77

Tab. B.1: (continued)

Specimen number	Length L [mm]	Breaking force F_{\max} [N]	Deformation dL at F_{\max} [mm]	Date of experiment	Date of production	Age [day]
P14-08	25.3	966	1.55	16.12.2011	20.10.2011	57
P17-08	24.4	809	1.20	16.12.2011	24.10.2011	53
P04-10	25.5	696	1.14	16.12.2011	14.9.2011	93
<i>LENGTH GROUP nr. 3: $l \sim 60$ mm</i>						
P04-12	62.0	747	1.78	19.10.2011	14.9.2011	35
P04-13	64.0	754	1.77	19.10.2011	14.9.2011	35
P05-11	58.0	640	1.68	19.10.2011	15.9.2011	34
P05-13	58.0	625	1.51	19.10.2011	15.9.2011	34
P11-08	60.0	729	1.88	19.10.2011	29.9.2011	20
P11-10	59.0	718	1.83	19.10.2011	29.9.2011	20
P09-08	58.2	918	2.13	29.10.2011	23.9.2011	36
P10-07	58.0	830	1.97	29.10.2011	24.9.2011	35
P12-07	58.6	827	2.13	29.10.2011	30.9.2011	29
P14-14	57.7	900	2.36	29.10.2011	20.10.2011	9
P03-11	59.2	515	1.46	1.11.2011	13.9.2011	49
P05-15	58.1	514	1.47	1.11.2011	15.9.2011	47
P06-14	57.2	628	1.78	1.11.2011	20.9.2011	42
P03-12	58.5	561	1.65	2.11.2011	13.9.2011	50
P04-14	62.4	643	1.75	2.11.2011	13.9.2011	50
P05-14	57.8	536	1.64	2.11.2011	15.9.2011	48
P05-19	57.8	812	2.09	2.11.2011	15.9.2011	48
P05-20	58.0	650	1.37	2.11.2011	15.9.2011	48
P06-12	57.1	743	1.50	2.11.2011	20.9.2011	43
P09-06	57.4	723	1.51	2.11.2011	23.9.2011	40
P10-08	59.2	831	1.41	2.11.2011	24.9.2011	39
P12-06	59.0	867	2.25	2.11.2011	30.9.2011	33
P14-12	58.0	862	2.09	2.11.2011	20.10.2011	13
P03-13	57.7	555	1.61	22.11.2011	13.9.2011	70
P05-17	57.9	753	1.88	22.11.2011	15.9.2011	68
P10-09	58.2	831	2.19	22.11.2011	24.9.2011	59
P12-09	59.0	878	2.34	22.11.2011	30.9.2011	53

Tab. B.1: (continued)

Specimen number	Length L [mm]	Breaking force F_{\max} [N]	Deformation dL at F_{\max} [mm]	Date of experiment	Date of production	Age [day]
P14-15	58.3	913	2.27	22.11.2011	20.10.2011	33
P03-15	58.8	484	1.32	23.11.2011	13.9.2011	71
P04-15	63.2	591	1.86	23.11.2011	14.9.2011	70
P05-18	59.0	670	2.09	23.11.2011	15.9.2011	69
P06-11	57.0	760	2.30	23.11.2011	20.9.2011	64
P09-09	57.3	834	2.34	23.11.2011	23.9.2011	61
P09-10	58.0	785	2.50	23.11.2011	23.9.2011	61
P10-10	59.0	915	2.56	23.11.2011	24.9.2011	60
P11-06	59.8	727	2.22	23.11.2011	29.9.2011	55
P12-10	59.4	804	2.37	23.11.2011	30.9.2011	54
P14-11	58.8	825	2.51	23.11.2011	20.10.2011	34
P03-14	58.5	520	1.28	16.12.2011	13.9.2011	94
P04-11	63.0	674	1.77	16.12.2011	14.9.2011	93
P05-12	58.0	944	1.55	16.12.2011	15.9.2011	92
P06-13	58.2	831	1.86	16.12.2011	20.9.2011	87
P09-07	57.6	647	1.66	16.12.2011	23.9.2011	84
P10-06	59.0	754	1.88	16.12.2011	24.9.2011	83
P11-07	58.8	785	1.99	16.12.2011	29.9.2011	78
P12-08	59.6	862	2.14	16.12.2011	30.9.2011	77
P14-13	58.6	830	2.06	16.12.2011	20.10.2011	57
P06-15	57.9	675	1.69	16.12.2011	20.9.2011	87
LENGTH GROUP nr. 4: $l \sim 130$ mm						
P03-17	128.0	528	2.22	19.10.2011	13.9.2011	36
P03-20	129.0	477	2.25	19.10.2011	13.9.2011	36
P05-22	129.0	669	2.81	19.10.2011	15.9.2011	34
P05-25	130.0	554	2.61	19.10.2011	15.9.2011	34
P10-11	126.0	662	2.67	19.10.2011	24.9.2011	25
P10-13	127.0	757	3.20	19.10.2011	24.9.2011	25
P04-25	131.8	620	2.60	29.10.2011	14.9.2011	45
P06-20	128.0	669	3.06	29.10.2011	20.9.2011	39
P08-14	127.8	727	3.08	29.10.2011	22.9.2011	37

Tab. B.1: (continued)

Specimen number	Length L [mm]	Breaking force F_{\max} [N]	Deformation dL at F_{\max} [mm]	Date of experiment	Date of production	Age [day]
P12-13	127.8	862	3.27	29.10.2011	30.9.2011	29
P04-24	131.0	580	2.47	1.11.2011	14.9.2011	48
P06-18	128.0	717	3.02	1.11.2011	20.9.2011	42
P09-12	127.0	746	2.89	1.11.2011	23.9.2011	39
P03-18	128.5	552	2.27	2.11.2011	13.9.2011	50
P03-19	129.2	541	2.79	2.11.2011	13.9.2011	50
P04-17	128.5	539	2.52	2.11.2011	14.9.2011	49
P04-22	131.3	661	2.87	2.11.2011	14.9.2011	49
P05-24	128.6	606	2.82	2.11.2011	15.9.2011	48
P06-17	126.8	685	2.96	2.11.2011	20.9.2011	43
P08-15	128.7	766	6.42	2.11.2011	22.9.2011	41
P10-14	125.8	833	3.35	2.11.2011	24.9.2011	39
P12-15	127.3	789	3.02	2.11.2011	30.9.2011	33
P16-02	128.0	768	3.06	2.11.2011	22.10.2011	11
P04-21	132.0	672	2.77	22.11.2011	14.9.2011	69
P04-23	132.4	687	3.26	22.11.2011	14.9.2011	69
P12-14	127.2	798	3.44	22.11.2011	30.9.2011	53
P16-25	129.1	807	3.21	22.11.2011	22.10.2011	31
P18-02	129.0	798	3.12	22.11.2011	25.10.2011	28
P03-16	128.9	593	2.67	23.11.2011	13.9.2011	71
P04-19	127.8	503	2.49	23.11.2011	14.9.2011	70
P05-21	129.9	592	2.81	23.11.2011	15.9.2011	69
P06-19	127.1	766	3.52	23.11.2011	20.9.2011	64
P08-12	128.1	744	3.49	23.11.2011	22.9.2011	62
P09-11	128.2	718	3.28	23.11.2011	23.9.2011	61
P10-12	125.6	842	3.56	23.11.2011	24.9.2011	60
P12-12	126.9	786	3.30	23.11.2011	30.9.2011	54
P16-01	128.8	751	3.27	23.11.2011	22.10.2011	32
P18-03	127.9	772	3.59	23.11.2011	25.10.2011	29
P04-18	129.3	532	2.36	16.12.2011	14.9.2011	93
P05-23	130.0	573	2.42	16.12.2011	15.9.2011	92
P06-16	127.5	762	2.79	16.12.2011	20.9.2011	87

Tab. B.1: (continued)

Specimen number	Length L [mm]	Breaking force F_{\max} [N]	Deformation dL at F_{\max} [mm]	Date of experiment	Date of production	Age [day]
P08-11	128.7	746	3.07	16.12.2011	22.9.2011	85
P08-13	129.2	790	3.08	16.12.2011	22.9.2011	85
P10-15	126.4	770	3.09	16.12.2011	24.9.2011	83
P12-11	128.0	713	2.94	16.12.2011	30.9.2011	77
P16-03	129.0	753	2.94	16.12.2011	22.10.2011	55
P16-04	127.8	824	3.08	16.12.2011	22.10.2011	55
P18-01	128.0	673	2.62	16.12.2011	25.10.2011	52
<i>LENGTH GROUP nr. 5: $l \sim 310$ mm</i>						
P06-23	308.0	622	2.17	19.10.2011	20.9.2011	29
P06-25	308.0	624	5.21	19.10.2011	20.9.2011	29
P07-09	307.0	683	5.18	19.10.2011	21.9.2011	28
P07-10	307.5	645	5.53	19.10.2011	21.9.2011	28
P09-17	306.5	696	5.75	19.10.2011	23.9.2011	26
P09-20	307.0	729	5.46	19.10.2011	23.9.2011	26
P03-24	308.0	608	4.98	29.10.2011	13.9.2011	46
P04-30	312.0	490	4.18	29.10.2011	14.9.2011	45
P05-30	309.0	452	4.42	29.10.2011	15.9.2011	44
P13-09	307.4	719	5.48	29.10.2011	5.10.2011	24
P05-28	310.0	469	4.07	1.11.2011	15.9.2011	47
P09-18	306.4	687	5.60	1.11.2011	23.9.2011	39
P13-10	308.0	684	5.37	1.11.2011	5.10.2011	27
P03-23	308.7	468	4.50	2.11.2011	13.9.2011	50
P04-27	311.3	616	4.88	2.11.2011	14.9.2011	49
P05-29	309.8	421	3.40	2.11.2011	15.9.2011	48
P06-22	306.0	650	5.89	2.11.2011	20.9.2011	43
P07-08	308.1	693	6.01	2.11.2011	21.9.2011	42
P09-24	306.0	607	5.11	2.11.2011	23.9.2011	40
P09-25	306.8	598	5.10	2.11.2011	23.9.2011	40
P13-08	308.9	706	6.15	2.11.2011	5.10.2011	28
P16-09	308.7	729	5.77	2.11.2011	22.10.2011	11
P18-08	310.0	733	5.68	2.11.2011	25.10.2011	8

Tab. B.1: (continued)

Specimen number	Length L [mm]	Breaking force F_{\max} [N]	Deformation dL at F_{\max} [mm]	Date of experiment	Date of production	Age [day]
P03-21	307.8	554	5.06	22.11.2011	13.9.2011	70
P04-29	311.0	615	5.28	22.11.2011	14.9.2011	69
P09-19	305.9	646	5.06	22.11.2011	23.9.2011	60
P16-10	309.4	642	5.12	22.11.2011	22.10.2011	31
P18-04	310.1	685	5.82	22.11.2011	25.10.2011	28
P03-22	307.6	534	4.51	23.11.2011	13.9.2011	71
P04-28	311.4	600	5.18	23.11.2011	14.9.2011	70
P05-26	309.4	517	4.47	23.11.2011	15.9.2011	69
P06-21	306.6	605	5.70	23.11.2011	20.9.2011	64
P07-07	307.4	648	5.38	23.11.2011	21.9.2011	63
P09-21	306.5	630	5.61	23.11.2011	23.9.2011	61
P09-23	307.0	628	5.85	23.11.2011	23.9.2011	61
P13-06	308.3	702	5.82	23.11.2011	5.10.2011	49
P16-06	309.7	679	5.70	23.11.2011	22.10.2011	32
P18-06	310.2	656	5.32	23.11.2011	25.10.2011	29
P03-25	307.7	526	4.46	16.12.2011	13.9.2011	94
P04-26	311.8	635	5.22	16.12.2011	14.9.2011	93
P05-27	308.9	485	3.83	16.12.2011	15.9.2011	92
P07-06	308.9	619	5.10	16.12.2011	21.9.2011	86
P09-16	307.2	596	5.15	16.12.2011	23.9.2011	84
P09-22	306.6	628	5.38	16.12.2011	23.9.2011	84
P13-07	307.5	704	5.46	16.12.2011	5.10.2011	72
P16-08	310.2	709	5.91	16.12.2011	22.10.2011	55
P18-05	309.0	723	5.82	16.12.2011	25.10.2011	52
P18-07	308.7	726	5.82	16.12.2011	25.10.2011	52
<i>LENGTH GROUP nr. 6: $l \sim 740$ mm</i>						
P03-29	740.0	358	6.47	19.10.2011	13.9.2011	36
P05-31	738.0	411	8.30	19.10.2011	15.9.2011	34
P05-32	739.0	352	7.68	19.10.2011	15.9.2011	34
P11-14	737.0	572	10.97	19.10.2011	29.9.2011	20
P11-15	737.0	565	11.23	19.10.2011	29.9.2011	20

Tab. B.1: (continued)

Specimen number	Length L [mm]	Breaking force F_{\max} [N]	Deformation dL at F_{\max} [mm]	Date of experiment	Date of production	Age [day]
P06-29	738.2	458	8.83	29.10.2011	20.9.2011	39
P08-16	740.0	583	10.98	29.10.2011	22.9.2011	37
P09-28	734.5	668	10.95	29.10.2011	23.9.2011	36
P13-11	738.8	497	8.92	29.10.2011	5.10.2011	24
P04-35	740.5	368	6.92	29.10.2011	14.9.2011	45
P04-32	740.0	395	7.76	1.11.2011	14.9.2011	48
P15-01	740.5	546	11.28	1.11.2011	21.10.2011	11
P03-28	740.0	361	6.58	2.11.2011	13.9.2011	50
P04-33	740.8	373	6.74	2.11.2011	14.9.2011	49
P05-35	739.5	376	7.89	2.11.2011	15.9.2011	48
P06-27	738.7	481	10.30	2.11.2011	20.9.2011	43
P08-17	739.0	493	9.58	2.11.2011	22.9.2011	41
P09-26	734.0	591	11.99	2.11.2011	23.9.2011	40
P13-12	737.0	649	11.15	2.11.2011	5.10.2011	28
P15-04	740.0	577	11.43	2.11.2011	21.10.2011	12
P17-11	739.2	448	8.70	2.11.2011	24.10.2011	9
P03-30	740.0	390	6.09	22.11.2011	13.9.2011	70
P06-28	740.0	466	9.48	22.11.2011	20.9.2011	63
P11-13	737.4	601	10.85	22.11.2011	29.9.2011	54
P13-15	737.9	494	9.23	22.11.2011	5.10.2011	48
P15-05	740.0	563	10.63	22.11.2011	21.10.2011	32
P17-12	738.5	566	11.34	22.11.2011	24.10.2011	29
P04-31	740.2	426	8.87	23.11.2011	14.9.2011	70
P05-34	737.6	476	7.74	23.11.2011	15.9.2011	69
P08-20	738.0	536	9.25	23.11.2011	22.9.2011	62
P09-27	732.8	581	10.44	23.11.2011	23.9.2011	61
P11-12	736.8	603	10.83	23.11.2011	29.9.2011	55
P13-13	737.5	550	10.21	23.11.2011	5.10.2011	49
P15-02	739.5	573	10.31	23.11.2011	21.10.2011	33
P17-14	738.4	511	11.00	23.11.2011	24.10.2011	30
P03-26	740.0	415	7.53	23.11.2011	13.9.2011	71
P04-34	740.3	421	8.20	16.12.2011	14.9.2011	93

Tab. B.1: (continued)

Specimen number	Length L [mm]	Breaking force F_{\max} [N]	Deformation dL at F_{\max} [mm]	Date of experiment	Date of production	Age [day]
P05-33	739.8	410	7.73	16.12.2011	15.9.2011	92
P06-26	740.8	485	8.75	16.12.2011	20.9.2011	87
P06-30	738.8	493	9.22	16.12.2011	20.9.2011	87
P08-18	737.7	519	10.91	16.12.2011	22.9.2011	85
P08-19	737.2	547	8.85	16.12.2011	22.9.2011	85
P09-29	733.7	547	9.80	16.12.2011	23.9.2011	84
P09-30	734.0	570	8.93	16.12.2011	23.9.2011	84
P11-11	738.2	536	9.43	16.12.2011	29.9.2011	78
P13-14	736.8	573	10.86	16.12.2011	5.10.2011	72
P15-03	740.3	534	10.62	16.12.2011	21.10.2011	56
P17-13	739.7	557	10.33	16.12.2011	24.10.2011	53
P17-15	739.4	534	10.41	16.12.2011	24.10.2011	53

Tab. B.2: Laboratory conditions: temperature and relative humidity with their extreme values in a certain time period.

date	time	temp. [°C]	hum. [%]	temp.		rel. hum.	
				max [°C]	min [°C]	max [°C]	min [°C]
20.10.2011	20:08	22.6	42.4	22.7	21.7	46.6	38.6
21.10.2011	12:40	21.4	40.7	22.9	20.6	46.6	38.6
	18:33	23.5	39.3	23.8	23.4	39.8	37.6
22.10.2011	12:20	21.4	38.0	23.7	20.6	40.2	38.0
27.10.2011	10:06	21.1	46.4	21.6	20.6	52.0	44.9
29.10.2011	11:30	20.9	43.8	21.3	20.4	47.0	42.8
	17:03	22.4	42.4	22.4	20.4	44.8	41.7
31.10.2011	9:45	20.0	44.8	22.5	19.8	45.8	41.8
	18:00	21.1	45.9	21.3	20.6	45.9	44.3
1.11.2011	10:00	20.9	42.8	21.3	20.3	45.9	42.8
	15:50	21.8	44.9	21.9	20.9	44.9	42.8
	18:50	22.6	44.0	22.6	21.8	45.0	43.9
2.11.2011	10:10	21.1	44.3	22.6	20.5	44.3	43.3
	16:40	22.9	43.5	22.9	21.0	44.8	42.3
	21:36	23.0	41.9	23.0	22.4	43.5	40.3
3.11.2011	14:20	21.8	42.3	23.1	21.2	42.3	39.6
21.11.2011	12:30	20.8	32.4	23.0	19.4	34.3	30.8
22.11.2011	15:00	21.3	30.8	21.3	20.4	33.0	30.8
23.11.2011	10:30	31.8	29.8	23.5	20.9	31.0	27.4
	21:00	23.8	28.8	23.9	21.8	32.0	25.3
24.11.2011	14:30	22.3	22.3	23.9	21.8	29.8	28.7
15.12.2011	12:45	21.0	35.5	24.1	19.5	36.3	29.6
16.12.2011	11:30	21.9	33.1	23.2	20.8	35.3	32.5